

Asteroid families classification: exploiting very large data sets

Andrea Milani^a, Alberto Cellino^b, Zoran Knežević^c, Bojan Novaković^d,
Federica Spoto^a, Paolo Paolicchi^e

^a*Dipartimento di Matematica, Università di Pisa, Largo Pontecorvo 5, 56127 Pisa, Italy*

^b*INAF–Osservatorio Astrofisico di Torino, 10025 Pino Torinese, Italy*

^c*Astronomical Observatory, Volgina 7, 11060 Belgrade 38, Serbia*

^d*Department of Astronomy, Faculty of Mathematics, University of Belgrade, Studentski
trg 16, 11000 Belgrade, Serbia*

^e*Dipartimento di Fisica, Università di Pisa, Largo Pontecorvo 3, 56127 Pisa, Italy*

Abstract

The number of asteroids with accurately determined orbits increases fast, and this increase is also accelerating. The catalogs of asteroid physical observations have also increased, although the number of objects is still smaller than in the orbital catalogs. Thus it becomes more and more challenging to perform, maintain and update a classification of asteroids into families. To cope with these challenges we developed a new approach to the asteroid family classification by combining the Hierarchical Clustering Method (HCM) with a method to add new members to existing families. This procedure makes use of the much larger amount of information contained in the proper elements catalogs, with respect to classifications using also physical observations for a smaller number of asteroids.

Our work is based on the large catalog of the high accuracy synthetic proper elements (available from AstDyS), containing data for > 330 000 numbered asteroids. By selecting from the catalog a much smaller number of large asteroids, we first identify a number of core families; to these we attribute the next layer of smaller objects. Then, we remove all the family members from the catalog, and reapply the HCM to the rest. This gives both halo families which extend the core families and new independent families, consisting mainly of small asteroids. These two cases are discriminated by another step

Email address: `milani@dm.unipi.it` (Andrea Milani)

of attribution of new members and by merging intersecting families. This leads to a classification with 128 families and currently 87095 members; the number of members can be increased automatically with each update of the proper elements catalog.

By using information from absolute magnitudes, we take advantage of the larger size range in some families to analyze their shape in the proper semimajor axis vs. inverse diameter plane. This leads to a new method to estimate the family age, or ages in cases where we identify internal structures. The analysis of the plot above evidences some open problems but also the possibility of obtaining further information of the geometrical properties of the impact process. The results from the previous steps are then analyzed, using also auxiliary information on physical properties including WISE albedos and SDSS color indexes. This allows to solve some difficult cases of families overlapping in the proper elements space but generated by different collisional events.

The families formed by one or more cratering events are found to be more numerous than previously believed because the fragments are smaller. We analyze some examples of cratering families (Massalia, Vesta, Eunomia) which show internal structures, interpreted as multiple collisions. We also discuss why Ceres has no family.

Keywords: Asteroids, Asteroid dynamics, Collisional evolution, Non-gravitational perturbations.

1. Introduction

Asteroid families are a powerful tool to investigate the collisional and dynamical evolution of the asteroid belt. If they are correctly identified, they allow to describe the properties of the parent body, the collisional event(s) generating the family and the subsequent evolution due to chaotic dynamics, non-gravitational perturbations, and secondary collisions.

However, asteroid families are statistical entities. They can be detected by density contrast with respect to a background in the phase space of appropriate parameters, but their reliability strongly depends upon the number of members, the accuracy of the parameters and the method used for the classification. The exact membership cannot be determined, because the portion of phase space filled by the family can have already been occupied by some

background asteroids, thus every family can and usually does have interlopers [45]. Moreover, the exact boundary of the region occupied by the family corresponds to marginal density contrast and thus cannot be sharply defined.

The problem is, the purpose of a classification is not just to get as many families as possible, but to obtain families with enough members, with a large enough spread in size, and accurate enough data to derive quantities such as number of family generating collisional events, age for each of them, size of parent bodies, size distribution of fragments (taking into account observational bias), composition, and flow from the family to Near Earth Asteroid (NEA) and/or cometary type orbits.

This has three important implications. First, the quality of a family classification heavily depends on the number of asteroids used, and upon the accuracy of the parameters used in the process. The number of asteroids is especially critical, because small number statistics masks all the information content in small families. Moreover, there is no way of excluding that families currently with few members are statistical flukes, even if they are found likely to be significant by statistical tests.

Second, different kinds of parameters have very different value in a family classification. This can be measured by the information content, which is, for each parameter, the base 2 logarithm of the inverse of relative accuracy, summed for all asteroids for which such data are available; see Section 2. By using this measure, it is easy to show that the dynamical parameters, such as the proper elements¹ a, e, I have a much larger information content than the physical observations, because the latter are either available only for much smaller catalogs of asteroids, or with worse relative accuracy, or both. As an example, absolute magnitudes are available for all asteroids with good orbits and accurate proper elements, but they are computed by averaging over inhomogeneous data with poorly controlled quality. There are catalogs with albedos such as WISE, described in [40, 36], and color indexes such as the Sloan Digital Sky Survey (SDSS), described in [28], but the number of asteroids included is smaller by factors 3 to 5 with respect to proper elements catalogs, and this already includes many objects observed with marginal S/N, thus poor relative accuracy.

Third, catalogs with asteroid information grow with time at a rapid and

¹As an alternative the corresponding frequencies n, g, s can be used, the results should be the same if the appropriate metric is used [10].

accelerating pace: e.g., we have used for this paper a catalog, distributed from AstDyS² with 336 219 numbered asteroids with synthetic proper elements computed up to November 2012. By April 2013 the same catalog had grown to 354 467 objects, i.e., 5.4% in 5 months. If the rate of asteroid numbering was to continue at this rate, a pessimistic assumption, in less than 8 years the catalog would be doubled. Catalogs of physical observations are also likely to grow, although in a less regular and predictable way. Thus the question is whether the increase of the catalogs will either confirm or contradict the conclusions we draw at present; or better, the goal should be to obtain robust conclusions which will pass the test of time.

As a consequence our purpose in this paper is not to make "yet another asteroid family classification", but to setup a classification which can be automatically updated every time the dataset is increased. We are going to use the proper elements first, that is defining "dynamical families", then use information from absolute magnitudes, albedos and generalized color indexes, when available and useful, as either confirmation or rejection, e.g, identification of interlopers and possibly of intersections of different collisional families. We will continue to update the classification by running at short intervals (few months) a fully automated "classification" computer program which attaches newly numbered objects to existing families.

This will not remove the need to work on the identification of new families and/or on the analysis of the properties of the already known families. Every scientist will be practically enabled to do this at will, since for our dataset and our classification we follow a strict open data policy, which is already in place when this paper is submitted: all the data on our family classification is already available on AstDyS, and in fact it has already been updated with respect to the version described in this paper.

We have also recently made operational a new graphic interface on AstDyS providing figures very much like the examples shown in this paper³. The senior authors of this paper have learned much on the books *Asteroids I* and *Asteroids II* which contained Tabulation sections with large printed tables of data. This has been abolished in *Asteroids III*, because by the the year 2000 the provision of data in electronic form, of which AstDyS is just one example, was the only service practically in use. It is now time to reduce

²<http://hamilton.dm.unipi.it/astdys2/index.php?pc=5>

³<http://hamilton.dm.unipi.it/astdys2/Plot/index.html>

the number of figures, especially in color, and replacing them with “graphic servers” providing figures based upon the electronically available data and composed upon request from the users: this is what the AstDyS graphic tool is proposing as an experiment which may be followed by others. Readers are warmly invited to take profit of this tool, although the most important statements we do in the discussion of our results are already supported by a (forcibly limited) number of explanatory figures.

The main purpose of this paper is to describe and make available some large data sets, only some of the interpretations are given, mostly as examples to illustrate how the data could be used. We would like to anticipate one major conceptual tool, which will be presented in the paper. This concerns the meaning of the word “family”, which has become ambiguous because of usage by many authors with very different background and intent.

We shall use two different terms: since we believe the proper elements contain most of the information, we perform a family classification based only upon them, thus defining *dynamical families*. A different term *collisional families* shall be used to indicate a set of asteroids in the catalog which have been formed at once by a single collision, be it either a catastrophic fragmentation or a cratering event. Note that there is no reason to think that the correspondence between dynamical families and collisional families should be one to one. A dynamical family may correspond to multiple collisional events, both on the same and on different parent bodies. A collisional family may appear as two dynamical families because of a gap due to dynamical instability. A collisional family might have dissipated long ago, leaving no dynamical family. A small dynamical family might be a statistical fluke, with no common origin for its members. In this paper we shall give several examples of these non-correspondences.

2. Dataset

In this section we list all datasets used in our classification and in its analysis contained in this paper.

2.1. Proper elements

Proper elements a , e , $\sin i$ are three very accurate parameters, and we have computed, over many years up to November 2012, synthetic proper elements [30, 31] for 336 319 asteroids. We made a special effort to recompute synthetic proper elements for asteroids missing in our database because of different

reasons: being close to strong resonances, suffering close encounters with major planets, or having high eccentricities and inclinations. In particular we aimed at increasing the number of objects in the high e, I regions, in order to improve upon the sparse statistics and the reliability of small families therein. We thus integrated orbits of a total of 2 222 asteroids, out of which the proper elements computation failed for only 62 of them. The rest are now included in the AstDyS synthetic proper elements files. This file is updated a few times per year.

For each individual parameter in this dataset there are available both standard deviation and maximum excursion obtained from the analysis of the values computed in sub-intervals [30]. If an asteroid has large instabilities in the proper elements, as it happens for high proper $e, \sin I$, then the family classification can be dubious.

The same catalog contains also absolute magnitudes and estimates of Lyapounov Characteristic Exponents, discussed in the following subsections.

2.2. Absolute magnitudes

Another piece of information is the set of absolute magnitudes available for all numbered asteroids computed by fitting the apparent magnitudes obtained incidentally with the astrometry, thus stored in the Minor Planet Center (MPC) astrometric database. The range of values for all numbered asteroids is 15.7, the accuracy is difficult to be estimated because the incidental photometry is very inhomogeneous in quality, and the information on both S/N and reduction method is not available.

The sources of error in the absolute magnitude data are not just the measurement errors, which are dominant only for dim asteroids, but also star catalog local magnitude biases, errors in conversion from star-calibrated magnitudes to the assumed V magnitude used in absolute magnitudes, and the lightcurve effect. Moreover, the brightness of an asteroid changes at different apparitions as an effect of shape and spin axis orientation, so strictly speaking the absolute magnitude is not a real constant. Last but not least, the absolute magnitude is defined at zero phase angle (ideal solar opposition) thus some extrapolation of observations obtained in different illumination conditions is always needed, and this introduces other significant errors, especially for high phase angles. The standard deviation of the apparent magnitude residuals has a distribution peaked at 0.5 mag: since numbered asteroids have in general many tens of magnitude observations, the formal error in the absolute magnitude, which is just a corrected average, is generally

very small, but biases can be very significant. Thus we do not have a reliable estimate of the accuracy for the large dataset of 336 219 absolute magnitudes computed by AstDyS, we can just guess that the standard deviation should be in the range $0.3 \div 0.5$ magnitudes.

The more optimistic estimate gives a large information content (see Table 1), which would be very significant, but there are many quality control problems. Other databases of photometric information with better and more consistent information are available, but the number of objects included is much smaller, e.g., 583 asteroids with accuracy better than 0.21 magnitudes [62]: these authors also document the existence of serious systematic size-dependent biases in the H values.

2.3. WISE and SDSS catalogs of physical observations

The WISE catalog of albedos⁴ has information on 94 632 numbered asteroids with synthetic proper elements, but the relative accuracy is moderate: the average standard deviation (STD) is 0.045, but the average ratio between STD and value is 0.28; e.g., the asteroids in the WISE catalog for which the albedo measured is < 3 times the STD are 26% (we are going to use measure > 3 times STD as criterion for using WISE data in Section 6).

This is due to the fact that WISE albedos, in particular for small asteroids, have been derived from a *measured* infrared flux and an *estimated* visible light flux derived from an adopted nominal value of absolute magnitude. Both terms are affected by random noise increasing for small objects, and by systematics in particular in the visible, as outlined in the previous subsection. In principle one should use a value of absolute magnitude not only accurate, but also corresponding to the same observation circumstances of the thermal IR observations, which is seldom the case. For comparatively large asteroids, albedo can be constrained also from the ratios between different infrared channels of WISE, thus the result may be less affected by the uncertainty of the absolute magnitude.

The 4th release of the SDSS MOC⁵ contains data for 471 569 moving objects, derived from the images taken in five filters, u , g , r , i , and z , ranging from 0.3 to 1.0 μm . Of those, 123 590 records refer to asteroids present in our catalog of proper elements. As many of these objects have more

⁴Available at URL http://wise2.ipac.caltech.edu/staff/bauer/NEOWISE_pass1

⁵Available at URL <http://www.astro.washington.edu/users/ivezic/sdssmoc/>

than one record in the SDSS catalog, a total number of asteroids present in both catalogs is 61 041. The latter number was then further decreased by removing objects having error in magnitude larger than 0.2 mag in at least one band (excluding the u -band which was not used in our analysis). This, non-conservative limit, is used to remove only obviously degenerate cases. Thus, we used the SDSS MOC 4 data for 59 975 numbered asteroids.

It is well known that spectrophotometric data is of limited accuracy, and should not be used to determine colors of single objects. Still, if properly used, the SDSS data could be useful in some situations, e.g. to detect presence of more than one collisional family inside a dynamical family, or to trace objects escaping from the families.

Following [61] we have used a^* , the first principal component⁶ in the $r-i$ versus $g-r$ color-color plane, to discriminate between C -type asteroids ($a^* < 0$) and S -type asteroids ($a^* \geq 0$). Then, among the objects having ($a^* \geq 0$) the $i-z$ values can be used to further discriminate between S - and V -type, with the latter one characterized by the $i-z < -0.15$. The average standard deviation of data we used is 0.04 for a^* , 0.08 for $i-z$.

2.4. Resonance identification

Another source of information available as an output of the numerical integrations used to compute synthetic proper elements is an estimate of the maximum Lyapounov Characteristic Exponent (LCE). The main use of this is to identify asteroids affected by chaos over comparatively short time scales (much shorter than the ages of the families)⁷. These are mostly due to mean motion resonances with major planets (only resonances with Jupiter, Saturn and Mars are affecting the Main Belt at levels which are significant for family classification). Thus we use as criterion to detect these “resonant/chaotic” asteroids the occurrence of at least one of the following: either a $LCE > 50$ per Million years (that is a Lyapounov time $< 20\,000$ years) or $STD(a) > 3 \times 10^{-4}$ au.

Note that the numerical integrations done to compute proper elements use a dynamical model not including any asteroid as perturber. This is done for numerical stability reasons, because all asteroids undergo mutual close

⁶According to [28] the first principal component in the $r-i$ vs $g-r$ plane is defined as $a^* = 0.89(g-r) + 0.45(r-i) - 0.57$.

⁷Every asteroid is affected by chaotic effects over timescales comparable to the age of the solar system, but this does not matter for family classification.

approaches and these would need to be handled accurately, which is difficult while integrating hundreds of asteroids simultaneously. Another reason for this choice is that we wish to identify specifically the chaos which is due to mean motion resonances with the major planets. As shown by [33], if even a few largest asteroids are considered with their mass in the dynamical model, then all asteroids are chaotic with Lyapounov times of a few 10 000 years. However, the long term effect of such chaos endogenous to the asteroid belt is less important than the chaos generated by the planetary perturbations [21].

The asteroid perturbers introduce many new frequencies, resulting in an enormous increase of the Arnold web of resonances, to the point of leaving almost no space for conditionally periodic orbits, and the Lyapounov times are short because the chaotic effects are driven by mean motion resonances. However, these resonances are extremely weak, and they do not result in large scale instability, not even over time spans of many thousands of Lyapounov times, the so called “stable chaos” phenomenon [49]. In particular, locking in a stable resonance with another asteroid is almost impossible, the only known exception being the 1/1 resonance with Ceres, see the discussion about the Hoffmeister family in Section 4.1.1 and Figure 3. This implies that the (size-dependent) Yarkovsky effect, which accumulates secularly in time in semimajor axis, cannot have secular effects in eccentricity and inclination, as it happens when there is capture in resonance.

We have developed a sensitive detector of mean motion resonances with the major planets, but we would like to know which resonance, which is the integer combination of mean motions forming the “small divisor”. For this we use the catalog of asteroids in mean motion resonances by [67], which has also been provided to us by the authors in an updated and computer readable form. This catalog will continue to be updated, and the information will be presented through the AstDyS site.

Asteroid families are also affected by secular resonances, with “divisor” formed with an integer combination of frequencies appearing in the secular evolution of perihelia and nodes, namely g, g_5, g_6 for the perihelia of the asteroid, Jupiter and Saturn, and s, s_6 for the ones in the nodes of the asteroid and Jupiter⁸. The data on the asteroids affected by secular resonances can

⁸In the Hungaria region even some resonances involving the frequencies g_3, g_4, s_4 for Earth and Mars can be significant [54].

be found with the analytic proper elements, computed by us with methods developed in the 90s [47, 48, 50]. In these algorithms, the small divisors associated with secular resonances appear as obstruction to the convergence of the iterative algorithm used to compute proper elements, thus error codes corresponding to the secular resonances are reported with the proper elements⁹.

Note that we have not used analytic proper elements as a primary set of parameters for family classification, since they are significantly less accurate (that is, less stable in time over millions of years) than the synthetic ones, by a factor about 3 in the low e and I portion of the main belt. The accuracy becomes even worse for high e, I , to the point that for $\sqrt{e^2 + \sin^2 I} > 0.3$ the analytical elements are not even computed [29]; they are also especially degraded in the outer portion of the main belt, for $a > 3.2$ au, due to too many mean motion resonances. On the other hand, analytic proper elements are available for multiopposition asteroids, e.g., for 98 926 of them in November 2012, but these would be more useful in the regions where the number density of numbered asteroids is low, which coincide with the regions of degradation: high e, I and $a > 3.2$ au. It is also possible to use proper elements for multiopposition asteroids to confirm and extend the results of family classification, but for this purpose it is, for the moment, recommended to use ad hoc catalogs of synthetic proper elements extended to multiopposition, as we have done in [54, 56].

2.5. Amount of information

For the purpose of computing the information content of each entry of the catalogs mentioned in this section, we use as definition of inverse relative accuracy the ratio of two quantities:

1. for each parameter, the useful range, within which most ($> 99\%$) of the values are contained;
2. the standard deviation, as declared in each catalog, for each individual computed parameter.

Then the content in bit of each individual parameter is the base 2 logarithm of this ratio. These values are added for each asteroid in the catalog,

⁹We must admit these codes are not user friendly, although a Table of conversion from the error codes to the small divisors is given in [47, table 5.1]. We shall try to improve the AstDyS user interface on this.

thus forming a total information content, reported in the last column of Table 1 in Megabits. For statistical purposes we give also the average number of bits per asteroid in the catalog.

Table 1: An estimate of the information content of catalogs. The columns give: parameters contained in the catalogs, minimum and maximum values and range of the parameters, average information content in bits for a single entry in the catalog, number of entries in the catalog and total information content.

parameter	min	max	range	av.bits	number	tot Mb
a (au)	1.80	4.00	2.20	16.7	336219	5.63
e	0.00	0.40	0.40	10.7	336219	3.59
sin I	0.00	0.55	0.55	15.1	336219	5.08
total						14.39
<hr/>						
H	3.30	19.10	15.8	5.7	336219	1.92
<hr/>						
albedo	0.00	0.60	0.60	4.5	94632	0.43
<hr/>						
a*	-0.30	0.40	0.70	4.4	59975	0.26
i-z	-0.60	0.50	1.10	4.0	59975	0.24
total						0.50
<hr/>						

Note that for the absolute magnitude we have assumed a standard deviation of 0.3 magnitudes for all, although this might be optimistic.

With the numbers in Table 1 we can estimate the information content of our synthetic proper element catalog to be about 14 Megabits, the absolute magnitudes provide almost 2 megabits with somewhat optimistic assumptions, the physical data catalogs WISE and SDSS are 1 Megabit together.

3. Method for large dataset classification

Our adopted procedure for family identification is largely based on applications of the classical Hierarchical Clustering Method (HCM) already adopted in previous families searches performed since the pioneering work by [76], and later improved in a number of papers [77, 78, 54, 56]. Since the

method has been already extensively explained in the above papers, here we will limit ourselves to a very quick and basic description.

We have divided the asteroid belt in zones, corresponding to different intervals of heliocentric distance, delimited by the most important mean-motion resonances with Jupiter. These resonances correspond to Kirkwood gaps wide enough to exclude family classification across the boundaries.

Table 2: Summary of the relevant parameters for application of the HCM.

Zone	$\sin I$	range a	N (total)	$H_{completeness}$ (when used)	$N(H_{completeness})$ (when used)	N_{min}	QRL (m/s)
1	> 0.3	$1.600 \div 2.000$	4249			15	70
2	< 0.3	$2.065 \div 2.501$	115004	15.0	15888	17	70
2	> 0.3	$2.065 \div 2.501$	2627			11	130
3	< 0.3	$2.501 \div 2.825$	114510	14.5	16158	19	90
3	> 0.3	$2.501 \div 2.825$	3994			9	140
4	< 0.3	$2.825 \div 3.278$	85221	14.0	14234	17	100
4	> 0.3	$2.825 \div 3.278$	7954			12	80
5	all	$3.278 \div 3.700$	991			10	120
6	all	$3.700 \div 4.000$	1420			15	60

As shown in Table 2, our “zone 1” includes objects having proper semi-major axes between 1.6 and 2 au. In this region, only the so-called Hungaria objects at high inclination ($\sin I \geq 0.3$) are dynamically stable [54]. Our “zone 2” includes objects with proper orbital elements between 2.067 and 2.501 au. The “zone 3” is located between 2.501 and 2.825 au, and “zone 4” between 2.825 and 3.278 au. Zones 2, 3 and 4 were already used in several previous analyzes by our team. In addition, we use also a “zone 5”, corresponding to the interval between 3.278 and 3.7 au., and a “zone 6”, extending between 3.7 and 4.0 au. (Hilda zone).

Moreover, some semi-major axis zones have been also split by the value of proper $\sin I$, between a moderate inclination region $\sin I < 0.3$ and a high inclination region $\sin I > 0.3$. In some zones the boundary value corresponds to a gap due to secular resonances and/or stability boundaries. E.g., in zone 1 the moderate inclination region is almost empty and contains very chaotic objects (interacting strongly with Mars). In zone 2 the $g - g_6$ secular resonance clears a gap below the Phocaea region. In zones 3 and 4 there is no

natural dynamical boundary which could be defined by inclination only, and indeed we have problems with families found in both regions. In zones 5 and 6 there are few high inclination asteroids, and a much smaller population.

A metric function has been defined to compute the mutual distances of objects in the proper element space. Here, we have adopted the so-called “standard metric” d proposed by [76], and since then adopted in all HCM-based family investigations. We remind that using this metric the distances between objects in the proper element space correspond to differences of velocity and are given in m/s.

Having adopted a metric function, the HCM algorithm allows the users to identify all existing groups of objects which, at any given value of mutual distance d , are linked, in the sense that for each member of a group there is at least one other member of the same group which is closer than d . The basic idea is therefore to identify groups which are sufficiently populous, dense and compact (i.e., include large numbers of members down to small values of mutual distance) to be reasonably confident, in a statistical sense, that their existence cannot be a consequence of random fluctuations of the distribution of the objects in the proper element space.

In this kind of analysis, which is eminently statistical, a few parameters play a key role. The most important ones are the minimum number of objects N_{min} required for groups to be considered as candidate families, and the critical level of distance adopted for family identification. As for N_{min} , it is evident that its choice depends on the total number of objects present in a given region of the phase space. At the epoch of the pioneering study by [76], when the total inventory of asteroids with computed proper elements included only about 4,000 objects in the whole main belt, its value was chosen to be 5. Since then, in subsequent analyzes considering increasingly bigger datasets, the adopted values of N_{min} were scaled as the square root of the ratio between the numbers of objects in the present dataset and the one in some older sample in the same volume of the proper element space. We follow this procedure also in the present paper, so we chose the new N_{min} values by scaling with respect to the N_{min} adopted by [78] for the low-I portions of zones 2, 3, and 4, and [56] for the high-I portions of the same zones. Zone 5 and 6 were analyzed for the first time, they contain relatively low numbers of objects, and for them we adopted N_{min} values close to 1% of the sample, after checking that this choice did not affect severely the results.

As for the critical distance level, it is derived by generating synthetic populations (“Quasi-Random Populations”) of fictitious objects occupying

the same volume of proper element space, and generated in such a way as to have *separately* identical distributions of a , e and $\sin I$ as the real asteroids present in the same volume. An HCM analysis of these fictitious populations is then performed, and this makes it possible to identify some critical values of mutual distance below which it is not possible to find groupings of at least N_{min} quasi-random objects. All groups of real objects which include N_{min} members at distance levels below the critical threshold, are then considered as dynamical families. Note also that we always looked at groupings found at discrete distance levels separated by steps of 10 m/s, starting from a minimum value of 10 m/s.

As for the practical application of the method described above, one might paradoxically say that this is a rare case, in the domain of astrophysical disciplines, in which the abundance of data, and not their scarcity, starts to produce technical problems. The reason is that the inventory of asteroids for which the orbital proper elements are available is today so big, that difficult problems of overlapping between different groupings must be faced. In other words, a simple application of the usual HCM procedures developed in the past to deal with much smaller asteroid samples would be highly problematic now in many respects, especially the phenomenon of *chaining* by which obviously independent families get attached together by a thin chain of asteroids.

For these reasons, when necessary (i.e., in the most populous zones of the asteroid belt) we have adopted in this paper a new, multistep procedure, allowing us to deal at each step with manageable numbers of objects, and developing appropriate procedures to link the results obtained in different steps.

3.1. Step 1: Core families

In order to cope with the challenge posed by the need of analyzing very big samples of objects in the most populous regions of the belt, namely the low-inclination portions of zones 2, 3 and 4, as a first step we look for the cores of the most important families present in these regions.

In doing this, we take into account that small asteroids below one or few km in size are subject to comparatively fast drifts in semi-major axis over time as the consequence of the Yarkovsky effect. Due to this and other effects (including low-energy collisions, see [22]) the cloud of smallest members of a newly born family tends to expand in the proper element space and the family borders tend to “blur” as a function of time. For this reason, we

first removed from our HCM analysis of the most populous regions the small asteroids. In particular, we removed all objects having absolute magnitudes H fainter than a threshold roughly corresponding to the completeness limit in each of the low- I portions of zones 2, 3 and 4. These completeness limits, listed in Table 2, were derived from the cumulative distributions of H ; for the purposes of our analysis, the choice of this threshold value is not critical. Having removed the objects having H fainter than the threshold value, we were left with much more manageable numbers of asteroids, see Table 2.

To these samples, we applied the classical HCM analysis procedures. As a preliminary step we considered in each zone samples of N completely random synthetic objects (N being the number of real objects present in the zone), in order to determine a distance value RL at which these completely random populations could still produce groups of N_{min} members. Following [78], in order to smooth a little the quasi-Random populations to be created in each region, groups of the real population having more than 10% of the total population at RL were removed and substituted by an equal number of fully-random objects. The reason of this preliminary operation is to avoid that in the real population, a few very big and dense groups could be exceedingly dominant and could affect too strongly the distributions of proper elements in the zone, obliging some bins of the $a, e, \sin I$ distribution, from which the QRL population is built (see below), to be over-represented. This could affect the generation of Quasi-Random objects, producing an exceedingly deep (low) Quasi-Random level (QRL) of distance, leading to a too severe criterion for family acceptance. In Zones 3 and 4 a few groups (only one group in Zone 3 and two groups in Zone 4) were first removed and substituted by equal numbers of randomly generated clones. In Zone 2, the RL turned out to be exceedingly high: 160 m/s, corresponding to a distance level at which practically the whole real population merges in a unique group. Removing real objects at that level would have meant to substitute nearly the whole real population by fully-random objects. So this substitution was *not* done in Zone 2.

After that, we ran the classical generations of quasi-random populations. In each zone, the distributions of proper a , e , and $\sin I$ to be mimicked by the quasi-random populations were subdivided in number of bins, as already done in previous papers. In each zone, we determined the minimum level of distance for which groupings of N_{min} objects could be found. We considered as the critical Quasi Random level QRL in each zone the minimum value obtained in ten generations. The QRL values adopted in each zone are also

listed in Table 2.

Then we run the HCM algorithm on the real proper elements. Families were defined as the groups having at least N_{min} members at distance levels 10 m/s lower than QRL , or just reaching QRL , but with a number of members $N \geq N_{min} + 2\sqrt{N_{min}}$. The families obtained in this first step of our procedure include only a small subset, corresponding to the largest objects, of the asteroids present in the low-I portion of zones 2, 3 and 4. For this reason, we call them “core families”: they represent the inner “skeletons” of larger families present in these zones, whose additional members are then identified by the following steps of the procedure (see below Figure 4).

In the case of the high-I portions of zones 2, 3 and 4, and the entire zones 1, 5 and 6, the number of asteroids is not extremely large, and we identified families within them by applying the classical HCM procedure, without multistep procedure. For each family, the members were simply all the objects found to belong to it at the resulting QRL value of the zone. In other words, we did not adopt a case-by-case approach based on looking at the details of the varying numbers of objects found within each group at different distance levels, as was done by [56] to derive memberships among high-inclination families.

3.2. Step 2: Attaching smaller asteroids to core families

The second step of the procedure in the low-I portions of zones 2, 3 and 4 was to *classify* individual asteroids, which had not been used in the core classification, by attaching some of them to the established family cores. For this we used the same QRL distance levels used in the identification of the family cores, but we allowed only single links for attachment, because otherwise we would get chaining, with the result of merging most families together. In other words, in step 2 we attribute to the core families the asteroids having a distance from at least one member (of the same core family) not larger than the QRL critical distance. The result is that the families are extended in the absolute magnitude/size dimension, not much in proper elements space, especially not in proper a (see Figure 4).

Since this procedure has to be used many times (see Section 3.6), it is important to use an efficient algorithm. In principle, if the distance has to be $d < QRL$, we need to compute all distances, e.g., with M proper elements we should compute $M \cdot (M - 1)/2$ distances, then select the ones $< QRL$. The computational load can be reduced by the partition into regions, but

with zones containing $> 100\,000$ asteroids with proper elements it is anyway a time consuming procedure.

This problem has a solution which is well known, although it may not have been used previously in asteroid family classification. Indeed, the problem is similar to the one of comparing the computed ephemerides of a catalog of asteroids to the available observations from a large survey [53, Section 11.3]. We select one particular dimension in the proper elements space, e.g, $\sin I$; we sort the catalog by the values of this proper element. Then, given the value of $\sin I_0$ for a given asteroid, we find the position in the sorted list, then scan the list starting from this position up and down, until the values $\sin I_0 + QRL$ and $\sin I_0 - QRL$, respectively, are exceeded. In this way the computational complexity for the computation of the distances $< QRL$ for M asteroids is of the order of $M \log_2(M)$, instead of M^2 . The large distances are not computed, even less stored in the computer memory.

3.3. Step 3: Hierarchical clustering of intermediate background

As an input to the third step in the low-I portion of zones 2, 3, and 4, we use the “intermediate background” asteroids, defined as the set of all the objects not attributed to any family in steps 1 and 2. The HCM procedure was then applied to these objects, separately in each of the three zones.

The numbers of objects left for step 3 of our analysis were 99399 in zone 2, 94787 in zone 3 and 57422 in zone 4. The corresponding values of N_{min} were 42, 46 and 34, respectively, adopting the same criterion [78] already used for core families. The same HCM procedures were applied, with only a few differences. In computing the critical QRL distance threshold, we did not apply any preliminary removal of large groupings of real objects, because *a priori* we were not afraid to derive in this step of our procedure rather low values of the QRL distance level threshold. The reason is that, dealing with very large numbers of small asteroids, we adopted quite strict criteria for family acceptance, in order to minimize the possible number of false grouping, and to reduce the chance of spurious family merging.

By generating in each of the three zones 10 synthetic quasi-random populations, and looking for the deepest groups of N_{min} objects to determine the QRL , we obtained the following QRL values: 50, 60 and 60 m/s for zones 2, 3 and 4, respectively. Following the same criteria used for core families, step 3 families need to be found as groupings having at least N_{min} members at 40 m/s in zone 2, and 50 m/s in the zones 3 and 4.

On the other hand, as mentioned above, in identifying step 3 families we are forced to be quite conservative. This is due to the known problems of overlapping between different families as a consequence of the intrinsic mobility of their smallest members in the proper element space, as a consequence of (primarily) Yarkovsky as well as of low-energy collisions. For this reason, we adopted a value of 40 m/s for step 3 family identification in all three zones. We also checked that adopting a distance level of 50 m/s in zones 3 and 4 would tend to produce an excessive effect of chaining, which would suggest merging of independent families.

If collisional processes produce overlapping of members of different families in the proper element space, we can reduce this effect on our family classification only at the cost of being somewhat conservative in the identification of family memberships.

Families identified at this step are formed by the population of asteroids left after removing from the proper elements dataset family members identified in steps 1 and 2 of our procedure. There are therefore essentially two possible cases: “step 3” families can either be fully independent, new families having no relation with the families identified previously, or they may be found to overlap “step 1+2” families, and to form “haloes” of smaller objects surrounding some family cores. The procedure adopted to distinguish these two cases is described in the following.

3.4. Step 4: Attaching background asteroids to all families

After adding the step 3 families to the list of core families of step 1, we repeat the procedure of attribution with the same algorithm of step 2. The control value of distance d for attribution to a given family is the same used in the HCM method as QRL for the same family; thus values are actually different for step 1 and step 3 families, even in the same zone.

If a particular asteroid is found to be attributed to more than one family, it can be considered as part of an intersection. A small number of these asteroids with double classification is unavoidable, as a consequence of the statistical nature of the procedure. However, the concentration of multiple intersections between particular families requires some explanation.

One possible explanation is due to the presence of families at the boundaries between high and low inclination regions in zones 3 and 4, where there is no gap between them. Indeed, the classification has been done for proper $\sin I > 0.29$ for the high inclination regions, for $\sin I < 0.3$ for the low inclination. This implies that in the overlap strip $0.29 < \sin I < 0.30$ some

families are found twice, e.g., family 729. In other cases two families are found with intersections in the overlap strip. This is obviously an artifact of our decomposition in zones and needs to be corrected by merging the intersecting families.

3.5. Step 5: Merging halo families with core families

Another case of family intersections, created by step 4, is the “halo families”. This is the case when a new family appears as an extension of an already existing family identified at steps 1 and 2, with intersections near the boundary.

In general for the merging of two families we require as a criterion multiple intersections. Visual inspection of the three planar projections of the intersecting families proper elements is used as a check, and sometimes allows to assess ambiguous cases.

Of the 77 families generated by HCM in step 3, we have considered 34 to be halo. Even 2 core families have been found to be halo of other core families and thus merged. There are of course dubious cases, with too few intersections, as discussed in Section 4.1.1. Still the number of asteroids belonging to intersections decreases sharply, e.g., in the two runs of single-step linkage before and after the step 5 mergers, the number of asteroids with double classification decreased from 1 042 to 29.

Note that the notion of “halo” we are using in this paper does not correspond to other definitions found in the literature, e.g., [7, 11]. The main difference is that we have on purpose set up a procedure to attach “halo families” formed on average by much smaller asteroids, thus we have used the absolute magnitude information to decompose the most densely populated regions. This is consistent with the idea that the smaller asteroids are more affected by the Yarkovsky effect, which is inversely proportional to the diameter: it spreads the proper elements a by the direct secular effect, $e, \sin I$ by the interaction with resonances encountered during the drift in a . This has very important consequences on the family classification precisely because we are using a very large proper elements catalog, which contains a large proportion of newly discovered smaller asteroids.

On the other hand, the other 43 families resulting from step 3 have been left in our classification as independent families, consisting mostly of smaller asteroids. As discussed in Sections 4.2 and 4.3, some of them are quite numerous and statistically very significant, some are not large and may require confirmation, but overall the step 3 families give an important contribution.

3.6. Automatic update

The rapid growth of the proper elements database due to the fast rate of asteroid discoveries and follow-up using modern observing facilities, and to the efficiency of the computation of proper elements, results in any family classification becoming quickly outdated. Thus we devised a procedure for an automatic update of this family classification, to be performed periodically, e.g., two-three times per year.

The procedure consists in repeating the attribution of asteroids to the existing families every time the catalog of synthetic proper elements is updated. What we repeat is actually step 4, thus the lists of core families members (found in step 1) and of members of smaller families (from step 3) are the same, and also the list of mergers (from step 5) is unchanged. Thus newly discovered asteroids, after they have been numbered and have proper elements, automatically are added to the already established families when this is appropriate.

There is a step which we do not think can be automated, and that is step 5: in principle, as the list of asteroids attached to established families grows, the intersection can increase. As an example, with the last update of the proper elements catalog with 18 149 additional records, we have added 3 586 new “step 4” family members. Then the number of intersections, that is members of two families, grows from 29 to 36. In some cases the new intersections support some merge previously not implemented because considered dubious, some open new problems, in any case to add a new merger is a delicate decision which we think should not be automated.

As time goes by, there will be other changes, resulting from the confirmation/contradiction of some of our interpretations as a result of new data: as an example, some small families will be confirmed by the attribution of new members and some will not. At some point we may be able to conclude that some small families are flukes and decide to remove them from the classification, but this is a complicated decision based on assessment of the statistical significance of the lack of increase.

In conclusion we can only promise we will keep an eye on the situation as the classification is updated and try to perform non-automated changes whenever we believe there is enough evidence to justify them. The purpose of both automated and non-automated upgrades of the classification is to maintain the validity of the information made public for many years, without the need for repeating the entire procedure from scratch. This is not only

to save our effort, but also to avoid confusing the users with the need of continuously resetting their perception of the state of the art.

3.7. *Some methodological remarks*

As it should be clear after the description of our adopted techniques, our approach to asteroid family identification is based on procedures which are in some relevant details different with respect to other possible approaches previously adopted by other authors.

In particular, we do not use any systematic family classifications in > 3 dimensional spaces, such as the ones based either upon proper elements and albedo, or proper elements and color indexes, or all three datasets. We make use in our procedure, when dealing with very populous zones, of the absolute magnitude, but only as a way to decompose into steps the HCM procedure, as discussed in Subsection 3.1. Any other available data are used only *a posteriori*, as verification and/or improvement, after a purely dynamical classification has been built. The reasons for this are explained in Table 1: less objects, each with a set of $4 \div 6$ parameters, actually contain less information.

We acknowledge that other approaches can be meaningful and give complementary results. The specific advantage of our datasets and of our methods is in the capability of handling large numbers of small asteroids. This allows to discover, or at least to measure better, different important phenomena. The best example of this is the radical change in perception about the cratering families, which have been more recently discovered and are difficult to appreciate in any approach biased against the use of information provided by small asteroids, as it is the case for classifications which require the availability of physical data (see Section 7).

Moreover, we do not make use of naked eye taxonomy, that is of purely visual perception as the main criterion to compose families. This is not because we disagree on the fact that the human eye is an extremely powerful instrument, but because we want to provide the users with data as little as possible affected by subjective judgments. We have no objection on the use of visual appreciation of our proposed families by the users of our data, as shown by the provision of a dedicated public graphic tool. But this stage of the work needs to be kept separate, after the classification has been computed by objective methods.

4. Results from dynamical classification

4.1. Large families

By “large families” we mean those having, in the classification presented in this paper, > 1000 members. There are 19 such families, and some of their properties are listed in Table 3.

Table 3: Large families with > 1000 members sorted by # tot. The columns give: family, zone, QRL distance (m/s), number of family members classified in steps 1, 3, 2+4 and the total number of members, family boundaries in terms of proper a , e and $\sin I$.

family	zone	QRL	1	3	2+4	tot	a_{min}	a_{max}	e_{min}	e_{max}	sI_{min}	sI_{max}
135	2	70	1141	5001	5286	11428	2.288	2.478	0.134	0.206	0.032	0.059
221	4	100	3060	310	6966	10336	2.950	3.146	0.022	0.133	0.148	0.212
4	2	70	1599	925	5341	7865	2.256	2.482	0.080	0.127	0.100	0.132
15	3	90	2713	0	4132	6845	2.521	2.731	0.117	0.181	0.203	0.256
158	4	100	930	0	4671	5601	2.816	2.985	0.016	0.101	0.029	0.047
20	2	70	86	3546	1126	4758	2.335	2.474	0.145	0.175	0.019	0.033
24	4	100	1208	0	2742	3950	3.062	3.240	0.114	0.192	0.009	0.048
10	4	100	511	50	1841	2402	3.067	3.241	0.100	0.166	0.073	0.105
5	3	90	27	1743	350	2120	2.552	2.610	0.146	0.236	0.054	0.095
847	3	90	176	175	1682	2033	2.713	2.819	0.063	0.083	0.056	0.076
170	3	90	785	0	1245	2030	2.523	2.673	0.067	0.128	0.231	0.269
93	3	90	641	0	1192	1833	2.720	2.816	0.115	0.155	0.147	0.169
145	3	90	327	0	1072	1399	2.573	2.714	0.153	0.181	0.193	0.213
1726	3	90	84	159	1072	1315	2.754	2.818	0.041	0.053	0.066	0.088
2076	2	70	140	528	477	1145	2.254	2.323	0.130	0.153	0.088	0.106
490	4	100	187	46	903	1136	3.143	3.196	0.049	0.079	0.151	0.172
434	1	70	662	0	455	1117	1.883	1.988	0.051	0.097	0.344	0.378
668	3	90	259	0	842	1101	2.744	2.811	0.188	0.204	0.129	0.143
1040	4	100	226	0	870	1096	3.083	3.174	0.176	0.217	0.279	0.298

The possibility of finding families with such large number of members results from our methods, explained in the previous section, to attach to the *core families* either families formed with smaller asteroids or individual asteroids which are suitably close to the core. The main effect of attaching individual asteroids is to extend the family to asteroids with higher H , that is smaller. The main effect of attaching families formed with smaller objects is to extend the families in proper a , which can be understood in terms of the Yarkovsky effect, which generates a drift da/dt inversely proportional to the diameter D .

As the most spectacular increase in the family size, the core family of (5) Astraea is very small, with only 27 members, growing to 2 120 members with steps 2–5: almost all the family members are small, i.e., $H > 14$.

For example: among the largest families, the ones with namesakes (135) Hertha and (4) Vesta are increased significantly in both ways, by attaching families with smaller asteroids on the low a side (the high a side being eaten up, in both cases, by the 3/1 resonance with Jupiter) and by attaching smaller asteroids to the core. In both cases the shape of the family, especially when projected on the proper a, e plane, clearly indicates a complex structure, which would be difficult to model with a single collisional event. There are two different reasons why these families contain so many asteroids: family 135 actually contains the outcome of the disruption of two different parents (see Section 6); family 4 is the product of two or more cratering events, but on the same parent body (see Section 5).

Another spectacular growth with respect to the core family is the one shown by the family of (20) Massalia, which is also due to a cratering event. The region of proper elements space occupied by the family has been significantly expanded by the attribution of the “halo families”, in yellow in Figure 1, on both the low a and the high a side. The shape is somewhat bilobate, and this, as already reported by [73], is due to the 1/2 resonance with Mars which is clearly indicated by chaotic orbits (marked in blue) and also by the obvious line of diffusion along the resonance. The border of the family on the high proper a side is very close to the 3/1 resonance with Jupiter; the instability effects due to this extremely strong resonance may be responsible for the difficulties of attributing to the family a number of objects currently classified as background (marked in black). We can anyway suggest that Massalia can be a significant source of NEA and meteorites through a chaotic path passing through the 3/1. On the contrary, there is no resonance affecting the border on the low a .

The families of (221) Eos and (15) Eunomia have also been increased significantly by our procedure, although the core families were already big. In both cases there is a complex structure, which makes it difficult to properly define the family boundaries as well as to model the collisional event(s).

On the contrary, the family of (158) Koronis was produced by an impact leading to complete disruption of the original parent body, since this family does not show any dominant largest member. Family 158 has no halo: this is due to being sandwiched between the 5/2 resonance and the 7/3 resonance with Jupiter. The same lack of halo occurs for the family of (24) Themis:

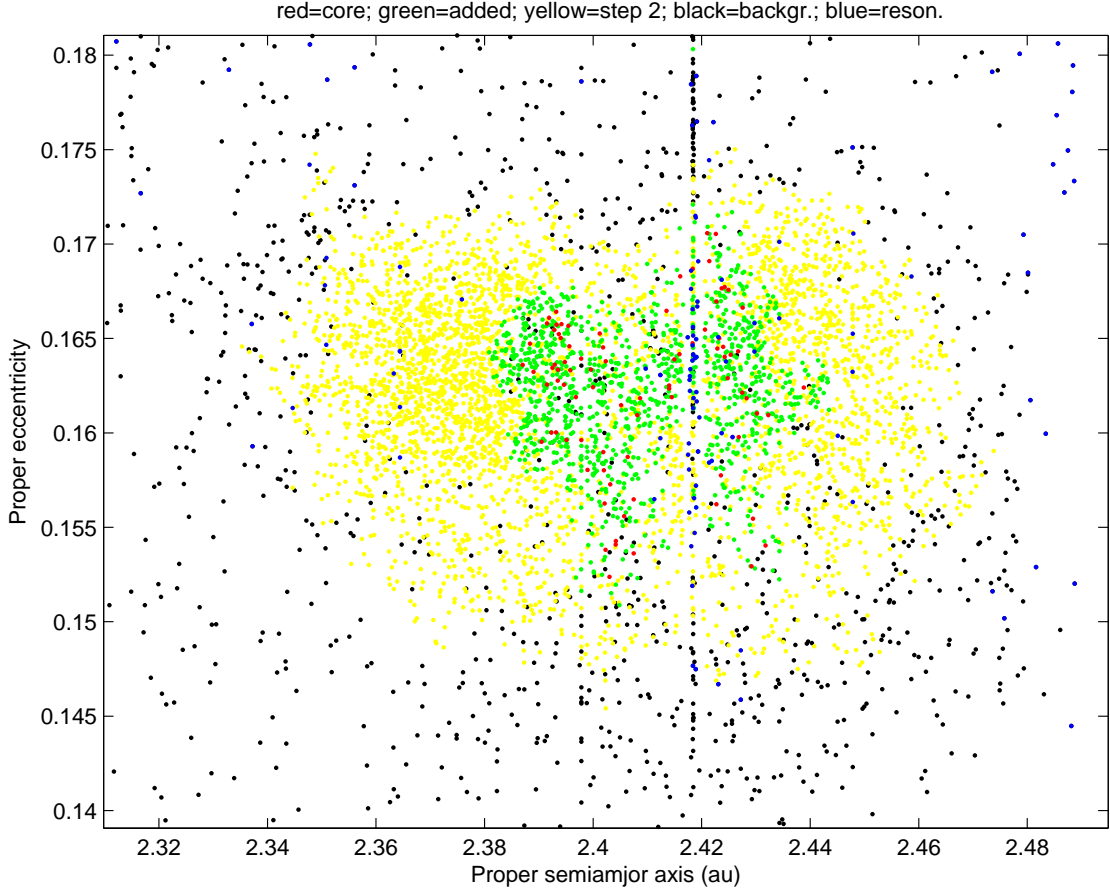


Figure 1: The family of Massalia as it appears in the $a-e$ plane. Red dots indicate objects belonging to the family core. Green dots refer to objects added in step 2 and 4 of the classification procedure, while yellow points refer to objects linked at step 3 (see text). Black dots are not recognized as nominal family members, although some of them might be, while others are background objects. Blue dots are chaotic objects, affected by the 2/1 resonance with Mars.

the 2/1 resonance with Jupiter explains the lack of halo on the high a , the 11/5 resonance has some influence on the low a boundary.

There has been some discussion in the past on the family 490, but as pointed out already in [51] the asteroid (490) Veritas is in a very chaotic orbit resulting in transport along a resonance (later identified as $5J - 2S - 2A$), thus it currently appears to be far away in proper e from the center of the

family, but still can be interpreted as the parent body. A significant fraction of family members are locked in the same resonance, thus giving the strange shape which can be seen in the right low portion of Figure 2.

We note that in our analysis we do not identify a family associated with (8) Flora. A Flora family was found in some previous family searches, but always exhibited a complicated splitting behavior which made the real membership to appear quite uncertain [78]. We find (8) Flora to belong to a step 1 grouping which is present at a distance level of 110 m/s, much higher than the adopted QRL for this zone (70 m/s). This grouping merges with both (4) and (20) at 120 m/s, obviously meaningless. In a rigorous analysis, the QRL cannot be increased arbitrarily just to accept as a family groupings like this one, which do not comply with our criteria.

4.1.1. *Halo problems*

We are not claiming that our method of attaching “halo” families to larger ones can be applied automatically and/or provide an absolute truth. There are necessarily dubious cases, most of which can be handled only by suspending our judgment. Here we are discussing all the cases in which we have found problems, resulting in a total of 29 asteroids belonging to family intersections.

For the family of (15) Eunomia, the 3/1 resonance with Jupiter opens a wide gap on the low a side. The 8/3 resonance appears to control the high a margin, but there is a possible appendix beyond the resonance, which is classified as the family of (173) Ino: we have found four intersections 15–173. A problem would occur if we were to merge the two families, because the proper $a = 2.743$ au of the large asteroid (173) appears incompatible with the dynamical evolution of a fragment from (15). The only solution could be to join to family 15 only the smaller members of 173, but we do not think that such a merge could be considered reliable at the current level of information.

The family of (221) Eos appears to end on the lower a side at the 7/3 resonance with Jupiter, but the high a boundary is less clear. There are two families 507 and 31811 having a small number (six) of intersections with 221: they could be interpreted as a continuation of the family, which would have a more complex shape. However, for the moment we do not think there is enough information to draw this conclusion. Other families in the same region have no intersections and appear separate: the $a, \sin I$ projection of Figure 2 shows well the separation of core families 179, 490, 845, and small families 1189 and 8737, while 283 is seen to be well separate by using an

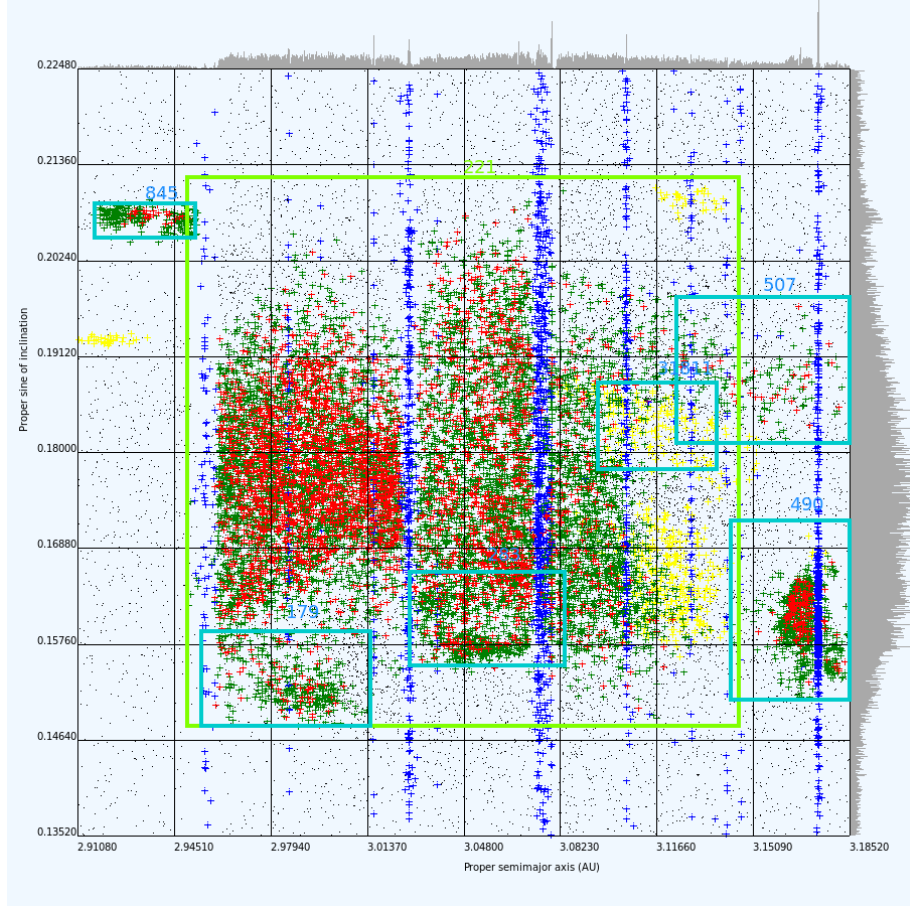


Figure 2: The region surrounding the family of (221) Eos in the proper a , proper $\sin I$ plane. Boxes are used to mark the location of families, some of which overlap family 221 in this projection but not in others, such as a, e . (This figure has been generated with the new AstDyS graphics server.)

$e, \sin I$ projection.

The family of (135) Hertha has few intersections (a total of four) with the small families 6138 (48 members) 6769 (45 members) 7220 (49 members). All three are unlikely to be separate collisional families, but we have not yet merged them with 135 because of too little evidence.

The family of (2076) Levin appears to be limited in the low a side by the 7/2 resonance with Jupiter. It has few (three) intersections with families 298 and 883. 883 is at lower a than the 7/2 resonance, and could be interpreted

as a halo, with lower density due to the ejection of family members by the resonance. Although this is an interesting interpretation which we could agree with, we do not feel this can be considered proven, thus we have not merged 2076–883. As for the family of (298) Baptistina, again the merge with 2076 could be correct, but the family shape would become quite complex, thus we have not implemented it for now. Note that a halo family, with lowest numbered (4375), has been merged with 2076 because of 38 intersection, resulting in a much larger family.

The family of (1040) Klumpkea has an upper bound of the proper $\sin I$ very close to 0.3, that is to the boundary between the moderate inclination and the high inclination zones, to which the HCM has been applied separately. This boundary also corresponds to a sharp drop in the number density of main belt asteroids (only 5.3% have proper $\sin I > 0.3$), which is one reason to separate the HCM procedure because of a very different level of expected background density. The small family of (3667) Anne-Marie has been found in a separate HCM run for high proper $\sin I$, but there are ten intersections with family 1040. The two families could have a common origin, but if we were to merge them the shape of the family would be bizarre, with a sharp drop in number density inside the family. This could have explanation either because of a stability boundary or because of an observational bias boundary. However, this would need to be proven by a very detailed analysis, thus we have not implemented this merge.

The family of (10) Hygiea has two intersections with family 1298, but the two are well separated in the $e, \sin I$ plane, thus they have not been merged.

The family of (1726) Hoffmeister has twenty intersection with the family 14970, formed with much smaller asteroids. Given such an overlap, merging the two families appears fully consistent with our procedure as defined in Section 3. However, the merged family has a strange shape, see Figure 3, in particular with a protuberance in the $\sin I$ direction which would not be easy to reconcile with a standard model of collisional disruption followed by Yarkovsky effect. Moreover, the strange shape already occurs in the core family, that is for the few largest asteroids, and thus should be explained by using perturbations not depending upon the size, that is gravitational ones.

Indeed, by consulting the database of analytic proper elements, it is possible to find that (14970) has a “secular resonance flag” 10, which can be traced to the effect of the secular resonance $g + s - g_6 - s_6$, see also [50, Figure 7]; the same flag is 0 for (1726). Indeed, the value of the “divisor” $g + s - g_6 - s_6$ computed from the synthetic proper elements is 0.1 arcsec/y

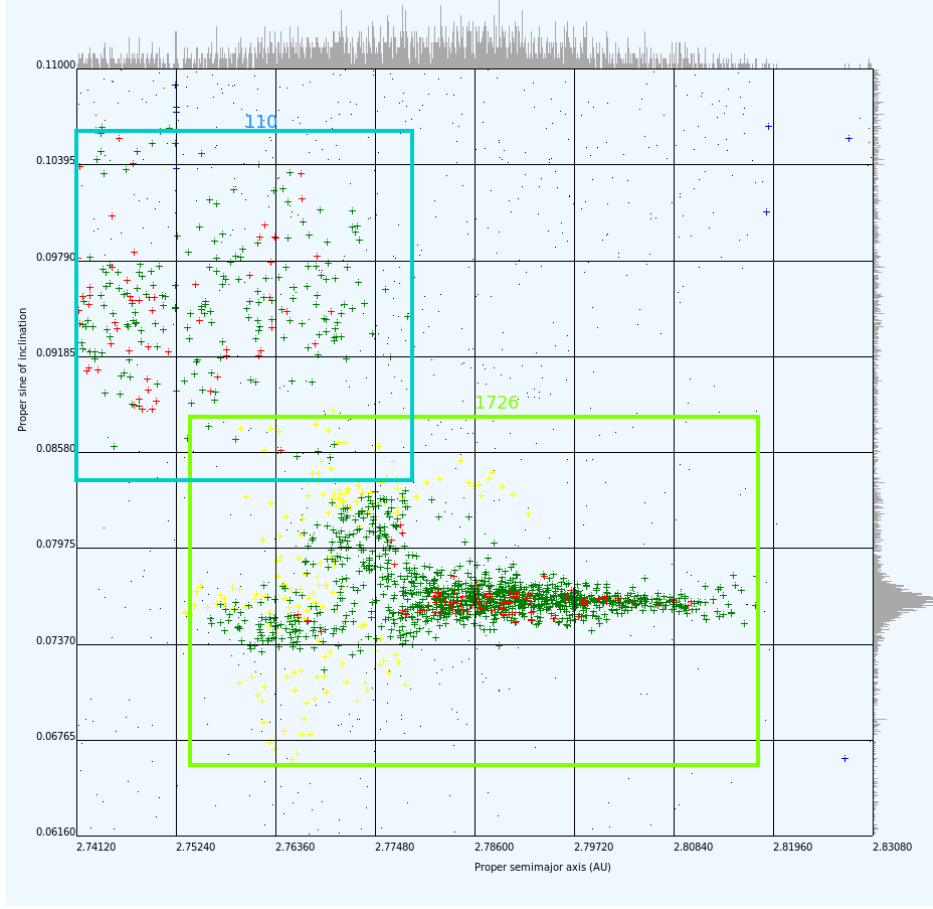


Figure 3: The strange shape of the family of (126) Hoffmeister is shown in the proper $a, \sin I$ projection. Some gravitational perturbations affect the low a portion of the family, including the halo family 14970. The family of (110) Lydia is nearby, but there is no intersection.

for (14970), 0.65 for (1726). On top of that, the proper semimajor axis of (1) Ceres is 2.7671 au, which is right in the range of a of the protuberance in proper $\sin I$, thus it is clear that close approaches and the 1/1 resonance with Ceres can play a significant role in destabilizing the proper elements [21]. We do not have a rigorous answer fully explaining the shape of the family, but we have decided to apply this merger because the number of intersection is significant and the strange shape did not appear as a result of the procedure to enlarge the core family.

From these examples, we can appreciate that it is not possible to define some algorithmic criterion, like a fixed minimum number of intersections, to automatize the process. All of the above cases can be considered as still open problems, to be more reliably solved by acquiring more information.

4.2. Medium families

By “medium families” we mean families we have found to have more than 100 and no more than 1 000 members; the properties of the 41 families in this group are given in Table 4.

Of course the exact boundaries 100 and 1 000 are chosen just for convenience: still the distinction between families based on these boundaries has some meaning. The medium families are such that the amount of data may not be enough for detailed studies of the family structure, including family age determination, size distribution, detection of internal structures and outliers. However, they are unlikely to be statistical flukes, they represent some real phenomenon, but some caution needs to be used in describing it.

In this range of sizes it is necessary to analyze each individual family to find out what can be actually done with the information they provide. As for the ones near the lower boundary for the number of members, they are expected to grow as the family classification procedure is applied automatically by the AstDyS information system to larger and larger proper elements datasets. As a result, they should over a time span of several years grow to the point that more information on the collisional and dynamical evolution process is available. The only other expected outcome is that some of them can become much stronger candidates for merging with big families (e.g., family 507 cited above as a possible appendix to 221). If some others were not to grow at all, even over a timespan in which there has been a significant increase in number density (e.g, 50%) in the region, this would indicate a serious problem in the classification and would need to be investigated.

Note that 14 of the medium families have been generated in step 3, that is they are formed with the intermediate background after removal of step 1 and 2 family members, roughly speaking with “smaller” asteroid.

4.2.1. Some remarkable medium families

The families of (434) Hungaria, (25) Phocaea, (31) Euphrosyne, and (480) Hansa, clustered around the 1 000 members boundary, are the largest high

Table 4: The same as in Table 3 but for medium families with $100 < \# \leq 1000$ members.

family	zone	QRL	1	3	2+4	tot	a_{min}	a_{max}	e_{min}	e_{max}	sI_{min}	sI_{max}
31	4	80	968	0	0	968	3.082	3.225	0.150	0.231	0.431	0.459
25	2	130	944	0	0	944	2.261	2.415	0.160	0.265	0.366	0.425
480	3	140	839	0	0	839	2.538	2.721	0.008	0.101	0.364	0.385
808	3	90	72	166	567	805	2.705	2.805	0.125	0.143	0.080	0.093
3	3	90	45	257	462	764	2.623	2.700	0.228	0.244	0.225	0.239
110	3	90	168	0	561	729	2.696	2.779	0.026	0.061	0.084	0.106
3827	3	90	29	310	332	671	2.705	2.768	0.082	0.096	0.080	0.094
3330	4	100	63	0	537	600	3.123	3.174	0.184	0.212	0.171	0.184
1658	3	90	98	172	288	558	2.546	2.626	0.165	0.185	0.123	0.142
375	4	100	229	0	273	502	3.096	3.241	0.059	0.130	0.264	0.299
293	4	100	38	0	405	443	2.832	2.872	0.119	0.133	0.256	0.264
10955	3	40	0	428	0	428	2.671	2.739	0.005	0.026	0.100	0.113
163	2	40	0	392	0	392	2.332	2.374	0.200	0.218	0.081	0.098
569	3	40	0	389	0	389	2.623	2.693	0.169	0.183	0.035	0.045
1128	3	40	0	389	0	389	2.754	2.817	0.045	0.053	0.008	0.018
283	4	100	49	0	320	369	3.029	3.084	0.107	0.124	0.155	0.166
179	4	100	60	0	306	366	2.955	3.015	0.053	0.080	0.148	0.159
5026	2	40	0	346	0	346	2.368	2.415	0.200	0.217	0.082	0.096
3815	3	40	0	283	0	283	2.563	2.583	0.138	0.143	0.145	0.164
1911	6	60	280	0	0	280	3.964	3.967	0.159	0.222	0.041	0.055
845	4	100	29	0	224	253	2.917	2.953	0.029	0.041	0.205	0.209
194	3	140	235	0	17	252	2.522	2.691	0.154	0.196	0.293	0.315
396	3	40	0	242	0	242	2.731	2.750	0.164	0.170	0.057	0.062
12739	3	40	0	240	0	240	2.682	2.746	0.047	0.060	0.031	0.041
778	4	100	29	0	200	229	3.158	3.191	0.240	0.261	0.243	0.253
945	3	140	219	0	0	219	2.599	2.659	0.190	0.289	0.506	0.521
1303	4	80	179	0	0	179	3.193	3.236	0.106	0.144	0.310	0.337
752	2	70	27	90	41	158	2.421	2.484	0.084	0.095	0.085	0.092
18466	3	40	0	155	0	155	2.763	2.804	0.171	0.182	0.229	0.236
173	3	90	29	0	125	154	2.708	2.770	0.159	0.180	0.229	0.239
606	3	40	0	153	0	153	2.573	2.594	0.179	0.183	0.166	0.168
507	4	100	38	0	111	149	3.124	3.207	0.049	0.075	0.181	0.198
13314	3	40	0	146	0	146	2.756	2.801	0.170	0.183	0.069	0.078
302	2	40	0	143	0	143	2.385	2.418	0.104	0.111	0.056	0.060
1298	4	100	69	0	74	143	3.088	3.220	0.105	0.123	0.104	0.123
87	5	120	119	0	20	139	3.459	3.564	0.046	0.073	0.162	0.179
883	2	70	46	0	86	132	2.213	2.259	0.140	0.151	0.092	0.102
298	2	70	43	0	88	131	2.261	2.288	0.146	0.161	0.100	0.114
19466	3	40	0	125	0	125	2.724	2.761	0.007	0.020	0.103	0.111
1547	3	40	0	108	0	108	2.641	2.650	0.267	0.270	0.211	0.212
1338	2	70	38	0	66	104	2.259	2.302	0.119	0.130	0.075	0.091

inclination families, one for each semimajor axis zone¹⁰. Given the lower number density for proper $\sin I > 0.3$ the numbers of members are remarkably high, and suggest that it may be possible to obtain information on the collisional processes which can occur at higher relative velocities. These four have been known for some time [54, 56, 31, 9], but now it has become possible to investigate their structure.

For family 480 the proper e can be very small: this results in a difficulty in computing proper elements (especially e and the proper frequency g) due to "paradoxical libration". We will try to fix our algorithm to avoid this, but we have checked that it has no influence on the family membership, because $e = 0$ is not a boundary.

The largest family in zone 5 is the one of (87) Sylvia, which is well defined, but with a big central gap corresponding to the resonance 9/5 with Jupiter. This family has in (87) such a dominant largest member that it can be understood as a cratering event, even if we do not have a good idea of how many fragments have been removed by the 9/5 and other resonances¹¹.

The largest family in zone 6, that is among the Hilda asteroid locked in the 3/2 resonance with Jupiter, is the one of (1911) Schubart. By the way, proper elements for Hildas, taking into account the resonance, have been computed by [66], but we have used as input to the HCM (step 1) procedure the synthetic proper elements computed without taking into account the resonance, thus averaging over the libration in the critical argument. This is due to the need to use the largest dataset of proper elements, and is a legitimate approximation because the contribution of even the maximum libration amplitude to the metrics similar to d , to be used for resonant asteroids, is more than an order of magnitude smaller than the one due to eccentricity.

4.3. *Small families*

The families we rate as "small" are those in the range between 30 and 100 members; data for 43 such families are in Table 5.

Note that 29 out 41 of these "small families" have been added in step 3, and have not been absorbed as halo families.

¹⁰Hungaria is included in our list of large families. Zones 5 and 6 have essentially no stable high inclination asteroids

¹¹This family is interesting also because (87) Sylvia has been the first recognized triple asteroid system, formed by a large primary and two small satellites [38]

Table 5: The same as in Table 3 but for small families with $30 < \# \leq 100$ members.

family	zone	QRL	1	3	2+4	tot	a_{min}	a_{max}	e_{min}	e_{max}	sI_{min}	sI_{max}
96	4	100	38	0	62	100	3.036	3.070	0.176	0.189	0.280	0.289
148	3	140	95	0	0	95	2.712	2.812	0.116	0.150	0.420	0.430
410	3	90	55	0	38	93	2.713	2.761	0.238	0.265	0.146	0.160
2782	3	90	21	0	71	92	2.657	2.701	0.185	0.197	0.061	0.072
31811	4	40	0	89	1	90	3.096	3.138	0.060	0.075	0.178	0.188
3110	3	40	0	86	0	86	2.554	2.592	0.134	0.145	0.049	0.065
18405	4	40	0	85	0	85	2.832	2.858	0.103	0.110	0.158	0.162
7744	3	40	0	78	0	78	2.635	2.670	0.069	0.075	0.042	0.049
1118	4	100	47	0	30	77	3.145	3.246	0.035	0.059	0.252	0.266
729	3	90	73	0	2	75	2.720	2.814	0.110	0.144	0.294	0.305
17392	3	40	0	75	0	75	2.645	2.679	0.059	0.070	0.036	0.042
4945	3	40	0	71	0	71	2.570	2.596	0.235	0.244	0.087	0.096
63	2	40	0	70	0	70	2.383	2.401	0.118	0.127	0.107	0.118
16286	4	40	0	68	0	68	2.846	2.879	0.038	0.047	0.102	0.111
1222	3	140	68	0	0	68	2.769	2.803	0.068	0.113	0.350	0.359
11882	3	40	0	66	0	66	2.683	2.708	0.059	0.066	0.031	0.040
21344	3	40	0	62	0	62	2.709	2.741	0.150	0.159	0.046	0.050
3489	2	40	0	57	0	57	2.390	2.413	0.090	0.096	0.103	0.109
6124	6	60	57	0	0	57	3.966	3.967	0.186	0.212	0.146	0.159
29841	3	40	0	53	0	53	2.639	2.668	0.052	0.059	0.033	0.040
25315	3	40	0	53	0	53	2.575	2.596	0.243	0.251	0.090	0.096
3460	4	100	28	0	24	52	3.159	3.218	0.187	0.209	0.016	0.028
2967	4	80	52	0	0	52	3.150	3.224	0.092	0.124	0.295	0.303
8905	3	40	0	49	0	49	2.599	2.620	0.181	0.190	0.084	0.091
7220	2	40	0	48	1	49	2.418	2.424	0.183	0.195	0.026	0.036
3811	3	40	0	49	0	49	2.547	2.579	0.101	0.110	0.185	0.190
6138	2	40	0	46	2	48	2.343	2.357	0.204	0.215	0.039	0.045
32418	3	40	0	48	0	48	2.763	2.795	0.255	0.261	0.152	0.156
53546	3	40	0	47	0	47	2.709	2.735	0.170	0.174	0.247	0.251
43176	4	40	0	47	0	47	3.109	3.152	0.065	0.074	0.174	0.183
618	4	40	0	46	0	46	3.177	3.200	0.056	0.059	0.270	0.277
28804	3	40	0	46	0	46	2.589	2.601	0.146	0.156	0.063	0.070
7468	4	40	0	45	0	45	3.031	3.075	0.087	0.091	0.060	0.061
6769	2	40	0	44	1	45	2.398	2.431	0.148	0.155	0.051	0.056
159	4	40	0	45	0	45	3.091	3.131	0.111	0.117	0.084	0.090
5651	4	100	20	0	22	42	3.097	3.166	0.112	0.128	0.231	0.241
21885	4	40	0	42	0	42	3.079	3.112	0.026	0.035	0.184	0.188
780	4	80	41	0	0	41	3.085	3.129	0.060	0.074	0.310	0.314
22241	4	40	0	40	0	40	3.082	3.096	0.126	0.133	0.087	0.096
2	3	140	38	0	0	38	2.756	2.791	0.254	0.283	0.531	0.550
1189	4	40	0	38	0	38	2.904	2.936	0.071	0.075	0.192	0.194
8737	4	40	0	37	0	37	3.116	3.141	0.112	0.121	0.207	0.211
3438	4	100	20	0	14	34	3.036	3.067	0.176	0.186	0.249	0.255

The families in this category have been selected on the basis of statistical tests, which indicates they are unlikely to be statistical flukes. Nevertheless, most of them need some confirmation, which may not be available due to small number statistics. Thus most of these proposed families are there waiting for confirmation, which may require waiting for more observational data.

The possible outcomes of this process, which requires a few years, are as follows: (i) the family is confirmed by growing in membership, as a result of automatic attachment of new numbered asteroids; (ii) the family is confirmed by the use of physical observations and/or modeling; (iii) the family grows and become attached as halo to a larger family; (iv) the family is found not to exist as collisional family because it does not increase with new smaller members; (v) the family is found not to exist as collisional family because of enough physical observations showing incompatible composition.

In other words, the tables published in this paper are to be used as reference and compared, at each enlargement of the proper elements database, with the automatically generated new table based on more asteroids, to see which family is growing¹².

However, there are cases in which some of these outcomes appear more likely, and we shall comment on a few of them.

4.3.1. *Small but convincing families*

The family of (729) *Watsonia* has been obtained by joining a high I and a low I families. We are convinced that it is robust, but it may grow unevenly in the high I and in the low I portions because of the drop in number density, whatever its cause. Other results on this family are given in Section 6.

The family of (2) *Pallas* has only 38 members, but it is separated, in proper a , by a gap from the tiny family 14916. The gap can be explained as the effect of resonances, the main one being the $3J - 1S - 1A$ 3-body resonance. Given the large escape velocity from *Pallas*, families 2 and 14916 together would be within the range of proper elements obtained from the ejection of the fragments following the cratering event. That is, the distribution of proper elements could be due to the initial spread of velocities rather

¹²The need for fixed lists to be cited over many years as a comparison with respect to the “current” number of members explains why these tables need to be published in printed form. The current family table can be downloaded from AstDyS at <http://hamilton.dm.unipi.it/~astdys2/propsynth/numb.famtab>

than to Yarkovsky, implying that they would contain no evidence for the age of the family. However, we have not merged these two families because this argument, although we believe it is correct, arises from a model, not from the data as such.

4.3.2. Small families which could belong to the halo of large families

On top of the small families already listed in Subsection 4.1.1, which are considered as possible halos because of intersections, there are other cases in which small families are very close to large ones, and thus could become candidates for merging as the size of the proper elements catalog increases.

To identify these cases we have used for each family the “box” having sides corresponding to the ranges in proper $a, e, \sin I$ listed in Tables 3–6, and we analyzed all the overlaps between them. The parameter we use as an alert of proximity between two families is the ratio between the volume of the intersection to the volume of the box for the smaller family. If this ratio is 100% then the smaller family is fully included within the box of the larger one; we have found 12 such cases. We found another 17 cases with ratio $> 20\%$. By removing the cases with intersections, or anyway already discussed in Sections 4.1 and 4.2, we are left with 17 cases to be analyzed.

One case of these overlapping-box families is about two medium families, namely family 10955 (with 428 members the largest of the step 3 families) and family 19466, which has 40% of its box contained in the box of 10955. The possibility of future merger cannot be excluded.

Among small/tiny families with boxes overlapping larger ones, we have found 10 cases we think could evolve into mergers with more data: 4-3489, 5-8905, 5-28804, 10-159, 10-22241, 221-31811, 221-41386, 375-2967, 480-34052, 1040-29185.

In two of the above cases there is already, from the first automatic update, supporting evidence: of the 7 new intersections, one is 10-22241 and another is 375-2967. We are not claiming this is enough evidence for a merge, but it shows how the automatic upgrade of the classification works.

In three cases we do not think there could be future mergers: 15-145, 15-53546, 221-21885. In another three cases the situation is too complicated to allow us to make any guess; 24-3460, 31-895, 4-63.

The conclusion from this discussion is clear: a significant fraction of the small families of Table 5, and few from Table 6, could be in the future included in the halo of larger families. Others could be confirmed as independent families, and some could have to be dismissed.

4.4. Tiny families

The “tiny families” are the ones with < 30 members; of course their number is critically dependent upon the caution with which the small clusters have been accepted as proposed families. In Table 6 we are presenting a set of 25 such families.

Table 6: The same as in Table 3 but for tiny families with < 30 members.

family	zone	QRL	1	3	2+4	tot	a_{min}	a_{max}	e_{min}	e_{max}	sI_{min}	sI_{max}
3667	4	80	25	0	3	28	3.087	3.125	0.184	0.197	0.294	0.301
895	4	80	25	0	0	25	3.202	3.225	0.169	0.183	0.438	0.445
909	5	120	23	0	1	24	3.524	3.568	0.043	0.058	0.306	0.309
29185	4	80	23	0	0	23	3.087	3.116	0.196	0.209	0.295	0.304
4203	3	140	22	0	0	22	2.590	2.648	0.124	0.135	0.473	0.486
34052	3	140	21	0	0	21	2.641	2.687	0.073	0.087	0.368	0.377
5931	4	80	19	0	0	19	3.174	3.215	0.160	0.172	0.302	0.313
22805	4	80	17	0	0	17	3.136	3.159	0.165	0.175	0.301	0.308
1101	4	80	17	0	0	17	3.229	3.251	0.030	0.037	0.363	0.375
10369	3	140	17	0	0	17	2.551	2.609	0.105	0.118	0.470	0.482
3025	4	80	16	0	0	16	3.192	3.221	0.059	0.066	0.368	0.378
14916	3	140	16	0	0	16	2.710	2.761	0.270	0.282	0.537	0.542
3561	6	60	15	0	0	15	3.962	3.962	0.127	0.133	0.149	0.156
45637	5	120	14	0	1	15	3.344	3.369	0.103	0.123	0.142	0.151
260	5	120	11	0	4	15	3.410	3.464	0.081	0.088	0.100	0.108
58892	4	80	14	0	0	14	3.121	3.154	0.153	0.162	0.300	0.308
6355	4	80	13	0	0	13	3.188	3.217	0.088	0.097	0.374	0.378
40134	3	140	13	0	0	13	2.715	2.744	0.223	0.235	0.429	0.438
116763	3	140	13	0	0	13	2.621	2.652	0.236	0.246	0.463	0.468
10654	4	80	13	0	0	13	3.207	3.244	0.051	0.056	0.368	0.374
10000	3	140	13	0	0	13	2.562	2.623	0.260	0.273	0.316	0.325
7605	4	80	12	0	0	12	3.144	3.153	0.065	0.073	0.447	0.453
69559	4	80	12	0	0	12	3.202	3.219	0.196	0.201	0.299	0.305
20494	3	140	12	0	0	12	2.653	2.690	0.119	0.132	0.470	0.480
23255	3	140	10	0	0	10	2.655	2.688	0.095	0.113	0.460	0.469

Given the cautionary statements we have given about the “small families”, what is the value of the “tiny” ones? To understand this, it is useful to check the zones/regions where these have been found: 3 tiny families belong to zone 5, 1 to zone 6, 12 to zone 4 high inclination, 9 to zone 3 high inclination. Indeed, groupings with such small numbers can be statistically significant only in the regions where the number density is very low.

These families satisfy the requirements to be considered statistically reliable according to the standard HCM procedure adopted in the above zones. It should be noted that, due to the low total number of objects present in these regions, the adopted minimum number N_{min} of required members to form a family turns out to be fairly low, and its choice can be more important with respect to more densely populated regions. In the case of high-I asteroids, [56] included in their analysis a large number of unnumbered objects which we are not considering in the present paper. The nominal application of the HCM procedure leads to accept the groups listed in Table 6 as families, but it is clear that their reliability will have to be tested in the future when larger numbers will be available in these zones.

Thus, each one of these groups is only a proposed family, in need of confirmation. There is an important difference with most of the small families listed in Table 5: there are two reasons why the number densities are much lower in these regions, one being the lower number density of actual asteroids, for the same diameters; the other being the presence of strong observational biases which favor discovering only objects of comparatively large size. In the case of the high inclination asteroids the observational bias is due to most asteroid surveys looking more often near the ecliptic, because there more asteroids can be found with the same observational effort. For the more distant asteroids the apparent magnitude for the same diameter is fainter because of both larger distance and lower average albedo.

If a family is small because of observational bias, it grows very slowly in membership unless the observational bias is removed, which means more telescope time is allocated for asteroid search/recovery at high ecliptic latitude and more powerful instruments are devoted to find more distant/dark asteroids. Unfortunately, there is no way to be sure that these resources will be available, thus some “tiny” families may remain tiny for quite some time. In conclusion, the list of Table 6 is like a bet to be adjudicated in a comparatively distant future. we can already confirm that many of these tiny families are slowly increasing in numbers. As already mentioned, while this paper was being completed, the proper elements catalog has already been updated, the automatic step 4 was completed, resulting in a new classification with a 4% increase in family membership. In this upgrade 14 out of 25 tiny families have increased their membership, although in most cases by just $1 \div 2$.

5. Use of absolute magnitude data

For most asteroids a direct measurement of the size is not available, whereas all the asteroids with an accurate orbit have some estimated value of absolute magnitude. To convert absolute magnitude data into diameter D , we need the albedo, thus D can be accurately estimated only for the objects for which physical observations, such as WISE data or polarimetric data, are available. However, it is known that families are generally found to be quite homogeneous in terms of albedo and spectral reflectance properties [14]. Therefore, by assuming an average albedo value to be assigned to all the members of a given family, we can derive the size of each object from its value of absolute magnitude. This requires that a family has one or more members with a known albedo, and we have reasons to exclude that they are interlopers.

The main applications of the statistical information on diameter D of family members are three: estimation of the total volume of the family, of the age of a collisional family, and of the size distribution.

5.1. The volume of the families

In case of a total fragmentation, the total volume of a collisional family can be used to give a lower bound for the size of the parent body. For cratering, the volume computed without considering the parent body can be used to constrain from below the size of the corresponding crater. In case of dubious origin, the total volume can be used to discard some possible sources if they are too small.

As an example let us choose the very large family of (4) Vesta. The albedo of Vesta has been measured as 0.423 [70], but more recently an albedo of 0.37 has been reported by [65], while a value around 0.30 is found by the most recent polarimetric investigations [16]¹³. Before computing the volume of fragments we need to remove the biggest interlopers, because they could seriously contaminate the result: asteroids (556) and (1145) are found to be interlopers because they are too big for their position with respect to the parent body, as discussed in the next subsection. If we assume albedo 0.423 for all family 4 members, we can compute the volume of all the family members at 32 500 km³. The volume would be 54 500 with albedo 0.3, thus

¹³By using WISE albedos, it can be shown that the most frequent albedos for members of family 4 are in the range spanning these measurements, see Figure 16

the volume of the known family can be estimated to be in this range. On Vesta there are two very large craters, Rheasilvia and Veneneia, with volumes of > 1 million km^3 . Thus it is possible to find some source crater.

Another example of cratering on a large asteroid is the family of (10) Hygiea. After removing Hygiea and interlopers with $D > 40$ km which should be too large for being ejected from a crater, and assuming a common albedo equal to the IRAS measure for (10), namely 0.072, we get a total volume of the family as $550\,000 \text{ km}^3$. This implies on the surface of (10) Hygiea there should be a crater with a volume at least as large as for Rheasilvia. Still the known family corresponds to only 1.3% of the volume of (10) Hygiea.

5.2. Family Ages

The computation of family ages is a high priority goal. As a matter of principle it can be achieved by using V-shape plots such as Figure 4, for the families old enough to have Yarkovsky effect dominating the spread of proper a . The basic procedure is as follows: as in the previous section by assuming a common geometric albedo p_v , from the absolute magnitudes H we can compute¹⁴ the diameters D . The Yarkovsky secular effect in proper a is $da/dt = c \cos(\phi)/D$, with ϕ the obliquity (angle of the spin axis with the normal to the orbit plane), and c a calibration depending upon density, thermal conductivity and spin rate. As a matter of fact c is weakly dependent upon D , but this cannot be handled by a general formula since the dependence of c from thermal conductivity is highly nonlinear [71, Figure 1]. Thus, as shown in [19, Appendix A], the power law expressing the dependence of c upon D changes from case to case. For cases in which we have poor information on the thermal properties (almost all cases) we are forced to use just the $1/D$ dependency.

Then in a plot showing proper a vs. $1/D$ for asteroids formed by the same collisional event we get straight lines for the same ϕ . We can try to fit to the data two straight lines representing the prograde spin and retrograde spin states ($\phi = 0^\circ$ and $\phi = 180^\circ$). The slopes of these lines contain information on the family age. Note that this procedure can give accurate results only if the family members cover a sufficient interval of D , which now is true for a large set of dynamical families thanks to the inclusion of many smaller objects (represented by green and yellow points in all the figures).

¹⁴ $D = 1\,329 \times 10^{-H/5} \times 1/\sqrt{p_v}$

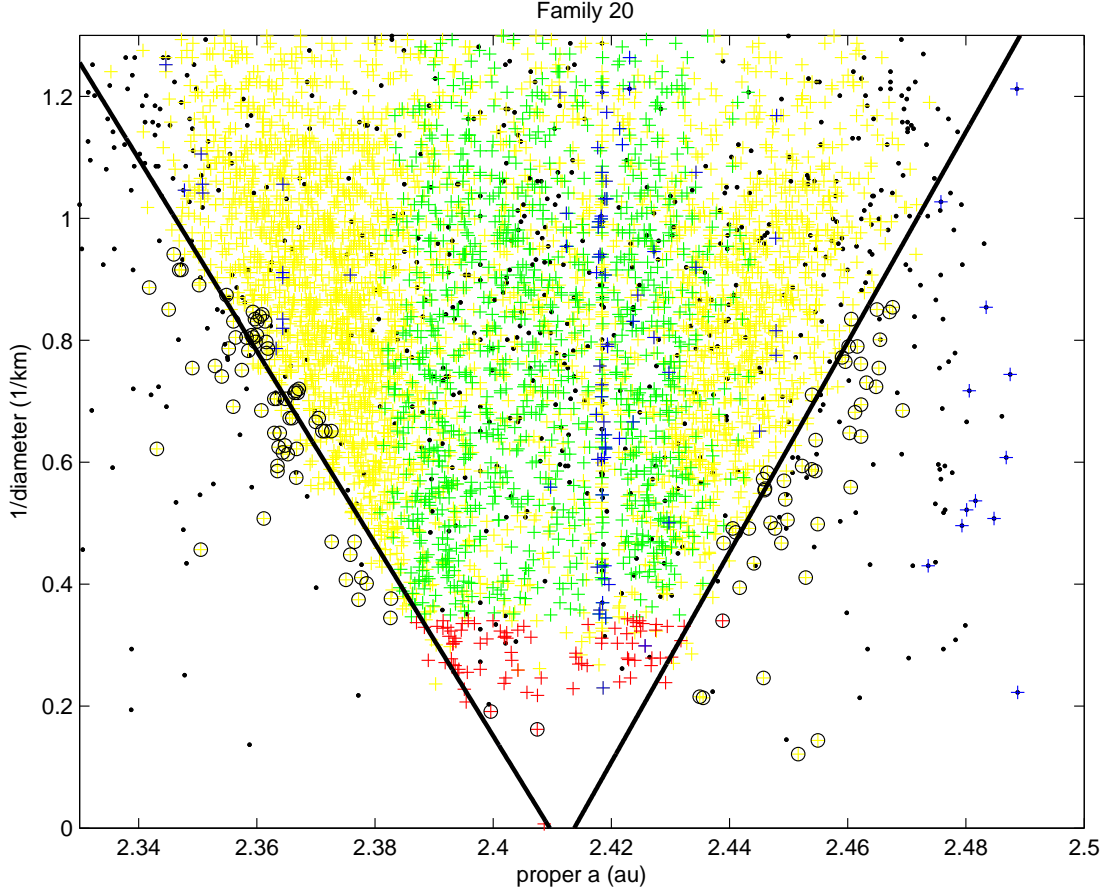


Figure 4: V-shape of the family 20 in the proper a vs. $1/D$ plane. The black lines are the best fit on the two sides; the black circles indicate the outliers.

As an example in Figure 4 we show two such lines for the Massalia family on both the low proper a and the high proper a side, that is representing the above mentioned retrograde and direct spin rotation state, respectively. This is what we call *V-shape*, which has to be analyzed to obtain an age estimate.

A method of age computation based on the V-shape has already been used to compute the age of the Hungaria family [54, Figure 20]. In principle, a similar method could be applied to all the large (and several medium) families. However, a procedure capable of handling a number of cases with different properties needs to be more robust, taking into account the following problems.

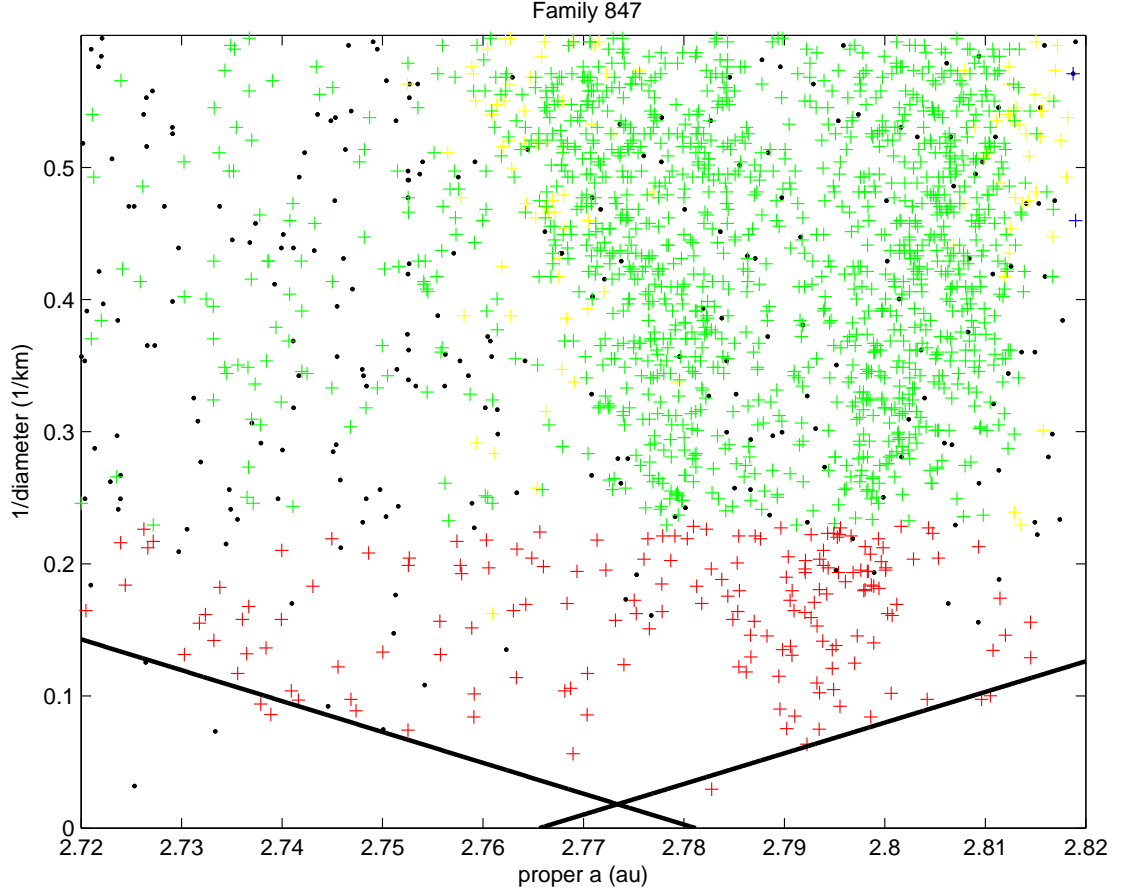


Figure 5: V-shape of the family 847 in the proper a vs. $1/D$ plane. The most striking feature is the presence of much denser substructure, which exhibits its own V-shape, shown in Figure 9.

- The method assumes all the family members have the same age, that is, it assumes the coincidence of the dynamical family with the collisional family. If this is not the case, the procedure is much more complicated: see Figure 5, which shows two superimposed V-shapes (the outer one is marked with a fit for the boundary) for the Agnia family, indicating at least two collisional events with different ages. Thus a careful examination of the family shape, not just in the $a, 1/D$ plot but also in all projections, is required to first decide on the minimum number of collisional events generating each dynamical family. If substructures

are found, with shape such that interpretation as the outcome of a separate collisional event is possible, their ages may in some cases be computed.

- To compute the age we use the inverse slope $\Delta a(D)/(1/D)$, with D in km, of one of the two lines forming the V-shape, which is the same as the value of Δa for an hypothetical asteroid with $D = 1$ km along the same line. This is divided by the value of the secular drift da/dt for the same hypothetical asteroid, giving the estimated age. However, the number of main belt asteroids for which we have a measured value of secular da/dt is zero. There are > 20 Near Earth Asteroids for which the Yarkovsky drift has been reliably measured (with $S/N > 3$) from the orbit determination [24, Table 2]. It is indeed possible to estimate the calibration c , thus the expected value of da/dt for an asteroid with a given D, a, e, ϕ , by scaling the result for another asteroid, in practice a Near Earth one, with different D, a, e, ϕ . However, to derive a suitable error model for this scaling is very complicated; see e.g. [25] for a full fledged Monte Carlo computation.
- The data points $(1/D, a)$ in the V-shape are not to be taken as exact measurements. The proper a coordinate is quite accurate, with the chaotic diffusion due to asteroid-asteroid interaction below 0.001 au [21], and anyway below the Yarkovsky secular contribution for $D < 19$ km; the error in the proper elements computation (with the synthetic method) gives an even smaller contribution. To the contrary, the value of D is quite inaccurate. Thus a point in the $1/D, a$ plane has to be considered as measurement with a significant error, especially in $1/D$, and the V-shape needs to be determined by a least squares fit, allowing also for outlier rejection.
- Most families are bounded, on the low- a side and/or on the high- a side, by resonances strong enough to eject the family members reaching the resonant value of a by Yarkovsky, into unstable orbits (at least most of them). Thus the V-shape is cut by vertical lines at the resonant values of proper a . The computation of Δa must therefore be done at values of $1/D$ below the intersection of one of the slanted sides of the V and the vertical line at the resonant value of a . For several families this significantly restricts the range of $1/D$ for which the V-shape can be measured.

- The dynamical families always contain interlopers, which should be few in number, but not necessarily representing a small fraction of the mass (the size distribution of the background asteroids is less steep). The removal of large interlopers is necessary not to spoil the computation of the slopes, and also of centers of mass.

As a consequence of the above arguments, we have decided to develop a new method, which is more objective than the previous one we have used, because the slope of the two sides of the V-shape is computed in a fully automated way as a least squares fit, with equally automatic outlier rejection. The following points explain the main features of this new method.

1. For each family we set up the minimum and maximum values of the proper semimajor axis and of the diameter for the fit. We may use different values for the inner and the outer side of the V, taking into account the possibility that they measure different ages. Note this is the only “manual” intervention.
2. We divide the $1/D$ -axis into bins, which are created in such a way to contain about the same number of objects. Hence:
 - the bins, which correspond to small values of $1/D$ are bigger than the ones which correspond to large values of $1/D$;
 - the inner side and the outer side of the family may have different bins.
3. We implement a linear regression for both sides. The method is iterative. For each iteration we calculate the residuals, the outliers and the kurtosis of the distribution of residuals. A point is an outlier if its residual is greater than 3σ . Then we remove the outliers and repeat the linear regression. Note that the outliers for the fit can be interlopers in the family, but also family members with low accuracy diameters.
4. We say that the method converges if the kurtosis of the residuals is 3 ± 0.3 or if there exists an iteration without additional outliers.
5. The two straight lines on the sides of the V-shape are computed independently, thus they do not need to cross in a point on the horizontal axis. We compute the *V-base* as the difference in the a coordinate of the intersection with the a axis of the outer side and of the inner side. This quantity has an interpretation we shall discuss in Section 5.2.7.

Table 7: Results of the fit for the low a (IN) and high a (OUT) sides for each considered family: number of iterations, minimum diameter D (in km) used in the fit, number of bins, number of outliers, value of the kurtosis and standard deviation of the residuals in $1/D$, and the value of the inverse of the slope (in au).

family		# iter.	min. D fit	# bins	# outliers	kurtosis	RMS(resid)	1/slope
20	IN	7	1.0	20	69	2.98	0.0371	-0.063
20	OUT	8	1.1	12	48	3.12	0.0118	0.058
4	IN	2	2.0	23	9	3.27	0.0364	-0.267
4	OUT	2	3.6	6	2	1.49	0.0060	0.537
15	IN	2	5.0	11	1	3.22	0.0021	-0.659
15	OUT	2	6.7	16	1	2.84	0.0027	0.502
158	IN	2	10.0	9	2	3.03	0.0013	-0.442
158	OUT	2	5.9	10	0	1.99	0.0024	0.606
847	IN	2	6.7	5	0	1.25	0.0004	-0.428
847	OUT	2	9.1	7	0	1.65	0.0003	0.431
3395	IN	10	1.8	7	43	2.92	0.0041	-0.045
3395	OUT	9	2.2	8	49	3.20	0.0053	0.045

Table 8: V-base and center of the V-base.

family	V-base	center of V-base
20	0.004	2.4117
4	-0.025	
15	0.009	2.6389
158	0.021	2.8774
847	-0.016	2.7734
3395	-0.008	2.7900

Let us emphasize that our main goal in this paper is to introduce methods which are objective and take as thoroughly as possible into account all the problems described above. Also we pay a special attention to the computation of quantities like Δa and the slopes, used to estimate the family age, but the determination of the ages themselves, involving the complicated calibra-

tion of the Yarkovsky effect, is performed only as an example, to demonstrate what we believe should be a rigorous procedure.

5.2.1. *Massalia*

One of the best examples of dynamical family for which the computation of a single age for a crater is possible is the one of (20) Massalia, see Figure 1. Massalia has an albedo 0.21 measured by IRAS¹⁵.

The two slopes of the inner and outer side of V-shape (Figure 4) have of course opposite sign, with the absolute value different by 9%, see Table 7. Taking into account that there is some dependence of the calibration on a , this indicates an accurate determination of the slope. This is due to the fact that the fit can be pushed down to comparatively small diameters, around 1 km, because the family is not cut by a resonance on the low a side, and is affected by the 3/1 resonance with Jupiter on the high a side, but only for $D < 1$ km. The V-base is small and positive (Table 8).

The internal structure of family 20 is further discussed in Section 7.1.

5.2.2. *Vesta*

For the V-shape and slope fit (Figure 6) we have used as common albedo 0.423. The Vesta family has a complex structure, which is discussed in Section 7.2: thus the presence of two different slopes on the two sides (Table 7) indicates that we are measuring the age of two different collisional events, the one forming the high a boundary of the family being older. In theory two additional slopes exist, for the outer boundary of the inner subfamily and for the inner boundary of the outer family, but they cannot be measured because of the significant overlap of the two substructures. Thus the negative V-base appearing in the figure has no meaning.

The family is cut sharply by the 3/1 resonance with Jupiter on the high a side and somewhat less affected by the 7/2 on the low a side. As a result the outer side slope fit is somewhat less robust, because the range of sizes is not as large. The fact that the slope is lower (the age is older) on the high a side is a reliable conclusion, but the ratio is not estimated accurately. The calibration constant is not well known, but should be similar for the two subfamilies with the same composition (with only a small difference due to the relative difference in a), thus the ratio of the ages is $\sim 2/1$.

¹⁵Massalia does not have a WISE albedo, but it is possible to use WISE data to confirm that 65% of the members of family 20 have albedo between 0.17 and 0.32.

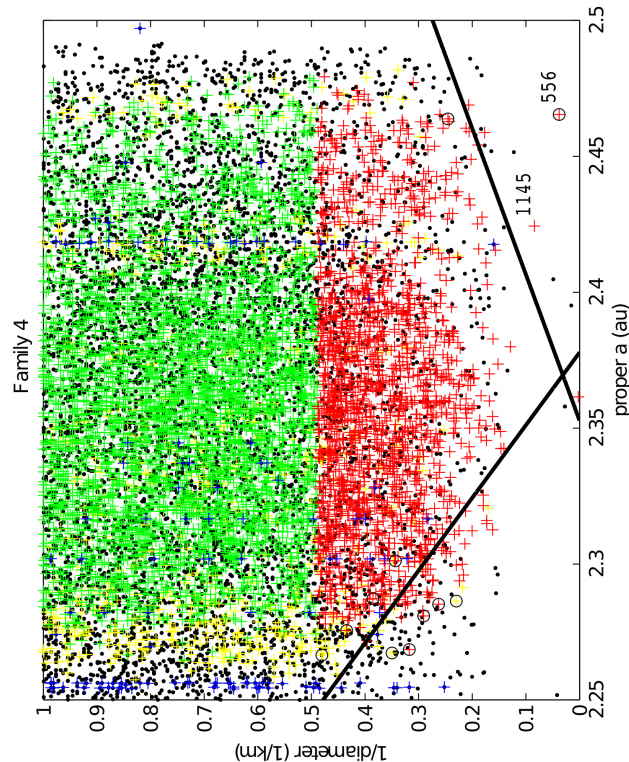


Figure 6: V-shape of the family 4. The lines identified by the fit have different slopes on the two sides; for the explanation see Section 7.2.

For the computation of the barycenter (Table 9) it is important to remove the interlopers (556) and (1145), which clearly stick out from the V-shape on the outer side, although (1145) is not rejected automatically by the fit¹⁶.

5.2.3. *Eunomia*

For the V-shape plot of Figure 7 we have used as common albedo the IRAS value for Eunomia which is 0.209. The inner and outer slopes of the V-shape for the Eunomia family are different by 31%. The slope on the outer side is affected by the 8/3 resonance with Jupiter, forcing us to cut the fit already at $D = 6.7$ km, thus the value may be somewhat less accurate. On the contrary the inner slope appears well defined by using $D > 5$ km, although the 3/1 resonance with Jupiter is eating up the family at lower

¹⁶By using the smaller WISE albedos, these two are even larger than shown in Figure 6.

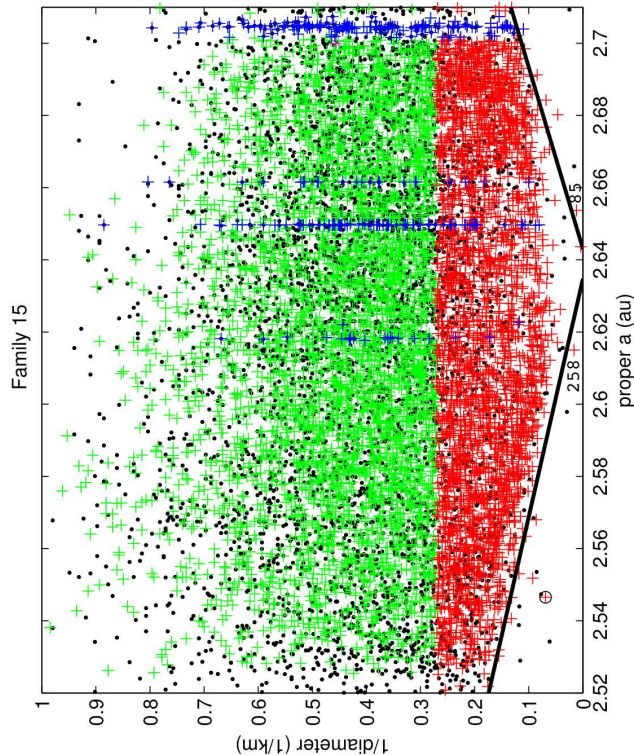


Figure 7: V-shape of the family 15 exhibiting two rather different slopes; for the explanation see Section 7.4.

diameters. The V-base is small and positive (Table 8). The possibility of an internal structure, affecting the interpretation of the slopes and ages, is discussed in Section 7.4.

For the computation of the barycenter (Table 9) it is important to remove the interlopers (85) and (258) which stick out from the V-shape, on the right and on the left, respectively, with the largest diameters after (15), see Figure 7¹⁷.

5.2.4. *Koronis*

The Koronis family has a V-shape sharply cut by the 5/2 resonance with Jupiter on the low a side, by the 7/3 on the high a side (Figure 8). This

¹⁷Moreover, the albedo of (85) Io is well known (both from IRAS and from WISE) to be incompatible with (15) Eunomia as parent body.

Table 9: Cratering families: family, proper a , e and $\sin I$ of the barycenter, position of the barycenter with respect to the parent body, escape velocity from the parent body. The barycenter is computed by removing the parent body, the interlopers and the outliers.

family	a_b	e_b	$\sin I_b$	$a_b - a_0$	$e_b - e_0$	$\sin I_b - \sin I_0$	v_e (m/s)
20	2.4061	0.1622	0.0252	-0.0025	0.0004	0.0004	102
4	2.3637	0.1000	0.1153	0.0022	0.0012	0.0040	363
4 (N \neq 1145)	2.3621	0.0993	0.1153	0.0006	0.0005	0.0040	
4 low e	2.3435	0.0936	0.1169	-0.0180	-0.0052	0.0056	
4 high e	2.3951	0.1094	0.1124	0.0336	0.0106	0.0011	
15	2.6346	0.1528	0.2276	-0.0091	0.0042	0.0010	176
15 (N \neq 85, 258)	2.6286	0.1495	0.2282	-0.0168	0.0010	0.0016	
15 low a	2.6090	0.1494	0.2294	-0.0347	0.0008	0.0028	
15 high a	2.6808	0.1501	0.2246	0.0371	0.0015	-0.0021	

results in a short range of diameters usable to compute the slope, especially on the low a side, where we have been forced to cut the fit at $D = 10$ km. This could be the consequence of an already well known phenomenon, by which leakage by Yarkovsky effect from family 158 into the 5/2 resonance occurs even for comparatively large objects [52, 72].

This implies a less accurate slope estimate on the inner side. This could explain the discrepancy by 37% of the two slopes, since we have no evidence for substructures which could affect the V-shape¹⁸. Anyway we recommend to use the outer slope for the age estimation.

5.2.5. Agnia

The Agnia family, as shown by Figure 5, has a prominent subfamily forming a V-shape inside the wider V-shape of the entire family. We call this structure the subfamily of (3395) Jitka.

For the entire family, almost identical values of the slopes on the two sides (Table 7) appear to correspond to the much older age of a wider and less dense family. The two slopes of the Jitka subfamily are also identical, but with inverse slopes lower by a factor > 9 . The V-base is negative in both cases (Table 8).

¹⁸There is a well known substructure, the Karin subfamily, which is perfectly visible in Figure 8, but does not affect the two sides of the V-shape.

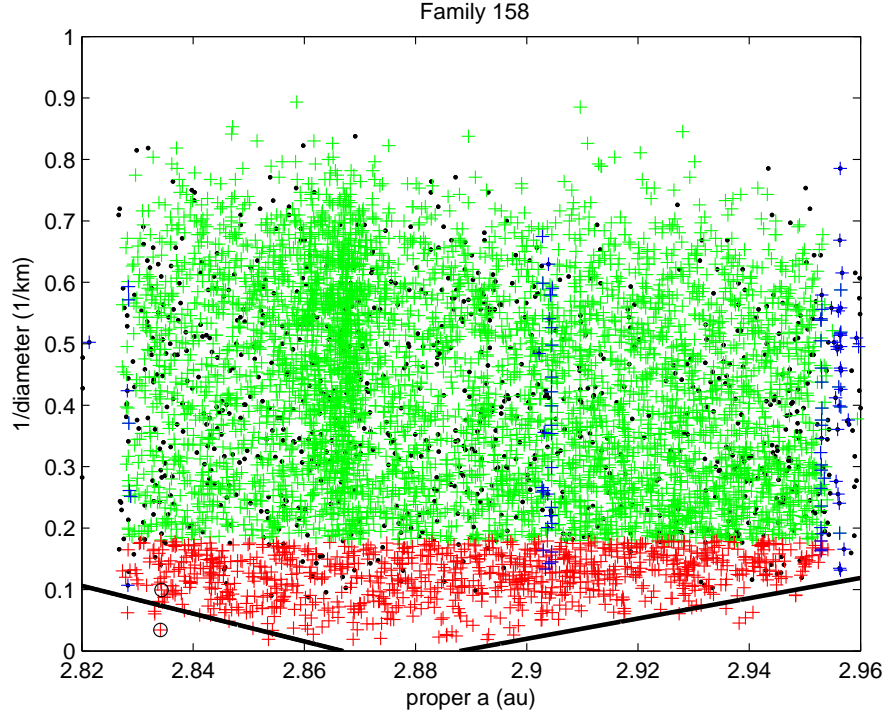


Figure 8: V-shape of the family 158. The Karin subfamily is clearly visible at about $a = 2.865$ au.

The Jitka subfamily shows in the V-shape plot (Figure 9) a depletion of the central portion, which should correspond to obliquities γ not far from 90° . This can be interpreted as a signature of the YORP effect, in that most members with $\gamma \sim 90^\circ$ would have had their spin axes evolved by YORP towards one of the two stable states, $\gamma = 0^\circ, 180^\circ$.

If the two collisional families belong to parent bodies with similar composition, then the ratio of the inverse slopes correspond to the ratio of the ages, independently from the calibration. Thus Jitka could be a catastrophic fragmentation of a fragment from another fragmentation 9 times older.

However, there are some problems if we use the WISE albedo data for family 847 members; there are 114 albedos with $S/N > 3$, which introduces some risk of small number statistics. Anyway, they indicate that the two subgroups, the 3395 subfamily and the rest of the 847 dynamical family, have a similar distribution of albedos, including dark interlopers. However, the

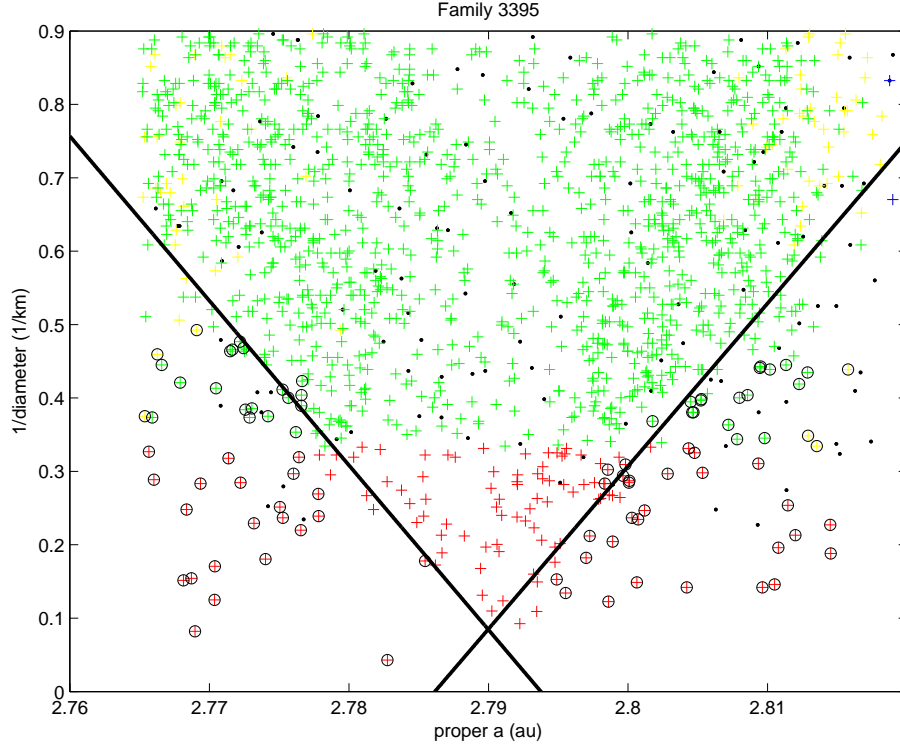


Figure 9: V-shape of the subfamily of (3395) Jitka. Most of the outliers, marked by a black circle, are members of the larger Agnia family, but not of the subfamily.

albedo of (847) Agnia 0.147 ± 0.012 is lower than most family members, while (3395) Jitka has 0.313 ± 0.045 which is more compatible with the family. Thus it is not clear whether (847) Agnia is the largest remnant or an interloper, and whether the parent body of the Jitka subfamily did belong to the first generation family.

5.2.6. Yarkovsky effect calibration and family age estimation

Recalling that there is not a single measurement of the Yarkovsky effect for the main belt asteroids, thus also for the families, we can perform the necessary calibration only by using the available measurements for the Near Earth Asteroids.

Thus, here the age estimation is obtained by scaling the results for the asteroid for which there is the best Yarkovsky effect determination [24], namely the low-albedo asteroid (101955) Bennu, with scaling taking into account the

Table 10: Fragmentation families: family, proper a , e and $\sin I$ of the barycenter. The barycenter is computed by removing the outliers.

family	a_b	e_b	$\sin I_b$
158	2.8807	0.0488	0.0371
847	2.7799	0.0715	0.0664
847 (w/o 3395)	2.7462	0.0725	0.0654
3395	2.7911	0.0728	0.0669

different values of D , a , e , ρ and A , where ρ is the density and A is the Bond albedo. The da/dt value for (101955) Bennu has a $S/N = 197.7$, thus a relative uncertainty $< 1\%$. The scaling formula we have used is:

$$\frac{da}{dt} = \frac{da}{dt} \Big|_{Bennu} \frac{\sqrt{a_{(Bennu)}}(1 - e_{Bennu}^2)}{\sqrt{a}(1 - e^2)} \frac{D_{Bennu}}{D} \frac{\rho_{Bennu}}{\rho} \frac{\cos(\phi)}{\cos(\phi_{Bennu})} \frac{1 - A}{1 - A_{Bennu}}$$

where $D = 1$ km used in this scaling formula is not the diameter of an actual asteroid, but is due to the use of the inverse slope and $\cos(\phi) = \pm 1$, as explained in the description of the method above.

It may appear that the use of the Yarkovsky effect measurements for asteroids more similar in composition to the considered families than Bennu would be more appropriate. So, for example, the asteroid (2062) Aten has the best determined da/dt value of all S-type asteroids. It has a $S/N = 6.3$, thus a relative uncertainty 0.16, which has to be taken into account in the calibration error. As for the scaling formula above, it introduces additional uncertainty, especially since there is no scaling term accounting for the different thermal properties.

Thus, using an S-class asteroid for scaling may not result in a better calibration, because the S-type asteroids are not all the same, e.g., densities and thermal properties may be different. In the case of (2062) Aten there is an error term due to the lack of knowledge on the obliquity ϕ , which can contribute an additional relative error up to 0.2. The other two S-type asteroids with measured Yarkovsky are (1685) Toro and (1620) Geographos, but with $S/N = 3.7$ and 3.0, respectively.

In the same way, for the family of (4) Vesta one would expect that the use of the Yarkovsky measurement for asteroid (3908) Nyx, presumably of V-type [3], should represent a natural choice for calibration. In fact, the same authors warn that this asteroid belongs to a small group of objects

with “sufficiently unusual or relatively low S/N spectra”, thus the taxonomic class may be different from nominal. This suspicion is further strengthened by the value of geometric albedo of only 0.16 ± 0.06 reported by [2], which is significantly lower than the typical value (~ 0.35) for a Vestoid. (3908) Nyx is apparently of extremely low density (Farnocchia and Chesley, private communication), thus it has too many properties inconsistent with Vestoids.

This is why we have decided to use (101955) Bennu as benchmark to be scaled for the Yarkovsky calibration of all families, because it is the known case with both the best estimate of Yarkovsky and best known properties, including obliquity, density, and size.

Table 11: Family age estimation: family, da/dt for $D = 1$ km obtained using (101955) Bennu for the calibration, for the two sides of the V-shape, and corresponding family age estimation.

family		da/dt (10^{-10} au/y)	Δt (Gy)
20	IN	-3.64	0.173
20	OUT	3.55	0.163
4	IN	-2.65	1.010
4	OUT	2.57	2.090
15	IN	-3.49	1.890
15	OUT	3.39	1.480
158	IN	-3.13	1.410
158	OUT	3.08	1.970
847	IN	-3.37	1.270
847	OUT	3.33	1.300
3395	IN	-3.35	0.134
3395	OUT	3.33	0.135

The results of our age computation for the considered families are given in Table 11, for the two sides of the V-shape.

As one can appreciate from these data, the estimations of the age of Massalia family from the two slopes differ by only a small amount, and they are also in good agreement with results obtained with a quite different

method by [73].

The Vesta family case is particularly interesting as the lower age appears to be compatible with the estimated age of one of the two largest craters on Vesta, Rheasilvia (~ 1 Gy) [37]. An age for the other big crater, Veneneia, has not been estimated, although it must be older because this crater is below the other. Our estimated $\sim 2/1$ ratio for the collisional families ages is an interesting result, although it should not be considered as a proof that the sources are the two known largest craters.

The difference of the values of the inner and outer slopes of the V-shape for the Eunomia could be interpreted as the age of two different events, see Section 7.4. There is no previous estimate of the age of Eunomia we are aware of, a “young age” being suggested on the basis of simulations of size distribution evolution by [43].

The estimation of the age of Koronis family as inferred from the longer outer side of the V-shape is consistent with the age (≤ 2 Gy) reported previously by [39], based on the observed size distribution of larger members, and by [18], based on the crater count on the surface of the Koronis family member (243) Ida. [4] give 2.5 ± 1 Gy, which is also consistent.

The age estimate for the Agnia family of < 140 My, provided by [74], is in a very good agreement with our result for the Jitka subfamily; the older age for the entire Agnia family has not been found previously because the low a component identified by us was not included in the family.

The two youngest according to our estimates, family 20 and subfamily 3395, have in common the presence of a lower density central region of the V-shape, more pronounced for Jitka, barely visible for Massalia. This suggests the following: the time scale for the YORP effect to reorient the rotation axis towards either full spin up or full spin down is much smaller than the time scale for randomization of a significant fraction of the spin states, which would fill the central gap.

We need to stress that the main uncertainty in the age computation is not due to the estimate of the slope (apart for the “bad” case of the inner slope of Koronis). The main error term is due to the calibration; we do not yet have enough information to derive a formal standard deviation estimate, but the relative uncertainty of the age should be of the order of $0.2 \div 0.3$.

5.2.7. Collisional Models and the interpretation of V-shapes

The method we have proposed for the computation of family ages has the advantage of using an objective measurement of the family V-shape, rather

than using a line placed “by eye” on a plot. However, because two parameters are fit for each boundary line, that is the slope and the intersection with a -axis, whenever both sides are accessible the output is a set of four parameters: the inverse slopes on both sides (Table 7), the V-base and the center of V-base (Table 8). To force the lines to pass from a single vertex on the horizontal axis would remove one fit parameter, to assign also the proper a of this vertex (e.g., at the value of some barycenter) would remove two parameters: by doing this we would bias the results and contradict the claimed objectivity of the procedure, which has to be defined by the family membership only.

On the other hand, our procedure does not use the V-base and its center to estimate the family age. Only the slopes of the leading edge of family members (for either high or low a) are used for the ages. This leads to two questions: which information is contained in the two parameters we are not using, and is it appropriate to obtain, e.g., a negative V-base, or is this an indication of a poor fit of at least one of the two lines?

The interpretation of the V-shape plots is not straightforward, because they are the outcome of a game involving three major players, each one producing its own effect. These players are: (1) the collisional history of a family, including the possible presence of overlapping multi-generation events; (2) the Yarkovsky effect, which in turn is influenced by the YORP effect; (3) the original field of fragment ejection velocities at the epoch of family formation. In addition, also the possible presence of strong nearby resonances plays an important role. Note also that in the present list of families several ones have been created by a cratering and not by a catastrophic disruption.

As for the effect (3), the existence of a correlation between the size and the dispersion in semi-major axis of family members has been known for several years. In the past, pre-Yarkovsky era (and with most of the recognized families resulting from catastrophic events), this correlation was assumed to be a direct consequence of the distribution of original ejection velocities, with smaller fragments being ejected at higher speeds. The ejection velocities derived from observed proper element differences, however, turned out to be too high to be consistent with the experiments, since they implied collisional energies sufficient to thoroughly pulverize the parent bodies.

Later, the knowledge of the Yarkovsky effect and the availability of more detailed hydrodynamic simulations of catastrophic fragmentation family-forming events (see, for instance, [43]) suggested a different scenario: most family members would be reaccumulated conglomerates, issued from merging of many fragments ejected at moderate velocities. In this scenario, the

original ejection velocities give a moderate contribution to the observed dispersion of proper elements. Then the V-shape plots discussed in the previous subsections would be essentially a consequence of such Yarkovsky-driven evolution (see [5] for a general reference). The extension of the above scenario to families formed by craterization events is not obvious, nor –at the present time– supported by numerical simulations, which are not yet capable to reach the required resolution [32]. However, the interpretation of the V-shape as a consequence of Yarkovsky effect should hold also for them.

Unfortunately, a fully satisfactory interpretation of the observed V-shape plots can hardly be achieved in such a purely Yarkovsky-dominated scenario: the original ejection velocities of fragments cannot be totally disregarded. For the Eos family [7], [75], assume, for bodies of a size of 5 km, average asymptotic relative velocities v_∞ of about 90 m/s. This is even more true for the families formed by cratering events on very large asteroids, since ejection velocities v_0 must be $> v_e$ (escape velocity) as to overcome the gravitational well of the parent body, and the v_∞ of the family members are both large and widely dispersed (see Section 7).

Due to the original dispersion of the family members, we cannot expect that the two sides of any given V-plot exactly intersect on the horizontal axis, as one might expect for a "pure" Yarkovsky model. The original extension of the family depends on the ejection velocities v_∞ of the bodies, while the Yarkovsky effect on every body of a given size depends on the orientation of the spin vector. If velocities and spin vectors are not correlated, the two terms should combine as independent distributions. If the Yarkovsky term is assumed to be the dominant signal, the original velocities provide a noise term; the noise/signal value is certainly significant for large objects, thus the two lines of the "V" should not intersect at $1/D = 0$, but in the halfplane $D < 0$. The "V-base" has therefore to be positive. Yet, this is not the case in 3 out of 6 examples presented in this paper. How to possibly explain this?

A more physical explanation may be tentatively suggested, based on an argument which has been previously discussed in the literature [34], [59] but yet not fully explored. According to the results of some laboratory fragmentation experiments [26], [27] the fragments ejected from a catastrophic disruption rotate, and the sense of spin is related to the ejection geometry: the fragments rotate away from the side of higher ejection velocity. Such behavior is clearly represented in [26, Fig. 1]. This experimental evidence was used in developing the so-called semi-empirical model [57, 58], assuming that fragment rotations are produced by the anisotropy in the velocity ejection

field.

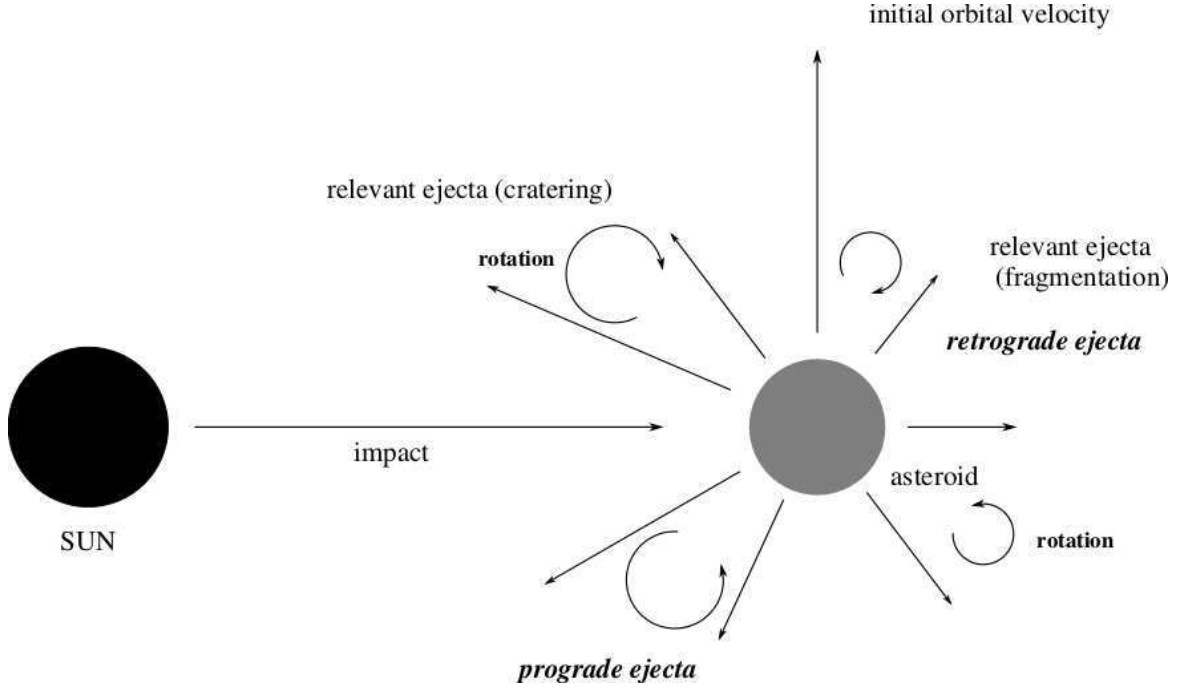


Figure 10: The possible correlation spin–ejection velocity for a radial impact from the interior of the Solar System. This is a projection on the orbital plane. For a cratering impact the ejecta are in the same hemisphere as the impact point, while for a catastrophic disruption the crater zone is pulverized, most sizable fragments are ejected from the antipodal hemisphere. In both cases the ejection velocity decreases with the angular distance from the impact point. If the rotation is connected to the velocity shear the fragment with a positive along track velocity (top of the figure) have a retrograde (clockwise) rotation, and viceversa. This is true both for the front side ejecta (cratering) and for the rear side fragments (disruption). In this case the correlation between the initial Δa and $\cos \gamma$ is negative, and the Yarkovsky effect tends initially to shrink the family in a .

In this scenario, the rotation of fragments created in a catastrophic process can be strongly correlated with the ejection velocity. For what concerns cratering events, as far as we know, there is not in this respect any experimental evidence mentioned in the literature. However, also in cratering events the ejection velocity field is strongly anisotropic (see, for instance, the popular Z–model by [42]), and a similar correlation between ejection velocity and spin

rate can be expected for the fragments. It is not obvious how significantly the reaccumulation of ejecta (a process which certainly is very important after catastrophic events) can affect this correlation. There are very few simulations taking into account the rotation of fragments recorded in the literature [63], [43], they are all about fragmentations, and their results do not solve the present question. However, if the fragments which stick together were ejected from nearby regions of the parent body, an original correlation might be preserved.

If this is the case, different impact geometries will result in different evolutions of the semi-major axis spread of the family. To model the geometry of the impact, let us call *crater radiant* the normal \hat{n} to the smoothed terrain before the crater is excavated (at the impact point). What matters are the angles between \hat{n} and the directions \hat{v} of the orbital velocity of the parent body, and \hat{s} towards the Sun (both at the epoch of the impact).

If $\hat{n} \cdot \hat{s} > 0$ (impact on the inner side) with $\hat{n} \cdot \hat{v} \simeq 0$ (impact radiant close to normal to the velocity) there are preferentially retrograde fragments on the side where ejection velocity adds up with orbital velocity, thus giving rise to larger a of fragments, preferentially prograde on the opposite, lower a side. This implies that the spread in proper a of the family initially decreases (ejection velocity and Yarkovsky term act in the opposite sense), then increases again, and the V-base is negative. If $\hat{n} \cdot \hat{s} < 0$ (impact on the outer side) with $\hat{n} \cdot \hat{v} \simeq 0$ there are preferentially prograde fragments at larger a , preferentially retrograde at lower a . This results in a large spread, even after a short time, of the family in proper a (ejection velocity and Yarkovsky term add), and the V-base is positive. Finally, in case of negligible $\hat{n} \cdot \hat{s}$, the original ejection velocities and Yarkovsky drift add up as a noise terms, the latter dominating in the long run; the V-base is positive but small. Note that, as shown by Figure 10, this argument applies equally to cratering and to fragmentation cases.

Thus, in principle, the properties of the V-base and of the family barycenter (Tables 8, 9, and 10) contain information on the impact geometry and on the original distribution of v_∞ . However, the interpretation of these data is not easy. A quantitative model of the ejection of fragments, describing the distribution of v_∞ , the direction of v_∞ , $\cos \gamma$, and D , taking into account all the correlations, is simply not available. We have just shown that some of these correlations (between direction and $\cos \gamma$) are not negligible at all, but all the variables can be correlated. Even less we have information on shapes, which are known to be critical for the YORP effect.

This does introduce error terms in our age estimates. The main problem is the dependence of the Yarkovsky drift in a , averaged over very long times, from D . According to the basic YORP theories (see [6] for a general reference) the bodies should preferentially align their rotation axes close to the normal to the orbital plane (both prograde and retrograde), with a timescale strongly dependent on the size. This result is also supported by the recent statistical work on the spin vector catalog [60]. Consequently, there should be a substantial fraction of the small bodies moving towards the borders of the V-plot, especially after times long with respect to the time scale for the YORP-driven evolution to the spin up/spin down stable states. Using a different database [73] have found for most families, a number density distribution in accordance to this idea. However, the maxima are not at the edges, but somewhere in between the symmetry axis of the V-shape and the edges: e.g., see Figure 9. It is not easy to draw general conclusions from this kind of data, because in most families the portions near the extreme values of proper a are affected by resonances and/or by the merging of step 3 families as haloes.

There are many models proposed in the literature to account for a form of randomization of the spin state, resulting in something like a Brownian motion along the a axis over very long time scales; e.g., [68] and [20] show that the YORP effect can be suddenly altered. Thus after a long enough time span, most family members may be random-walking between the two sides of the V-shape, and the central area is never emptied. However, what we are measuring is not the evolution in a of the majority of family members, but the evolution of the members fastest in changing a . Our method, indeed any method using only the low and high a boundaries of the family, should be insensitive to this effect for large enough families. In a random effect a portion of the family with a spin state remaining stable at $\cos \gamma \simeq \pm 1$ will be maintained for a very long time, and this portion is the one used in the V-shape fit.

Our method is mathematically rigorous in extracting from the family data two components of the evolution of proper a after the family formation, a term which is constant in time (from the original distribution of velocities) and independent from D , and a term which is proportional to $1/D$ and to the time elapsed. If the situation is much more complicated, with a larger number of terms with different dependence on both D and t , we doubt that the current dataset is capable of providing information on all of them, independently from the method used. Moreover, some terms may not be dis-

criminated at all, such as an $1/D$ dependency not due to a pure Yarkovsky term $\Delta t/D$.

5.3. Size distributions

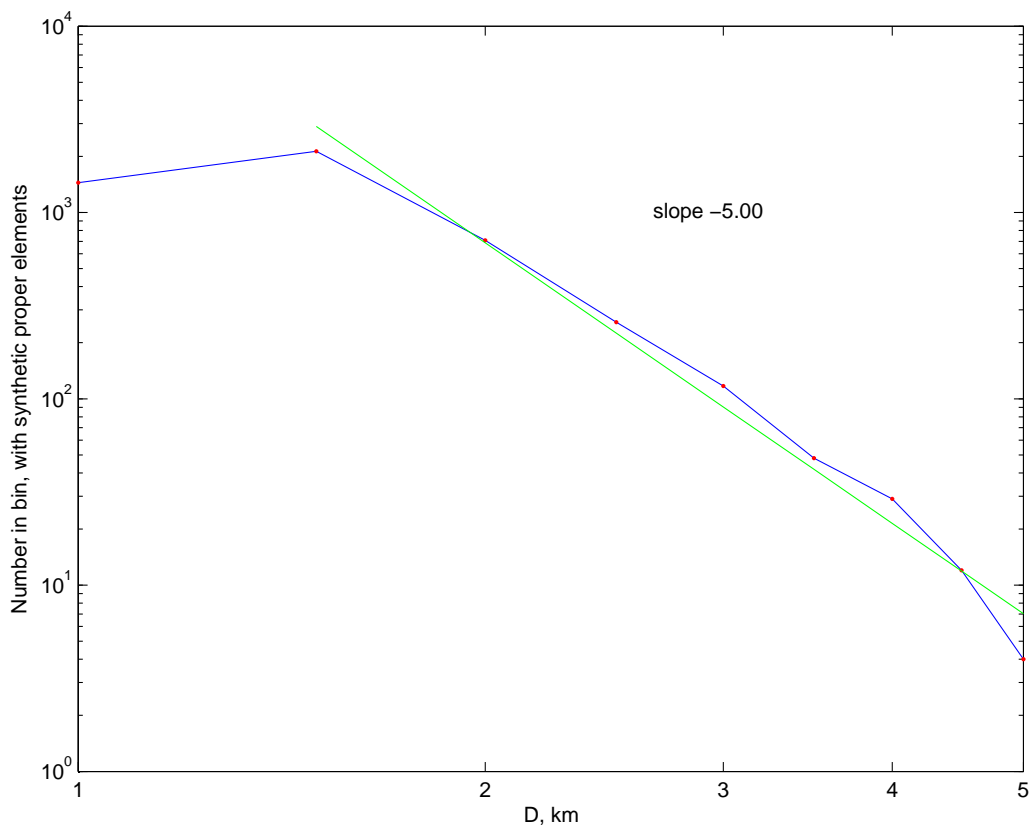


Figure 11: Size distribution of family 20 using the range $1.5 < D < 5$ km.

Another use of the diameters deduced from absolute magnitudes assuming uniform albedo is the possibility of computing a size distribution. This is a very delicate computation, depending strongly upon the range of diameters used. Numbers of members at too small diameters are affected by incompleteness, while too large diameters are affected by small number statistics, especially for cratering events. The utmost caution should be used in these estimates for families less numerous and/or with a more complex structure.

In Figure 11 we show the result of a size distribution power law fit for family 20, by using the range from $D = 1.5$ to 5 km, thus excluding (20)

and the two outliers identified above as well as two others above 5 km. The resulting best fit differential power law is proportional to $1/D^5$, that is the cumulative distribution is proportional to $1/D^4$; this value suggests that the fragments are not yet in collisional equilibrium, thus supporting a comparatively young age for the family. The results are somewhat dependent upon the range of diameters considered, as it is clear by the much lower value for diameters $D < 1$ km with respect to the fit line (in green): this is a clear signature of observational incompleteness.

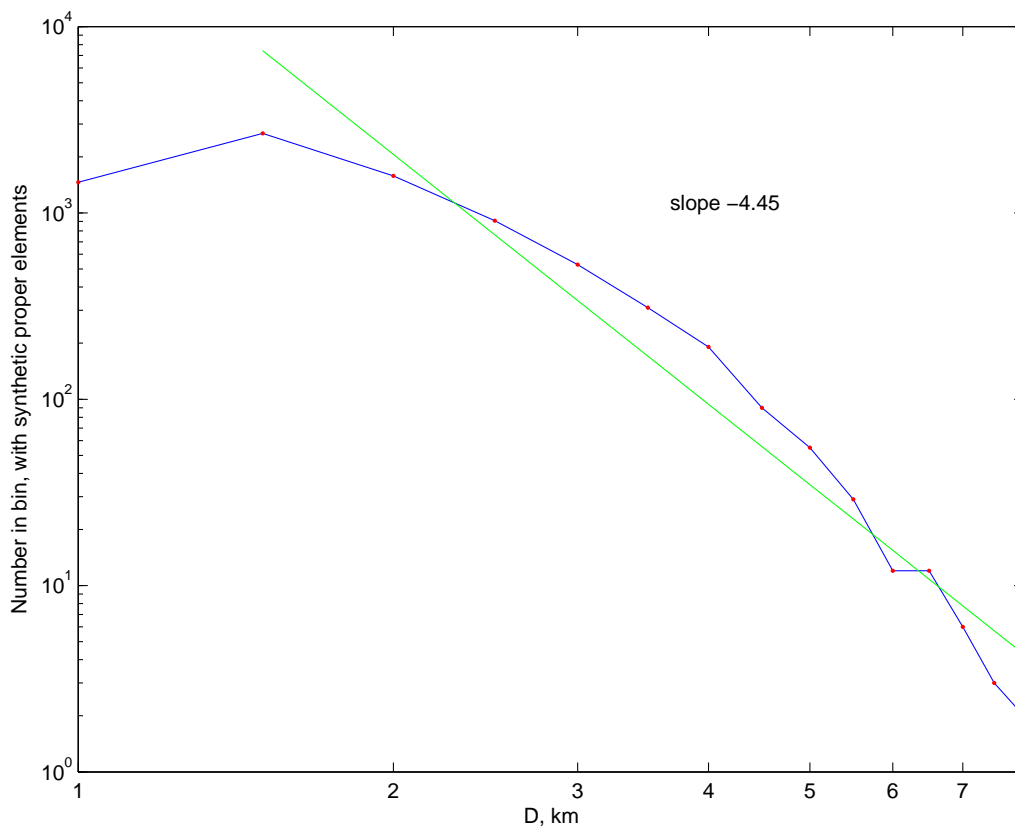


Figure 12: Size distribution of family 4 using the range $1.5 < D < 8$ km.

In Figure 12 we show the size distribution power law fit for family 4; to improve the estimates of the diameters, we have used as a common albedo 0.35 because it is more representative for the small members of the family, see Figure 16. We have used the range from $D = 1.5$ to 8 km, thus excluding (4) and the interlopers (556) and (1145) as well as another member

marginally larger than $D = 8$. The differential power law is $1/D^{4.5}$, that is the cumulative is $1/D^{3.5}$; this value also suggests that collisional equilibrium has not been reached, the family appears somewhat less steep, which should mean it is older, in agreement with the estimates from the previous subsection. Because of the larger span in D the figure shows, besides the incompleteness of family members with diameter $D < 2$ km, an additional phenomenon, namely a tendency to decrease the number of members with respect to the power law at comparatively large diameters $D > 5$. However, a complete interpretation of the size distribution should not be attempted without taking into account the results of Section 7.2, proposing a complex structure for the family.

The fact that the size distribution of families formed in cratering events usually exhibits such kind of concavity, is in agreement with available fragmentation models [69, 23]. The concavity in the size distribution tends to disappear when the parent body to largest member size ratio decreases, and this can be qualitatively explained in terms of available volume for the production of larger fragments [69].

Another constraint on the low D side comes from the fact that a slope larger than 4 for the differential size distribution corresponds to an infinite total volume of all the fragments of diameter in the interval $D_{max} > D > 0$. This implies that, even if there was no observational bias, the slope must decrease below some critical value of D . The problem is, we do not know what this critical size is; thus we cannot discriminate between observational bias and possible detection of a real change in slope.

6. Refinement with physical data

The data from physical observations of asteroids, especially if they are available in large and consistent catalogs like WISE and SDSS, are very useful to solve some of the problems left open by purely dynamical classifications such as the one discussed in the previous sections. This happens when there are enough consistent and quality controlled data, and when the albedo and/or colors can discriminate, either between subsets inside a family, or between a family and the local background, or between nearby families. (See also examples in Section 7.)

6.1. The Hertha–Polana–Burdett complex family

The most illustrative example of discrimination inside a dynamical family is the case of the family with lowest numbered asteroid (135) Hertha; when defined by purely dynamical arguments, it is the largest family with 11 428 members. Its shape is very regular in the $a, \sin I$ proper element projection, but has a peculiar $>$ -shape in the a, e projection (Figure 13), which has been strongly enhanced by the addition of the smaller asteroids of the halo (in yellow).

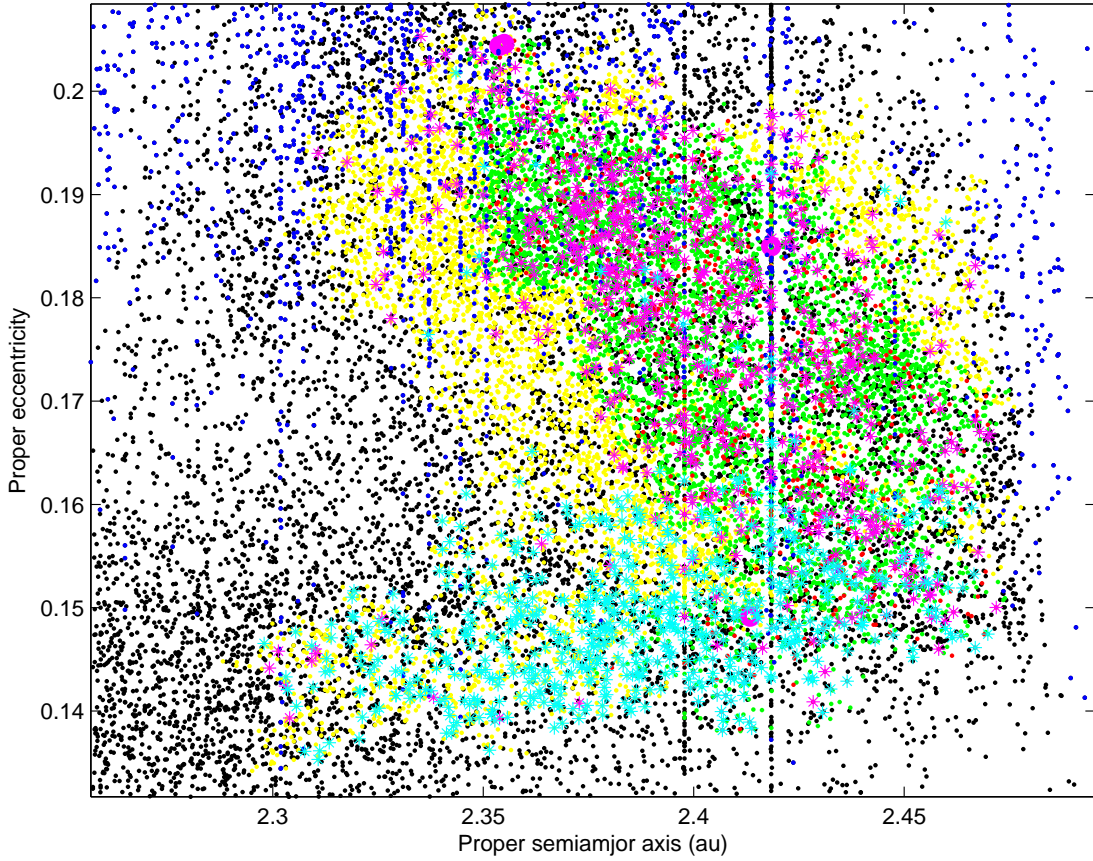


Figure 13: The Hertha dynamical family in proper a, e plane. Bright objects (magenta stars) and dark objects (cyan stars) forming a characteristic $>$ -shape indicate two partly overlapping collisional families.

Already by using absolute magnitude information some suspicion arises

from the V-shape plot, from which it appears possible to derive a consistent “slope” neither from the inner nor for the outer edge. Problems are already well known to arise in this family from the very top, that is (142) Polana which is dark (WISE albedo 0.045) and diameter $D \simeq 60$ km, and (135) Hertha which is of intermediate albedo 0.152 and $D \simeq 80$ km, also known to be an M type asteroid, but exhibiting the $3 \mu\text{m}$ spectral feature of hydrated silicates [64].

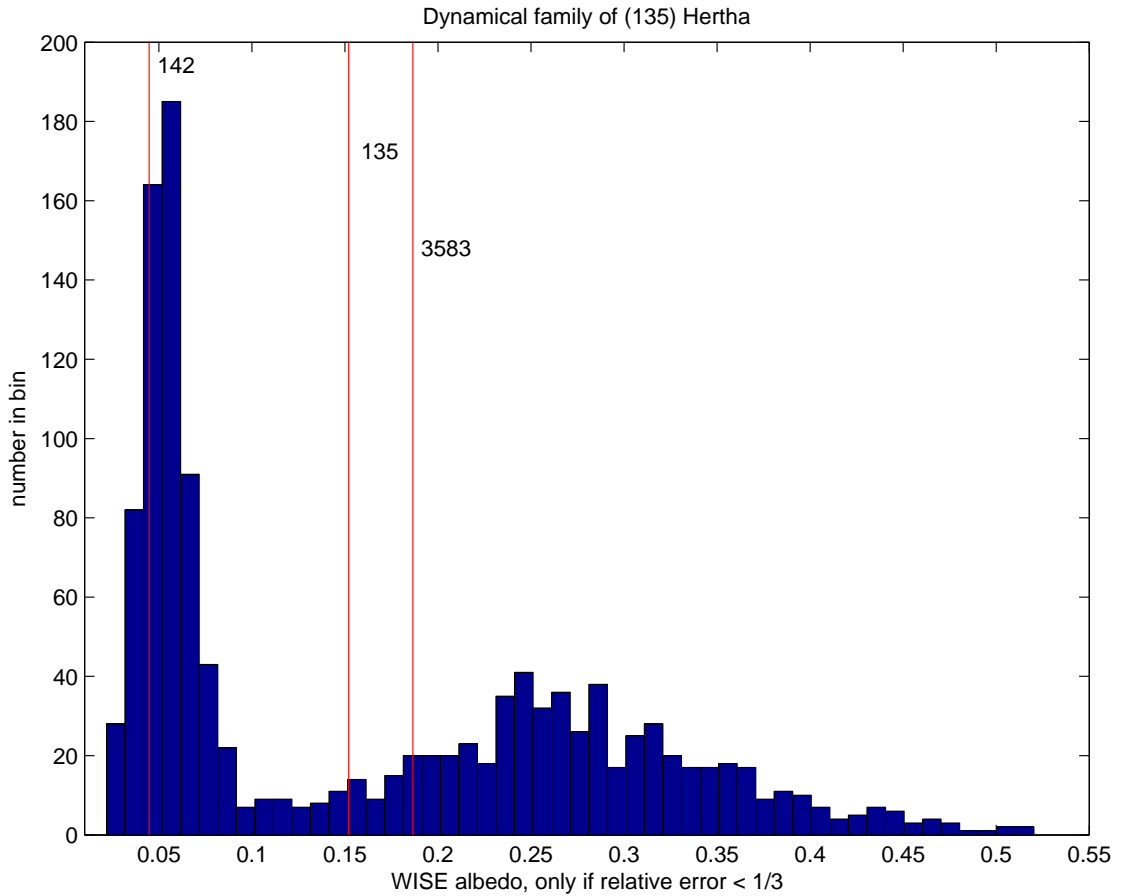


Figure 14: The distribution of WISE albedos for the 135 dynamical family with the locations of the three namesakes indicated by red lines. The distribution is clearly bimodal supporting the scenario with two collisional families.

By using systematically the WISE albedo, limited to the asteroids for which the albedo uncertainty is less than $1/3$ of the nominal value (1247

such data points in the 135 dynamical family), we find the sharply bimodal distribution of Figure 14. (142) Polana is by far the largest of the “dark” population (for the purpose of this discussion defined as albedo < 0.09 , 611 asteroids) as well as the lowest numbered. The “bright” population (albedo > 0.16 , 568 asteroids) does not have a dominant large member, the largest being (3583) Burdett (albedo 0.186 ± 0.02 , $D \simeq 7.6$ km)¹⁹

In Figure 13 we have plotted with magenta stars the “bright”, with cyan stars the “dark”, and it is clear that they are distributed in such a way that the >-shape in the proper a, e plane can be explained by the presence of two separate collisional families, the Polana family and the Burdett family, with a significant overlap in the high a , low e portion of the Hertha dynamical family. Because the WISE dataset is smaller than the proper elements dataset, we cannot split the list of members of the 135 dynamical family into Polana and Burdett, because such a list would contain an overwhelming majority of “don’t know”. Erosion of the original clouds of fragments by the 3/1 resonance with Jupiter must have been considerable, thus we can see only a portion of each of the two clouds of fragments. Based on the total volume of the objects for which there are good albedo data, the parent body of Polana must have had $D > 76$ km, the one of Burdett $D > 30$ km.

Note that we could get the same conclusion by using the a^* parameter of the SDSS survey: among the 1019 asteroids in the 135 dynamical family with SDSS colors and a^* uncertainty less than $1/3$ of the nominal value, 184 have $-0.3 < a^* < -0.05$ and 835 have $+0.05 < a^* < 0.3$, thus there is also a bimodal distribution, which corresponds to the same two regions marked in magenta and cyan in Figure 13, with negative a^* corresponding to low albedo and positive a^* corresponding to high albedo, as expected [61, Figure 3]. The lower fraction of “dark” contained in the SDSS catalog, with respect to the WISE catalog, is an observation selection effect: dark objects are less observable in visible light but well observable in the infrared.

Because of its very different composition (135) Hertha can be presumed to belong to neither the one nor the other collisional family, although strictly

¹⁹The asteroid (878) Mildred was previously cited as namesake of a family in the same region: Mildred is very likely to be “bright”, although the WISE data are not conclusive (albedo = 0.40 ± 0.22), but is very small ($D \simeq 2.5$ km). The fact that (878) was imprudently numbered in 1926 after the discovery and then lost is a curious historical accident explaining a low numbered asteroid which is anomalously small. Thus we are going to use Burdett as the namesake of the “bright” component.

speaking this conclusion cannot be proven from the data we are using, listed in Section 2, but requires some additional information (e.g., taxonomic classification of Hertha) and suitable modeling (e.g., excluding that a metallic asteroid can be the core of a parent body with ordinary chondritic mantle). All these conclusions are a confirmation, based on a statistically very significant information, of the results obtained by [13] on the basis of a much more limited dataset (spectra of just 20 asteroids). Other authors, such as [41], have first split the asteroids by albedo then formed families by proper elements, and they get the same conclusion on two overlapping families, but the total number of family members is lower by a factor ~ 3 .

6.2. *The Eos family boundaries*

Unfortunately, in many other cases in which the dynamical classification raises doubts on the family structure the physical observations databases are not sufficient to solve the problem. An example is the family of (221) Eos, which on the basis of the proper elements only cannot be neatly separated from the two smaller families of (507) Laodica and (31811) 1999 NA41 (there are a few members in common), as discussed in Section 4. The Eos family mostly contains intermediate albedo asteroids, including (221) Eos (WISE albedo = 0.165 ± 0.034) belonging to the unusual K taxonomic class, but the surrounding region predominantly contains low albedo objects, including (31811) (albedo 0.063 ± 0.014) and the majority of the members of the 507 family for which WISE data are available; (507) Laodica itself has an albedo = 0.133 ± 0.009 which is compatible with the Eos family. From this we are able to give the negative conclusion: attaching families 507 and 31811 to 221 would not be supported by physical observations, but leaving them separate is not much better.

6.3. *Watsonia and the Barbarians*

The family of (729) Watsonia had been already identified in the past by [56], who adopted a proper element data base including also a significant number of still unnumbered, high-inclination asteroids, not considered in our present analysis. This family is interesting because it includes objects called “Barbarians”, see [15], which are known to exhibit unusual polarization properties. Two of us (AC and BN) have recently obtained VLT polarimetric observations [17] showing that seven out of nine observed members of the Watsonia family exhibit the Barbarian behavior. This result strongly confirms a common origin of the members of the Watsonia family. On the

other hand, the presence of another large (around 100 km in size) Barbarian, (387) Aquitania, which has proper semi-major axis and inclination within the limits of the Watsonia family, but shows a difference in proper eccentricity of about 0.1, exceedingly large to include it in the family, indicates that the situation can be fairly complex and opens interpretation problems, including a variety of possible scenarios which are beyond the scopes of the present paper.

7. Cratering families

As a result of the availability of accurate proper elements for smaller asteroids, our classification contains a large fraction of families formed by cratering events.

Modeling of the formation of cratering families needs to take into account the escape velocity v_e from the parent body, which results in the parent body not being at the center of the family as seen in proper elements space. This is due to the fact that fragments which do not fall back on the parent body need to have an initial relative velocity $v_0 > v_e$, and because of the formula giving the final relative velocity $v_\infty = \sqrt{v_0^2 - v_e^2}$ the values of v_∞ have a wide distribution even for a distribution of v_0 peaking just above v_e . The mean value of v_∞ is expected to be smaller than v_e , at most of the same order. Thus immediately after the cratering event, the family appears in the proper elements space as a region similar to an ellipsoid, which is centered at a distance d of the order of v_e from the parent body. Of course this effect is most significant for the very largest parent bodies.

Moreover, it is important not to forget that cratering events typically occur multiple times over the age of the solar system, since the target keeps the same impact cross section. The outcomes can appear either as separate dynamical families or as structures inside a single one.

We use as criterion for identification of a cratering family that the fragments should add up to $\leq 10\%$ of the parent body volume; we have tested only the large and medium families, and used the common albedo hypothesis to compare volumes. In this way 12 cratering families have been identified with the asteroids (2), (3), (4), (5), (10), (15), (20), (31), (87), (96), (110), (179), and (283) as parent bodies. Other large asteroids do not appear to belong to families. We will discuss some interesting examples.

7.1. The Massalia family

Although the V-shape plot (Figure 4) does not suggest any internal structure for the family 20, the inspection of the shape of the family in the space of all three proper elements suggests otherwise.

The distribution of semimajor axes is roughly symmetrical with respect to (20) Massalia, while these of eccentricity and inclination are, on the contrary, rather asymmetrical. The eccentricity distribution is skewed towards higher eccentricities (third moment positive), this is apparent from Figure 1 as a decrease of number density for $e < 0.157$; the inclination one is skewed towards lower inclinations (third moment negative).

Thus the barycenter of the ejected objects appears quite close to the parent body (20), see Table 9: if the differences in $e, \sin I$ are scaled by the orbital velocity they correspond to about 7 m/s, which is much smaller than the escape velocity. Even if the distributions are skewed in number density, fragments appear to have been launched in all directions, and this is not possible for a single cratering event.

These arguments lead us to suspect a multiple collision origin of the dynamical family. At $e < 0.157$ there seems to be a portion of a family with less members which does not overlap the other, more dense collisional family. The more dense family has been ejected in a direction such that e increases and $\sin I$ decreases, the other in a direction with roughly opposite effect.

However, the presence of the low e subfamily does not affect the age computation, which only applies to the high e subfamily, due to the fact that the extreme values of a are reached in the high e region. Thus there are two concordant values for the slopes on the two sides, and a single value of the age we can compute, which refers only to the larger, high e subfamily.

7.2. The Vesta family substructures

The Vesta family has a curious shape in the proper a, e plane, see Figure 15, which is even more curious if we consider the position of (4) Vesta in that plane.

In proper a , the family 4 is bound by the 3/1 resonance with Jupiter on the outside and by the 7/2 inside. Closer inspection reveals the role of another resonance at $a \simeq 2.417$ au, which is the 1/2 with Mars. Indeed, the low e portion of the family has the outside boundary at the 1/2 resonance with Mars. By stressing the position of Vesta, as we have done with the cyan cross in Figure 15, we can appreciate the existence of a group of roughly oval shape with proper e lower than, or only slightly above, the one of Vesta (which

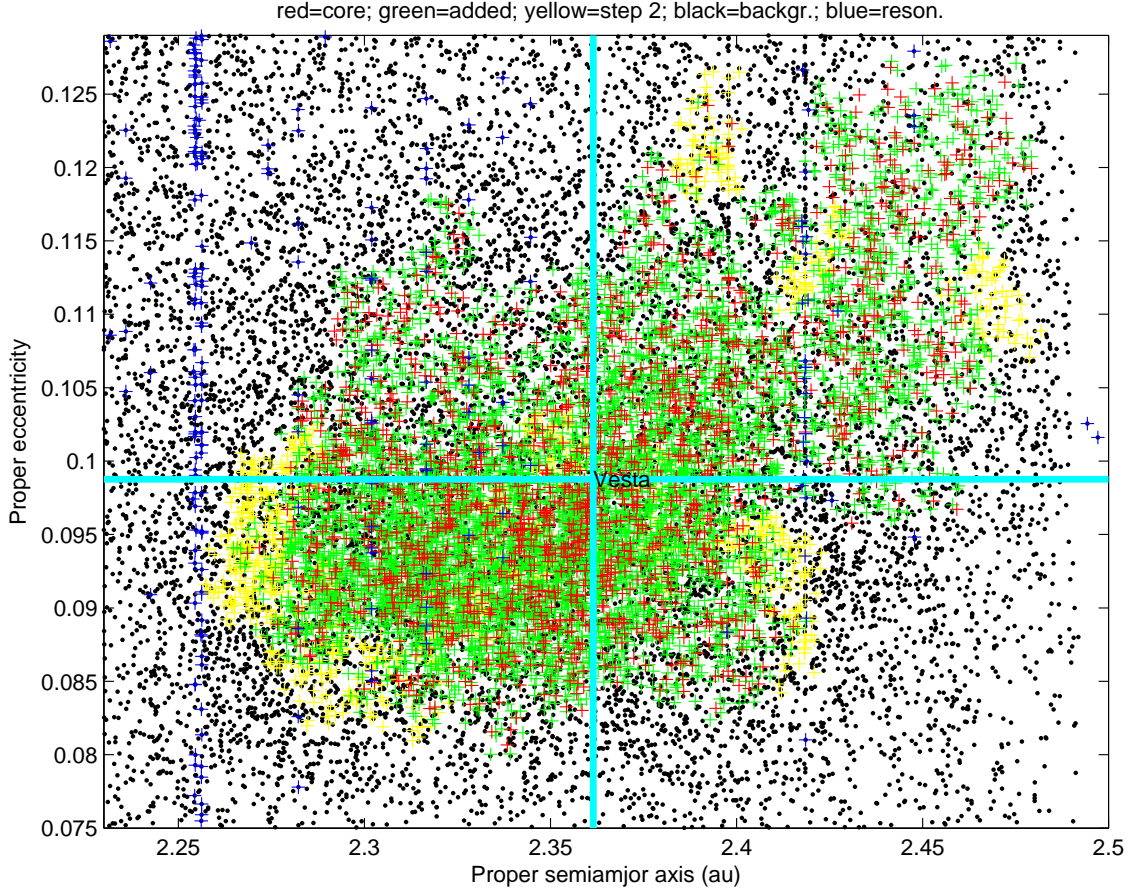


Figure 15: The family 4 shown in the proper a, e plane. The halo families merged in step 5 of our classification procedure (yellow dots) extend the family closer to the 3/1 resonance with Jupiter on the right and to the 7/2 resonance on the left. The position of (4) Vesta is indicated by the cyan cross, showing that the parent body is at the center of neither of the two concentrations of members, at lower e and at higher e . This because of the strongly anisotropic distribution of velocities v_∞ for a cratering event.

is 0.099). This can be confirmed by a histogram of the proper a for family 4 members, showing for $2.3 < a < 2.395$ a denser core containing about 2/3 of the family members. We can define a subgroup as the family 4 members with $a < 2.417$ and $e < 0.102$, conditions satisfied by 5 324 members. We shall call this group with the non-committing name of “low e subfamily”.

By assuming for sake of simplicity that albedo and density are the same, we can compute the center of mass, which is located at $a = 2.3435$ and $e = 0.0936$. To get to such values the relative velocity components after escape from Vesta should have been -76 and -98 m/s, respectively²⁰. Since the escape velocity from Vesta surface is ~ 363 m/s, this is compatible with the formation of the low e subfamily from a single cratering event, followed by a Yarkovsky evolution significant for all, since no member has $D > 8$ km.

What is then the interpretation of the rest of the family 4? We shall call “high e subfamily” all the members not belonging to the low e portion defined above, excluding also asteroids (556) and (1145) which have been found to be interlopers. This leaves 2538 members, again with size $D < 8$ km. It is also possible to compute a center of mass: the necessary relative velocities after escape are larger by a factor ~ 2 , still comparable to the escape velocity from Vesta, although this estimate is contaminated by the possible inclusion of low e , low a members into the low e subfamily. Anyway, the shape of this subfamily is not as simple as the other one, thus there could have been multiple cratering events to generate it.

This decomposition provides an interpretation of the results from Section 5.2, in which there was a large discrepancy, by a factor ~ 2 , between the age as computed from the low a side and from the high a side of the V-shape in $a, 1/D$. Indeed, if the low e subfamily ends for $a < 2.417$, while the high e subfamily ends at $a \sim 2.482$, then the right side of the V-shape belongs to the high e subfamily. From Figure 15 we see that the low a side of the family appears to be dominated by the low e subfamily.

As a consequence of this model, the two discordant ages computed in Section 5.2 belong to two different cratering events. This interpretation is consistent with the expectation that cratering events, large enough to generate an observable family, occur multiple times on the same target.

As for the uncertainties of these ages, they are dominated by the poor a priori knowledge of the Yarkovsky calibration constant c for the Vesta family. Still the conclusion that the two ages should be different by a factor ~ 2 appears robust. From the DAWN images, the age of the crater Rheasilvia on Vesta has been estimated at about 1 Gy [37], while the underling crater Veneneia must be older, its age being weakly constrained. Thus both

²⁰The negative sign indicates a direction opposite to the orbital velocity for a , and a direction, depending upon the true anomaly at the collision, resulting in decrease of e .

the younger age and the ratio of the ages we have estimated in Section 5.2 are compatible with the hypothesis that the low e subfamily corresponds to Rheasilvia, the high e subfamily (or at least most of it) corresponds to Veneneia. We are not claiming we have a proof of this identification.

Unfortunately, for now there are no data to disentangle the portions of the two collisional families which overlap in the proper elements space. Thus we can compute only with low accuracy the barycenter of the two separate collisional families, and to model the initial distributions of velocities would be too difficult. However, there are some indications [8] that discrimination of the two subfamilies by physical observations may be possible.

In conclusion, the current family of Vesta has to be the outcome of at least two, and possibly more, cratering events on Vesta, not including even older events which should not have left visible remnants in the family region as we see it today.

7.3. *Vesta Interlopers and lost Vestoids*

Another possible procedure of family analysis is to find interlopers, that is asteroids classified as members of a dynamical family, not belonging to the same collisional family, because of discordant physical properties; see as an example of this procedure Figure 25 and Table 3 of [54].

In the dynamical family of (4) Vesta there are 695 asteroids with reasonable (as afore) WISE albedo data. We find the following 10 asteroids with albedo < 0.1 : (556), (11056), (12691), (13411), (13109), (17703), (92804), (96672), (247818), (253684); the first is too large ($D \simeq 41$ km) and was already excluded, the next 3 are larger than 7.5 km, that is marginally too large for typical Vestoids; we had also excluded in Section 5.1 (1145), which has an intermediate albedo but is also too large ($D \simeq 23$ km). We think these 11 are reliably identified as interlopers, of which 10 belong to the C-complex. By scaling to the total number 7 865 of dynamic family members, we would expect a total number of interlopers belonging to the C-complex $\simeq 120$.

The problem is how to identify the interlopers belonging to the S-complex, which would be expected to be more numerous. For this task the WISE albedo data are not enough, as shown by Figure 16. The albedos of most family members are in the range between 0.16 and 0.5, which overlaps the expected for the S-complex, but there is no ostensible bimodality in this range.

The background asteroids, with $2.2 < a < 2.5$, for which significant WISE albedos are available, clearly have a dark component, 34% of them

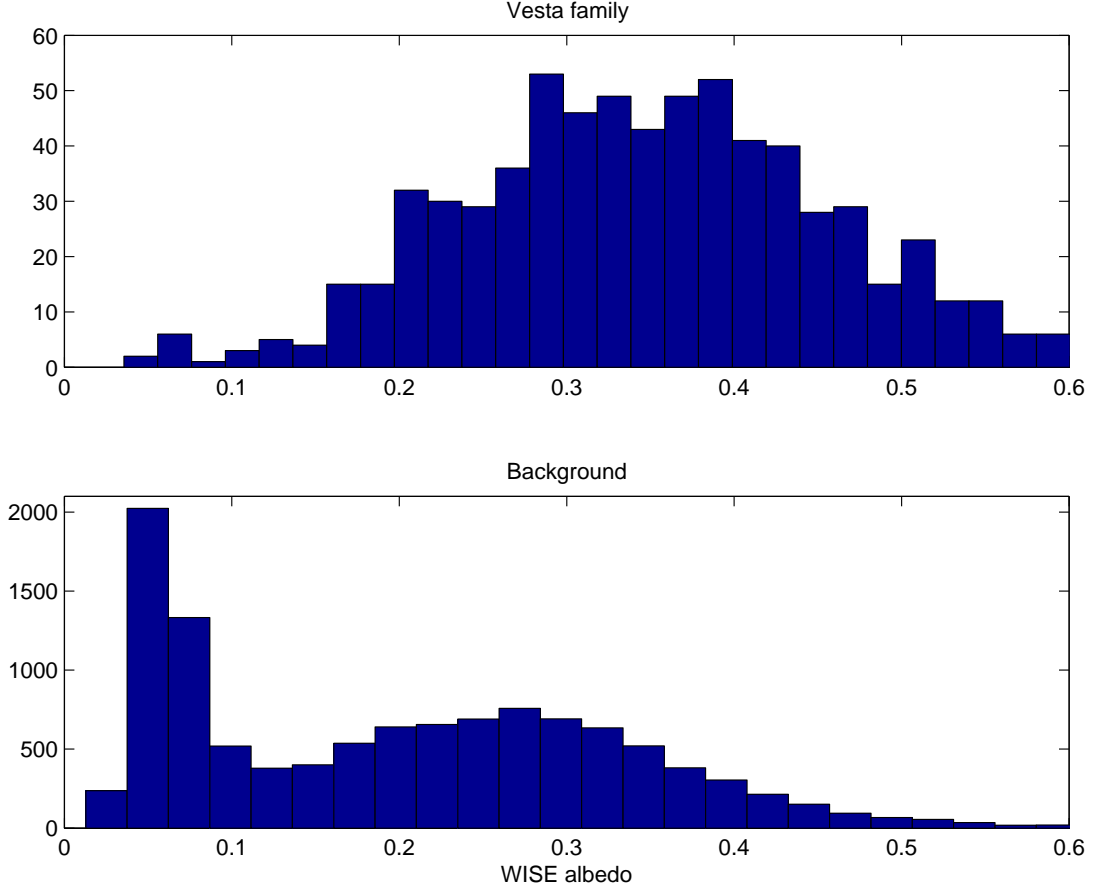


Figure 16: Histogram of albedo measured by WISE with $S/N > 3$: above for the asteroids belonging to family 4; below for the background asteroids with $2.2 < \text{proper } a < 2.5$ au. The uneven distribution of “dark” asteroids (albedo < 0.1) is apparent. The asteroids with $0.27 < \text{albedo} < 0.45$, corresponding to the bulk of the family 4, are present, but as a smaller fraction, in the background population.

with albedo < 0.1 , but the majority have albedos compatible with the S-complex, a large fraction also compatible with V-type.

The estimated value of the albedo is derived from an assumed absolute magnitude, which typically has an error of 0.3 magnitudes (or worse). This propagates to a relative error of 0.3 in the albedo. Thus the values of albedo for S and V type are mixed up as a result of the measurement errors, both in the infrared and in the visible photometry. The only class of objects

which are clearly identified from the albedo data are the dark C-complex ones, because the main errors in the albedo are relative ones, thus an albedo estimated at < 0.1 cannot correspond to an S-type, even less to a V-type.

In conclusion, by using only the available albedo data there is no way to count the interlopers in the Vesta family belonging to the S-complex; it is also not possible to identify “lost Vestoids”, originated from Vesta but not included in the dynamical family.

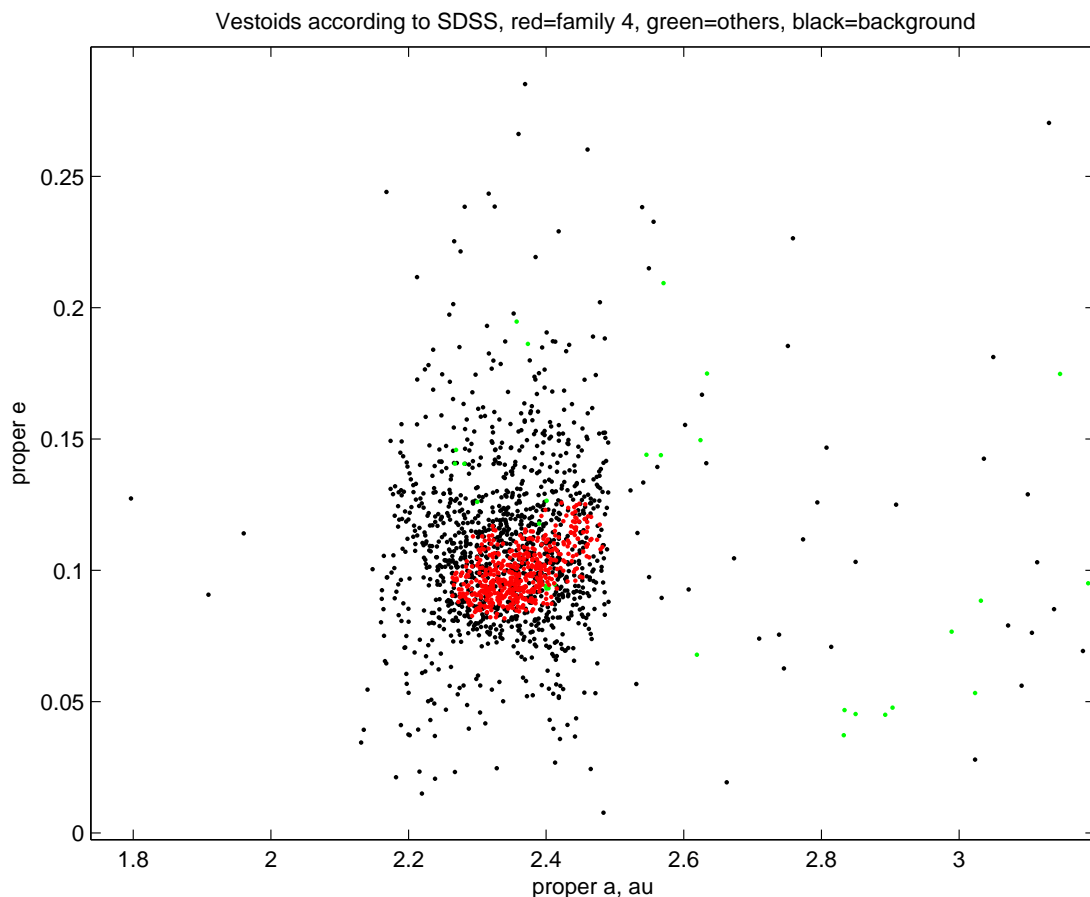


Figure 17: Asteroids complying with the [61] criterion for V-type. Red points: members of family 4, green: members of other families, black: background asteroids. The background asteroids apparently matching the color properties of Vestoids are, among objects with significant SDSS data, at least twice more numerous than the family 4 members with the same colors.

The question arises whether it would be possible to use the SDSS data to solve these two problems. According to [61] the V-type objects should correspond to the region with $a^* > 0$ and $i - z < -0.15$ in the plane of these two photometric parameters. However, as it is clear from [61, Figure 3], these lines are not sharp boundaries, but just probabilistic ones. Thus this criterion is suitable to reliably identify neither family 4 interlopers, nor lost Vestoids.

On the other hand, the Parker et al. criterion can be used to estimate the V-type population in a statistical sense. To select the asteroids which have a large probability of being V-type we require $a^* - 2\text{STD}(a^*) > 0$ and $i - z + 2\text{STD}(i - z) < -0.15$; we find 1 758 asteroids, of which 55 with $a > 2.5$ au; they are plotted on the proper a, e plane in Figure 17. The number of asteroids of V-type beyond the 3/1 resonance with Jupiter should be very small, anyway 55 is an upper bound on the number of false positive for the V-type criterion in that region.

Of the V-type with $a < 2.5$ au, 504 are members of the dynamical family 4 and 1 199 are not. In conclusion, even taking into account the possible number of false positive, there are at least twice as many V-types in the inner belt outside of the dynamical family rather than inside.

Conversely, if we define “non-V type” by the criterion either $a^* + 2\text{STD}(a^*) < 0$ or $i - z - 2\text{STD}(i - z) > -0.15$ we find in the inner belt $a < 2.5$ as many as 8 558 non-V, out of which only 42 belong to the dynamical family 4, which means the number of S-type interlopers is too small to be accurately estimated, given the possibility of “false negative” in the V-type test.

This gives an answer to another open question: where are the “lost Vestoids”, remnants of cratering events on Vesta which occurred billions of years ago? The answer is everywhere, as shown by Figure 17, although much more in the inner belt than in the outer belt, because the 3/1 barrier deflects most of the Vestoids into planet crossing orbits, from which most end up in the Sun, in impacts on the terrestrial planets, etc. Still there is no portion of the asteroid main belt which cannot be reached, under the effect of billions of years of Yarkovsky effect and chaotic diffusion combined. We should not even try to find families composed with them, because they are too widely dispersed. All but the last two (possibly three) family-forming cratering events have completely disappeared from the Vesta family.

7.4. *The Eunomia Family*

The number frequency distributions of the family members' proper elements indicate that some multiple collisions interpretation is plausible: the distribution of semimajor axes exhibits a gap around $a = 2.66$ au, close to where Eunomia itself is located²¹. The distribution of family members on all sides of the parent body for all three proper elements, and the barycenter of the family (not including Eunomia) very close to (15), are discordant with the supposed anisotropic distribution of velocities of a single cratering event.

All these pieces of evidence indicate that a single collisional event is not enough to explain the shape of the dynamical family 15. Then the discrepancy in the slopes on the two sides could be interpreted as the presence of two collisional families with different ages. Since the subfamily with proper $a > 2.66$ dominates the outer edge of the V-shape, while the inner edge is made only from the rest of the family, we could adopt the younger age as that of the high a subfamily, the older as the age of the low a subfamily. However, the lower range of diameters, starting only from $D > 6.7$ km on the outer edge, and the ratio of ages too close to 1 result in a difference of ages which is poorly constrained.

Still the most likely interpretation is that the Eunomia dynamical family was generated by two cratering events, with roughly opposite crater radiants, such that one of the two collisional families has barycenter at $a > a(15)$, the other at $a < a(15)$, see Table 9. The WISE albedo distributions of the two subfamilies are practically the same, which helps in excluding more complex interpretations in which one of the two subfamilies has a different parent body. In conclusion, the interpretation we are proposing is similar to the one of the Vesta family.

7.5. *The missing Ceres family*

(1) Ceres in our dynamical classification does not belong to any family, still there could be a family originated from Ceres. The escape velocity from Ceres is $v_e \sim 510$ m/s, while the QRL velocity used to form families in zone 3 was 90 m/s. An ejection velocity v_0 just above v_e would result in a velocity at infinity larger than 90 m/s: $v_0 = 518$ m/s is enough.

Thus every family moderately distant from Ceres, such that the relative velocity needed to change the proper elements is $< v_e$, is a candidate for

²¹A narrow resonance occurs at about the location of the gap, but it does not appear strong enough to explain it.

a family from Ceres. Family 93 is one such candidate²². By computing the distance d between the proper element set of (1) and all the family 93 members, we find the minimum possible $d = 153$ m/s for the distance (in terms of the standard metric) between (1) and (28911). Although the relationship between d and v_∞ is not a simple one (depending upon the true anomaly at the impact), anyway v_∞ would be of the same order as d , thus corresponding approximately to $v_0 = 532$ m/s.

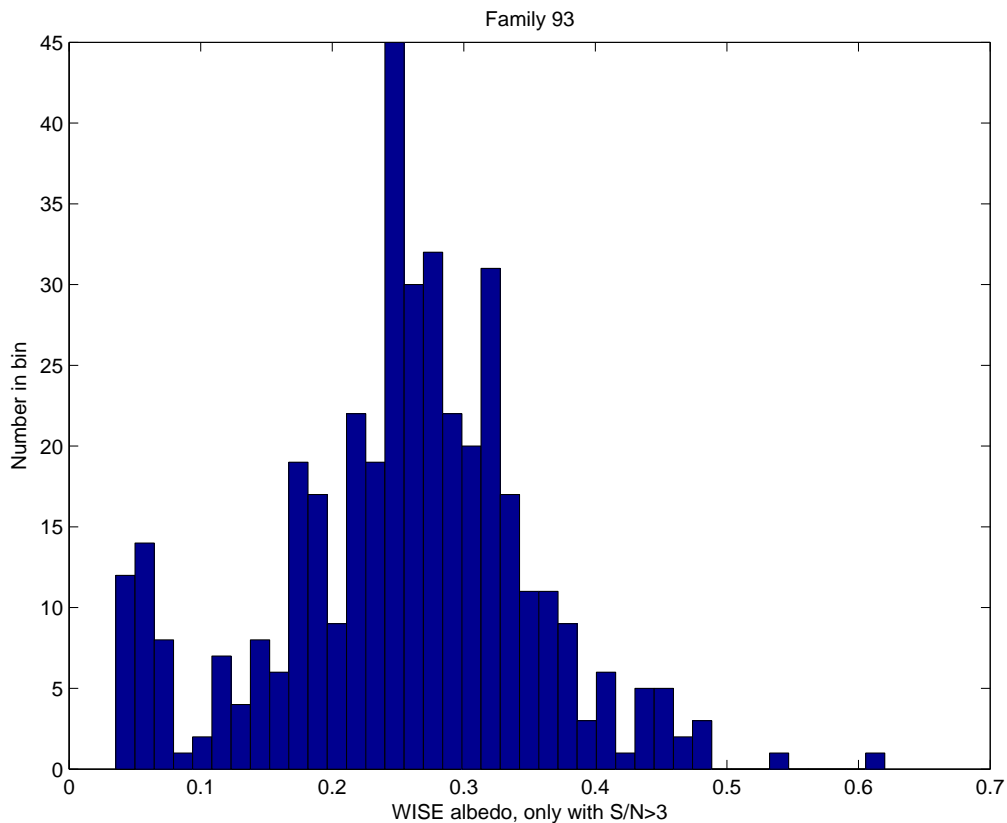


Figure 18: Histogram of the albedos measured by WISE with $S/N > 3$ among the members of the family 93. There is an obvious “dark” subgroup with albedo < 0.1 and a large spread of higher estimated albedos. Most members have intermediate albedos typical of the S-complex.

²²Other authors have proposed family classifications in which (1) is a member of a family largely overlapping with our family 93.

This is a hypothesis, for which we seek confirmation by using absolute magnitudes and other physical observations, and here comes the problem.

The albedo of (1) is 0.090 ± 0.0033 according to [35]. The surface of Ceres has albedo inhomogenities, but according to the HST data reported by [35] the differences do not exceed 8% of the value.

The WISE albedos of the family 93 (again accepting only the 403 data with $S/N > 3$) are much brighter than that of Ceres, apart from a small minority: only 37, that is 9%, have albedo < 0.1 . (93) has albedo 0.073 from IRAS, but we see no way to eject a $D \sim 150$ km asteroid in one piece from a crater; also (255) belongs to the dark minority, and is too large for a crater ejecta. No other family member, for which there are good WISE data, has diameter $D \geq 20$ km. Actually, from Figure 18 the albedo of Ceres is a minimum in the histogram. By using the SDSS data we also get a large majority of family 93 members in the S-complex region.

We cannot use V-shape diagrams composed with the same method used in Section 5.2, because the assumption of uniform albedo is completely wrong, as shown by Figure 18. As an alternative, to study possible internal structures we use only the 403 objects with good WISE data, and use a color code to distinguish low albedo, high albedo and intermediate. The Figure 19 in the proper $a, \sin I$ plane and the one in the proper a, e plane show no concentration of objects with low, not even with intermediate, albedo. Thus there appears to be no family originated from Ceres, but only a family of bright and (possibly) intermediate asteroids, having to do neither with (1), nor with (93), nor with (255).

Thus the family 93 is the only one suitable, for its position in proper elements space, to be a cratering family from Ceres, after removing the two large outliers. However, physical observations (albedo and colors) contradict this origin for an overwhelming majority of family members. Should we accept the idea that the bright/intermediate component of family 93 is the result of a catastrophic fragmentation of some S-complex asteroid, and the fact of being very near Ceres is just a coincidence?

Moreover, why Ceres would not have any family? This could not be explained by assuming that Ceres has been only bombarded by much smaller projectiles than those impacting on (2), (4), (5) and (10): Ceres has a cross section comparable to the sum of all these four others.

"How often have I said to you that when you have eliminated the impos-

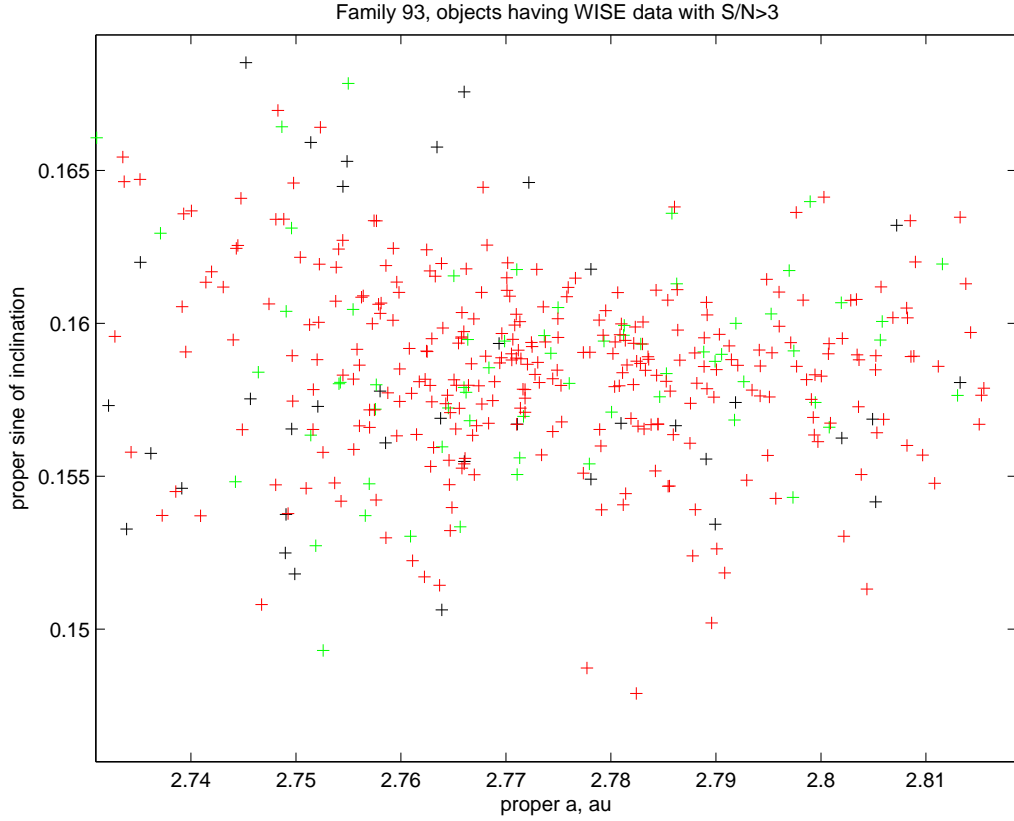


Figure 19: The members of the dynamical family 93 for which significant WISE data are available, plotted in the proper $a, \sin I$ plane. Red= albedo > 0.2 , green=albedo between 0.1 and 0.2, black=albedo < 0.1 .

sible, whatever remains, however improbable, must be the truth?”²³.

Following the advise above, we cannot discard the “coincidence” that a family of bright asteroids is near Ceres, but then all the dark family members have to be interlopers. This means we can assign 366 “bright and intermediate” (with albedo > 0.1 measured by WISE with $S/N > 3$) members of family 93 to the Gerantina collisional family, from the lowest numbered member, (1433) Gerantina, which has albedo 0.191 ± 0.017 , from which $D \simeq 15$. The volume of these 366 is estimated at $49\,000 \text{ km}^3$, equivalent to a sphere

²³Sherlock Holmes to dr. Watson, in: C. Doyle, *The Sign of the Four*, 1890, page 111.

with $D \simeq 45$ km. This can be interpreted as a catastrophic fragmentation of some S-complex asteroid with a diameter $D > 50$ km, given that a good fraction of the fragments has disappeared in the 5/2 resonance.

As for the missing family from Ceres, before attempting an explanation let's find out how significant are our family classification data, that is whether our classification could just have missed a Ceres family.

This leads to a question, to which we can give only a low accuracy answer: which is the largest family from Ceres which could have escaped our classification? This question has to be answered in two steps: first, how large could be a family resulting from cratering on Ceres which could be superimposed to the family 93? 37 dark interlopers out of 403 with good WISE data could be roughly extrapolated to 168 out of 1 833 members of family 93²⁴.

Second, how large could be a Ceres family separate from 93 and not detected by our classification procedure? In the low proper I zone 3, the three smallest families in our classification have 93, 92 and 75 members. Although we do not have a formal derivation of this limit, we think that a family with about 100 members could not be missed.

By combining these two answers, families from Ceres cratering with up to about 100 members could have been missed. The comparison with the family of (10) Hygiea, with 2 402 members, and the two subfamilies of Vesta, the smallest with $> 2,538$ members, suggests that the loss in efficiency in the generation of family members in the specific case of Ceres is at least by a factor 20, possibly much more.

Thus as an explanation for the missing Ceres family, the only possibility would be that there is some physical mechanism preventing most fragments which would be observable, currently those with $D > 2$ km, either from being created by a craterization, or from being ejected with $v_0 > 510$ m/s, or from surviving as asteroids. We are aware of only two possible models.

One model can be found in [35, section 6.3]: “The lack of a dynamical family of small asteroids associated with Ceres, unlike Vesta’s Vestoids, is consistent with an icy crust that would not produce such a family.” We have some doubts on the definition of an “icy” crust with albedo < 0.1 , thus we generalize the model from [35] by assuming a comparatively thin

²⁴This is an upper bound, since some dark interlopers from the background are expected to be there: in the range of proper semimajor axis $2.66 < a < 2.86$ au we find that 59% of background asteroids have albedo < 0.1 .

crust effectively shielding the mantle volatiles, with whatever composition is necessary to achieve the measured albedo. When Ceres is impacted by a large asteroid, $20 < D < 50$ km, the crust is pierced and a much deeper crater is excavated in an icy mantle. Thus the efficiency in the generation of family asteroids (with albedo similar to the crust) is decreased by a factor close to the ratio between average crater depth and crust thickness. The ejected material from the mantle forms a family of main belt comets, if they have enough water content they quickly dissipate by sublimation and splitting. This would be one of the most spectacular events of solar system history; unfortunately, it is such a rare event that we have no significant chance of seeing it²⁵. Thus a crust thickness of few km would be enough to explain a loss of efficiency by a factor > 20 and the possible Ceres family could be too small to be found.

A second possible model is that there is a critical value for the ejection velocity v_0 beyond which asteroids with $D > 2$ km cannot be launched without going into pieces. If this critical velocity v_c is > 363 m/s for V-type asteroids, but is < 510 m/s for the composition of Ceres ejecta (presumably with much lower material strength), then Vesta can have a family but Ceres can not. Of course it is also possible that the number of large ejecta with $v_0 > 510$ is not zero but very small. Thus even a very large impact on Ceres does generate few observable objects, it does not matter whether they are asteroids or comets, leading to a family too small to be detected. However, if the crater is deeper than the crust, Ceres itself behaves like a main belt comet for some time, until the crater is “plugged” by dirt thick enough to stop sublimation. This would be spectacular too.

The fact is, little is known of the composition and geological structure of Ceres. This situation is going to change abruptly in 2015, with the visit by the DAWN spacecraft. Then what these two models would predict for the DAWN data?

With both models, larger impacts would leave only a scar, resulting from the plugging of the mantle portion of the crater (because Ceres does not have large active spots). What such a big scar looks like is difficult to be predicted, they could be shallow if the mantle restores the equilibrium shape, but still

²⁵The exceptional presence of some 10 000 comets could perhaps be detected in an extrasolar planetary system, but since we know only of the order of 1 000 extrasolar systems, also this is a low probability event.

be observable as albedo/color variations. If there is a thin crust, then craters should have low maximum depth and a moderate maximum diameter. At larger diameters only scars would be seen. If the family generation is limited by the maximum ejection velocity, the crust could be thicker: there would be anyway craters and scars, but the craters can be larger and the scars would be left only by the very large impact basins.

8. Binaries and couples

Table 12: Binary (or multiple) systems belonging to some family identified in the present paper. Confirmed binary systems are listed in bold.

Binary asteroid		Family
(87)	Sylvia	87
(90)	Antiope	24
(93)	Minerva	93
(243)	Ida	158
(283)	Emma	283
(379)	Huenna	24
(1338)	Duponta	1338
(3703)	Volkonskaya	4
(3782)	Celle	4
(5477)	Holmes	434
(5481)	Kiuchi	4
(10208)	Germanicus	883
(11264)	Claudiomaccone	5
(15268)	Wendelinefroger	135
(17246)	2000 GL74	158
(22899)	1999 TO14	158
(76818)	2000 RG79	434

Having defined a list of asteroid families, an interesting investigation is to look at the list of currently known binary or multiple asteroid systems, to see whether these systems tend to be frequent among family members. This because a possible origin of binary systems is related to collisional events.

This is true especially for objects above some size limit, for which rotational fission mechanisms related to the YORP effect become less likely.

By limiting our attention to main belt asteroids, the list of binary systems includes currently a total of 88 asteroids²⁶, including 34 systems which are not definitively confirmed. Among them, 17 (including 6 binaries still needing confirmation) are family members according to our results; see Table 12.

The data set of definitively confirmed is still fairly limited, but it is interesting to note that 17 out of 88, or 11 out of 54 objects if we consider only certain binary systems, turn out to be family members. The relative abundance is of the order of 20%, so we cannot conclude that binary asteroids are particularly frequent among families. Looking more in detail at the data shown in Table 12, we find that binaries tend to be more abundant in the Koronis, Hungaria and Themis families, while the situation is not so clear in the case of Vesta, due to the still uncertain binary nature of some objects. We also note that binary asteroids tend also to be found among the biggest members of some families, including Sylvia, Minerva and Duponta.

8.1. Couples

One step of our family classification procedure is the computation of the distance in proper elements space between each couple of asteroids; the computation is needed only if the distance is less than some control d_{min} . If the value of d_{min} is chosen to be much smaller than the QRL values used in the family classification, a new phenomenon appears, namely the *very close couples*, with differences in proper elements corresponding to few m/s.

A hypothesis for the interpretation of asteroid couples, very close in proper elements, has been proposed long ago, see [46][p. 166-167]. The idea, which was proposed by the late P. Farinella, is the following: the pairs could be obtained after *an intermediate stage as binary*, terminated by a low velocity escape through the so-called fuzzy boundary, generated by the heteroclinic tangle at the collinear Lagrangian points.

The procedure to actually prove that a given couple is indeed the product of the split of a binary is complex, typically involving a sequence of filtering steps, followed by numerical integrations (with a differential Yarkovsky effect, given the differences in size) to find an epoch for the split and confirm that

²⁶A list of identified binary systems is maintained by R. Johnston at the URL <http://johnstonsarchive.net/astro/asteroidmoons.html>

Table 13: Very close couples among the numbered asteroids: the d distance corresponds to < 0.5 m/s.

name	H	name	H	d	$\delta a_p/a_p$	δe_p	$\delta \sin I_p$
92652	15.11	194083	16.62	0.1557213	0.0000059	-0.0000011	0.0000011
27265	14.72	306069	16.75	0.2272011	0.0000076	0.0000021	-0.0000029
88259	14.86	337181	16.99	0.2622311	-0.0000091	0.0000019	-0.0000011
180906	17.41	217266	17.44	0.2649047	0.0000069	-0.0000049	-0.0000013
60677	15.68	142131	16.05	0.3064294	0.0000090	0.0000021	0.0000052
165389	16.31	282206	16.85	0.3286134	0.0000019	0.0000080	0.0000022
188754	16.29	188782	16.90	0.3384864	-0.0000059	-0.0000019	0.0000087
21436	15.05	334916	18.14	0.3483815	-0.0000041	-0.0000081	0.0000016
145516	15.39	146704	15.57	0.4131796	-0.0000142	-0.0000062	0.0000046
76111	14.55	354652	16.55	0.4137084	0.0000174	0.0000033	-0.0000011
67620	15.35	335688	16.91	0.4225815	0.0000017	0.0000027	0.0000105
52009	15.15	326187	17.22	0.4459464	0.0000079	0.0000115	-0.0000020
39991	14.15	340225	17.90	0.4495984	0.0000003	-0.0000101	-0.0000061
64165	15.14	79035	14.54	0.4501940	-0.0000018	0.0000010	0.0000127
57202	15.34	276353	17.45	0.4543033	-0.0000027	0.0000103	0.0000052
180255	16.85	209570	17.08	0.4686305	0.0000185	-0.0000026	0.0000003
39991	14.15	349730	17.35	0.4686824	0.0000182	-0.0000020	-0.0000043
56285	14.98	273138	16.72	0.4958970	0.0000199	-0.0000061	0.0000025

the relative velocity was indeed very small. Many authors have worked on this, including ourselves [54] and [22], who analyzed the efficiency of non-disruptive collisional events in leading to binary “evaporation”. Our goal for this paper is not to confirm a large number of split couples, but just to offer the data for confirmation by other authors, in the form of a very large list of couples with very similar proper elements.

Currently we are offering a dataset of 14 627 couples with distance < 10 m/s, available from AstDyS²⁷. A small sample of these couples is given in Table 13, for $d < 0.5$ m/s.

To assess the probability of finding real couples in this large sample, it is enough to draw an histogram of the distance d . It shows the superposition of two components, one growing quadratically with d and one growing linearly. Since the incremental growth of volume is quadratic in d , this should correspond to the fraction of couples which are random and to the ones which result from a very different phenomenon, such as split followed by drift due

²⁷<http://hamilton.dm.unipi.it/~astdys2/propsynth/numb.near>

to differential Yarkovsky. It turns out that from the histogram it is possible to compute that, out of 14 627 couples, about half belong to the “random” sub-population, half to the linear growth component.

9. Conclusions and Future Work

By performing an asteroid family classification with a very enlarged dataset the results are not just “more families”, but there are interesting qualitative changes. These are due to the large number statistics, but also to the larger fraction of smaller objects contained in recently numbered asteroids and to the accuracy allowing to see many structures inside the families²⁸.

Another remarkable change is that we intend to keep this classification up to date, by the (partially automated) procedures we have introduced.

In this section we would like to summarize some of these changes, and also to identify the research efforts which can give the most important contribution to this field. Note that we do not necessarily intend to do all this research ourselves, given our complete open data policy this is not necessary.

9.1. How to use HCM

The size increase of the dataset of proper elements has had a negative effect on the perception about the HCM method in the scientific community, because of the chaining effect which tends to join even obviously distinct families. Thus some authors have either reduced the dataset by asking that some physical observations are available, or used QRL values variable for each family, or even reverted to visual methods.

We believe that this paper shows that there is no need to abandon the HCM method, provided a more complex multistep procedure is adopted. In short, our procedure amounts to using a truncation QRL for the larger members belonging to the core family different from the one used for smaller members. This is justified from the statistical point of view, because the smaller asteroids have larger number density.

We are convinced that our method is effective in adding many smaller asteroids to the core families, without expanding the families with larger

²⁸Note that these three are reasons to discard the usage of physical observation data as primary parameters for classification. Consistent catalogs of physical observation are available for less asteroids, they are also observationally biased against smaller asteroids, which are either absent or present with very low accuracy data.

members. As a result we have a large number of families with very well defined V-shapes, thus with a good possibility of age estimation. We have also succeeded in identifying many families formed only with small asteroids, or at most with very few large ones, as expected for cratering.

The portion of the procedure on which we intend to work more is the step 5, merging, which is still quite subjective (indeed, even visual inspection plays a significant role). This procedure is cumbersome and not automated at all, and may become even more difficult in the future with the expected large increase of the dataset size, thus further improvements are needed.

9.2. Stability of the classification

We have established a procedure to maintain our family classification up to date, by adding the newly discovered asteroids, as soon as their orbital elements are stable enough because determined with many observations. First the proper elements catalogs are updated, then we attribute some of the new entries as new members to the already known families. This last step 6 (see Section 3) is performed in a fully automated way, just by running a single computer code (with CPU times of the order of 1 hour), which is actually the same code used for steps 2 and 4.

We already have done this for the proper elements catalog update of April 2013, and we continue with periodic updates. The results are available, as soon as computed, on the AstDyS information system.

The classification is meant to be methodologically stable but frequently updated in the dataset. In this way, the users of our classification can download the current version. They can find a full description of the methods in this paper, even if specific results (e.g., number and list of members of some family) should not be taken from the paper but from the updated web site.

Some changes in the classification such as mergers are not automatic, thus we are committed to apply them periodically, until when we will be able to automatize this too.

9.3. Magnitudes

As shown in Table 1, the absolute magnitudes computed with the incidental photometry could contribute a significant fraction of the information used in family classification and analysis. However, the accuracy is poor, in most cases not estimated; better data are available for smaller samples, not enough for statistical purposes, such as the analysis of Section 5. This does not affect the classification, but has a very negative impact on the attempt

to compute ages, size distributions, and volumes. It also affects the accuracy of the albedos, and has serious implications on the population models.

The question is what should be done to improve the situation. One possibility would be a statistically rigorous debiasing and weighting of the photometry collected with the astrometry. The problem is, the errors in the photometry, in particular the ones due to difference in filters and star/asteroid colors, are too complex for a simple statistical model, given that we have no access to a complete information on the photometric reduction process.

Thus we think that the only reliable solution is to have an optimally designed photometric survey, with state of the art data processing, including the new models of the phase effect [55]. This requires a large number (of the order of 100) photometric measurements per asteroid per opposition, with a wide filter, and with enough S/N for most numbered main belt asteroids. These appear tough requirements, and a dedicated survey does not appear a realistic proposal. However, it turns out that these requirements are the same needed to collect enough astrometry for a NEO wide survey, aiming at discovering asteroids/comets on the occasion of close approaches to the Earth. Thus a “magnitude survey” could be a byproduct of a NEO discovery survey, provided the use of many different filters is avoided.

9.4. Yarkovsky effect and ages

One of our main results is that for most families, large enough for statistically significant analysis of the shape, the V-shape is clearly visible.

We have developed our method to compute ages, which we believe is better than those used previously (including by ourselves, [54]) because it is more objective and takes into account the error in the estimate of the diameter by the common albedo hypothesis, which is substantial.

We believe our new method tackles in an appropriate way all the difficulties of the age estimation discussed in Section 5.2, but for one: the calibration. The difficulty in estimating the Yarkovsky calibration, due to the need to extrapolate from NEAs with measured da/dt to main belt asteroids, is in most cases the main limitation to the accuracy of the age estimation.

Thus the research effort which could most contribute to the improvement of age estimation (for a large set of families) would be either the direct measurement of Yarkovsky effect for some family members (with known obliquity) or the measurement of the most important unknown quantities affecting the scaling from NEA, such as thermal conductivity and/or density. These

appear ambitious goals, but they may become feasible by using advanced observation techniques, in particular from space, e.g., GAIA astrometry, Kuiper infrared observations, and radar from the ground.

9.5. Use of physical observations

In this paper we have made the choice of using the dynamical data first, to build the family classification, then use all the available physical data to check and refine the dynamical families.

This is best illustrated by the example of the Hertha/Polana/Burdett complex dynamical family, in which the identification of the two collisional families Polana and Burdett can be obtained only with the physical data. This leaves us with more understanding, but with an incomplete classification because the majority of the members of the Hertha dynamical family there are no physical data. If we had a much larger database of accurate albedos and/or colors, we would be very glad to use the separation by physical properties as part of the primary family classification. The same argument could apply to the separation of the two collisional families of Vesta.

In other words, the use of dynamical parameters first is not an ideological choice, but is dictated by the availability and accuracy of the data. We would very much welcome larger catalogs of physical data, including much smaller asteroids and with improved S/N for those already included. However, we are aware that this would require larger aperture telescopes.

9.6. Cratering vs. Fragmentation

Our procedure, being very efficient in the inclusion of small asteroids in the haloes of core families, has allowed to identify new cratering families and very large increases of membership for the already known ones.

As a result of the observational selection effect operating against the cratering families, because they contain predominantly small asteroids (e.g., $D < 5$ km), in the past the cratering events have been less studied than the catastrophic fragmentations. On the contrary, elementary logic suggests that there should be more cratering than fragmentation families, because the target of a cratering remains available for successive impacts, with the same cross section. The number of recognized cratering families is reduced because small asteroids from craterizations have a shorter lifetime, thus the observable cratering families have a limited age. As the observational bias against small asteroids is progressively mitigated, we expect that the results on cratering will become more and more important.

This argument also implies that multiple cratering collisional families should be the rule rather than the exception. They necessarily intersect because of the common origin but do not overlap completely because of the different crater radiants. Although we have studied only some of the cratering families (listed in Section 7), all the examples we have analyzed, namely the families of (4), (20), (15), show a complex internal structure.

For the catastrophic fragmentation families, the two examples we have analyzed, (158) and (847), appear to contain significant substructures (named after Karin and Jitka). The general argument could be used that fragments are smaller, thus should have collisional lifetimes shorter than the parent body of the original fragmentation family. Thus we should expect that as fragmentation families become larger in membership and include smaller asteroids, substructures could emerge in most of the families.

A full fledged collisional model for the ejection velocities and rotations of fragments from both cratering and fragmentation needs to be developed, possibly along the lines of the qualitative model of Section 5.2.7. This will contribute both to the age determination and to the understanding of the family formation process. As for future research, there is the need to search for substructures and to classify as cratering/fragmentation, this for all the big families of Table 3 and many of the medium families of Table 4.

9.7. Comparison with space mission data

When on-site data from spacecraft, such as DAWN, become available for some big asteroid, a family classification should match the evidence, in particular from craters on the surface. For Vesta the main problem is the relationship between the dynamical family 4 and the two main craters Rheasilvia and Veneneia. The solution we are suggesting is that the two subfamilies found from internal structure of family 4 correspond to the two main craters. We have found no contradiction with this hypothesis in the data we can extract from the family, including ages. However, to prove this identification of the source craters requires more work: more accurate age estimates for both subfamilies and craters, and more sophisticated models of how the ejecta from a large crater are partitioned between ejecta reaccumulated, fragments in independent orbits but too small, and detected family members.

Because the problem of the missing Ceres family is difficult, due to apparently discordant data, we have tried to build a consistent model, with an interpretation of the dynamical family 93 (without the namesake) and two possible physical explanations of the inefficiency of Ceres in generating

families. We are not claiming these are the the only possible explanations, but they appear plausible. The data from DAWN in 2015 should sharply decrease the possibilities and should lead to a well constrained solution.

Acknowledgments

The authors have been supported for this research by: the Ministry of Science and Technological Development of Serbia, under the project 176011 (Z.K. and B.N.). We thank S. Marchi, M. Micheli and S. Bus for discussions which have contributed to some of the ideas of this paper.

References

- [1] Ph. Bendjoya & Zappalà, V.: 2002, Asteroid Family Identification, in *Asteroids III*, (W.F. Bottke Jr., A. Cellino, P. Paolicchi, and R.P. Binzel, Eds), University of Arizona Press Tucson, pp. 613-618.
- [2] Benner L.A.M., S.J. Ostro, R.S. Hudson, K.D. Rosema, R.F. Jurgens, D.K. Yeomans, & 3 coauthors: 2002, Radar observations of Asteroid 3908 Nyx, *Icarus* **158**, 379–388.
- [3] Binzel R.P., A.S. Rivkin, J.S. Stuart, A.W. Harris, S.J. Bus, & T.H.. Burbine: 2004, Observed spectral properties of near-Earth objects: results for population distribution, source regions, and space weathering processes, *Icarus* **170**, 259–294.
- [4] Bottke, W.F., *Science* **294** 1693
- [5] Bottke W.F., D. Vokrouhlický, D.F. Rubincam & M. Brož: 2002. The effect of Yarkovsky Thermal Forces on the Dynamical Evolution of Asteroids and Meteoroids, in *Asteroids III*, (W.F. Bottke Jr. et al., Eds), University of Arizona Press Tucson, pp. 395-408.
- [6] Bottke W.F., Vokrouhlický D., Rubincam D.F. & D. Nesvorný: 2006, The Yarkovsky and YORP effects: Implications for Asteroid Dynamics, *Ann. Rev. Earth and Planet. Sci.* **34**, 157-191.
- [7] Brož, M. & A. Morbidelli: 2013, The Eos family halo, *Icarus* **223**, 844–849.

- [8] Bus, S.J.: 2013, A Record of Multiple Cratering Events in the Vesta Asteroid Family, *American Astronomical Society*, DPS meeting #45, #208.05.
- [9] Carruba, V.: 2009, An analysis of the region of the Phocaea dynamical family, *Mon. Not. R. Astron. Soc.* **398**, 1512–1526.
- [10] Carruba, V. & T.A. Michtchenko: 2007, A frequency approach to identifying asteroid families, *Astron. Astrophys.* **475**, 1145–1158.
- [11] Carruba, V., R.C. Domingos, D. Nesvorný, F. Roig, M.E. Huaman & D. Souami: 2013, A multidomain approach to asteroid families’ identification, *Mon. Not. R. Astron. Soc.* **433**, 2075–2096.
- [12] Cellino, A., P. Michel, P. Tanga, V. Zappalà, P. Paolicchi, & A. Dell’Oro: 1999, The Velocity-Size Relationship for Members of Asteroid Families and Implications for the Physics of Catastrophic Collisions, *Icarus* **141**, 79-95.
- [13] Cellino, A., V. Zappalà, A. Doressoundiram, M. Di Martino, Ph. Bendjoya, E. Dotto, & 1 coauthor: 2001, The Puzzling Case of the NysaPolana Family, *Icarus* **152**, 225–237.
- [14] A. Cellino, S. J. Bus, A. Doressoundiram, & D. Lazzaro: 2002, Spectroscopic properties of asteroid families, in *Asteroids III*, (W. F. Bottke Jr., A. Cellino, P. Paolicchi, & R. P. Binzel, Eds), University of Arizona Press, Tucson, pp. 633–643.
- [15] Cellino, A., I. N. Belskaya, Ph. Bendjoya, M. di Martino, R. Gil-Hutton, K. Muinonen, & 1 coauthor: 2006, The strange polarimetric behavior of asteroid (234) Barbara, *Icarus* **180**, 565-567.
- [16] Cellino, A., R. Gil-Hutton, A. Dell’Oro, Ph. Bendjoya, M. Cañada-Assandri, & M. Di Martino: 2011, A new calibration of the albedo-polarization relation for the asteroids, *J. Quant. Spectr. Rad. Trans.* **113**, 2552–2560.
- [17] Cellino, A., S. Bagnulo, P. Tanga, B. Novaković, & M. Delbò: 2013, A successful hunt for hidden Barbarians in the Watsonia asteroid family, *submitted*.
- [18] Chapman, C.R., E.V. Ryan, W.J. Merline, G. Neukum, R. Wagner, P.C. Thomas, & 2 coauthors: 1996, Cratering on Ida, *Icarus* **120**, 77-86.

- [19] Chesley, S.R., D. Farnocchia, M.C. Nolan, D. Vokrouhlický, P.W. Chodas, A. Milani, & 14 coauthors: 2013, Orbit and Bulk Density of the OSIRIS-REx Target Asteroid (101955) Bennu, *submitted*.
- [20] Cotto-Figueroa, D., Statler T.S., Richardson D.C., & P. Tanga: 2013, Killing the YORP Cycle: A stochastic and Self-Limiting YORP Effect, *American Astronomical Society*, DPS meeting #45 (October), #106.09.
- [21] Delisle, J.-B. & J. Laskar: 2012, Chaotic diffusion of the Vesta family induced by close encounters with massive asteroids, *Astron. Astrophys.* **540**, A118, 1–8.
- [22] Dell’Oro, A., A. Cellino, & P. Paolicchi: 2012, Non-destructive collisions and the evolution of the orbits of binary asteroid systems in the Main Belt, *Mon. Not. R. Astron. Soc.* **425**, 1492–1503.
- [23] Durda, D.R., W.F. Bottke, D. Nesvorný, B.L. Enke, W.J. Merline, E. Asphaugh, & 1 coauthor: 2007, Size-frequency distributions of fragments from SPH/ N-body simulations of asteroid impacts: Comparison with observed asteroid families, *Icarus* **186**, 498-516.
- [24] Farnocchia, D., S. R. Chesley, D. Vokrouhlický, A. Milani, F. Spoto, & W. F. Bottke: 2013, Near Earth Asteroids with measurable Yarkovsky effect, *Icarus* **224**, 1–13.
- [25] Farnocchia, D., S. R. Chesley, P. W. Chodas, M. Micheli, D. J. Tholen, A. Milani, & 2 coauthors: 2013, Yarkovsky-driven impact risk analysis for asteroid (99942) Apophis, *Icarus* **224**, 199–200.
- [26] Fujiwara A., Cerroni P., Davis D., Ryan E., & M. Di Martino: 1989, Experiments and scaling laws for catastrophic collisions, *Asteroids II*, (R. P. Binzel, T. Gehrels, & M.S. Matthews, Eds.), University of Arizona Press, Tucson, pp. 240-265.
- [27] Holsapple K., GIBLIN I., Housen K., Nakamura A. & Ryan E.:2002, in *Asteroids III*, (W. F. Bottke Jr., A. Cellino, P. Paolicchi, & R. P. Binzel, Eds), University of Arizona Press, Tucson, pp. 443-462.
- [28] Ivezić, Ž., S. Tabachnik, R. Rafikov, R. H. Lupton, T. Quinn, M. Hammergren, & 26 coauthors: 2001, Solar System Objects Observed in the

- Sloan Digital Sky Survey Commissioning Data, *Astron. J.*, **122**, 2749–2784.
- [29] Z. Knežević, Ch. Froeschlé, A. Lemaitre, A. Milani & A. Morbidelli: 1994, Comparison between two theories of asteroid proper elements, *Astron. Astrophys.* **293**, 605–612.
 - [30] Knežević Z., & Milani A.: 2000 Synthetic proper elements for outer main belt asteroids, *Cel. Mech. Dyn. Astron.* **78**, 17–46.
 - [31] Knežević Z., & Milani A.: 2003, Proper element catalogs and asteroid families, *Astron. Astrophys.* **403**, 1165–1173.
 - [32] Jutzi M., Asphaug E., Gillet P., Barrat J.A. & Benz W.: 2013, The structure of the asteroid 4 Vesta as revealed by models of planet-scale collisions, *Nature* **494**, 207–210.
 - [33] Laskar, J., M. Gastineau, J.-B. Delisle, A. Farrés, & A. Fienga: 2011, Strong chaos induced by close encounters with Ceres and Vesta, *Astron. Astrophys.* **532**, L4, 1–4.
 - [34] La Spina A., Paolicchi P. and Penco U.:2005. Yarkovsky-evolved asteroid dynamical families: a correlation between their present properties and the impact geometry? American Astronomical Society, DPS meeting #37, #15.14; Bulletin of the American Astronomical Society, 37, 641.
 - [35] Li, J.-Y.; L. A. McFadden, J. W. Parker, & Wm. Joel: 2006, Photometric analysis of 1 Ceres and surface mapping from HST observations, *Icarus* **182**, 143–160.
 - [36] Mainzer, A., J. Bauer, T. Grav, J. Masiero, R. M. Cutri, J. Dailey, & 29 coauthors: 2011, Preliminary results from NEOWISE: An enhancement to the Wide-field Infrared Survey Explorer for Solar System science, *Astrophys. J.* **731**:53.
 - [37] Marchi, S., H. Y.McSween, D.P. O’Brien, P. Schenk, M.C. De Sanctis, R. Gaskell, & 6 coauthors: 2012, The Violent Collisional History of Asteroid 4 Vesta, *Science* **336**, 690–694.
 - [38] Marchis F., P. Descamps, D. Hestroffer, & J. Berthier: 2005, Discovery of the triple asteroidal system 87 Sylvia, *Nature* **436**, 822–824.

- [39] Marzari F., D. Davis, & V. Vanzani: 1995, Collisional Evolution of Asteroid Families, *Icarus* **113**, 168–178.
- [40] Masiero J. R., A. K. Mainzer, T. Grav, J. M. Bauer, R. M. Cutri, J. Dailey, & 12 coauthors: 2011, Main belt asteroids with WISE/NEOWISE. I. Preliminary albedos and diameters, *Astrophys. J.* **741**, 68.
- [41] Masiero J. R., A. K. Mainzer, J. M. Bauer, T. Grav, C.R. Nugent, & R. Stevenson: 2013, Asteroid family identification using the hierarchical clustering method and WISE/NEOWISE physical properties, *Astrophys. J.* **770**, 7.
- [42] Maxwell D.E.:1977. Simple Z model of cratering,ejection and the overturned flap; Impact and Explosion Cratering, *Pergamon Press*, New York (USA), 1003–1008.
- [43] Michel. P., W. Benz, P. Tanga & D.C. Richardson: 2001, Collisions and Gravitational Reaccumulation: Forming Asteroid Families and Satellites, *Science* **294**, 1696–1700.
- [44] Michel P. & Richardson D. C.:2013, Collision and gravitational reaccumulation: Possible formation mechanism of the asteroid Itokawa, *Astronomy & Astrophysics* **554**, L1.
- [45] Migliorini F., V. Zappalà, R. Vio, & A. Cellino: 1995, Interlopers within asteroid families, *Icarus* **118**, 271–291.
- [46] Milani, A.: 1994, The dynamics of the Trojan asteroids, in: A. Milani, M. Di Martino and A. Cellino (eds), *Asteroids, Comets, Meteors 1993*, Kluwer Acad. Publ. Dordrecht, pp. 159–174.
- [47] A. Milani & Z. Knežević: 1990. Secular perturbation theory and computation of asteroid proper elements, **49**, 347–411.
- [48] Milani, A., & Z. Knežević: 1992, Asteroid proper elements and secular resonances, *Icarus* **98**, 211–232.
- [49] Milani, A. & A. M. Nobili: 1992, An example of stable chaos in the solar system, *Nature* **357**, 569–571.
- [50] Milani, A., & Z. Knežević: 1994, Asteroid proper elements and the Dynamical Structure of the Asteroid Main Belt, *Icarus* **107**, 219–254.

- [51] A. Milani & P. Farinella: 1994, The age of the Veritas asteroid family deduced by chaotic chronology, *Nature* **370**, 40–42.
- [52] A. Milani & P. Farinella: 1995, An asteroid on the brink, *Icarus* **115**, 209–212.
- [53] A. Milani & Gronchi, G.F.: 2010, *Theory of Orbit determination*, Cambridge University Press, Cambridge, UK.
- [54] Milani, A., Z. Knežević, , B. Novaković, & A. Cellino: 2010, Dynamics of the Hungaria asteroids, *Icarus* **207**, 769–794.
- [55] Muinonen, K., I.N. Belskaya, A. Cellino, M. Delbò, A-C. Levasseur-Regourd, A. Penttilä, Antti; & 1 coauthor: 2010, A three-parameter magnitude phase function for asteroids, *Icarus* **209**, 542–555.
- [56] Novaković, B., A. Cellino, & Z. Knežević: 2011, Families among high-inclination asteroids, *Icarus* **216**, 69–81.
- [57] Paolicchi P., Cellino A., Farinella P. & V. Zappalà: 1989, A semiempirical model of catastrophic breakup processes, *Icarus* **77**, 187–212.
- [58] Paolicchi P., Verlicchi A. & A. Cellino: 1996, An improved semiempirical model of catastrophic impact processes, *Icarus* **121**, 126–157.
- [59] Paolicchi P. & M. Micheli: 2008, The non-gravitational effects on the dynamical evolution and on the rotational properties of the asteroids, *Memorie della Società Astronomica Italiana, Supplement* **12**, 145–150.
- [60] Paolicchi P. & A. Kryszczyńska: 2012, Spin vectors of asteroids: Updated statistical properties and open problems, *Planet. and Space Science* **73**, 70–74.
- [61] Parker, A., Ž. Ivezić, M. Jurić, R. Lupton, M. D. Sekora, & A. Kowalski: 2008, The size distributions of asteroid families in the SDSS Moving Object Catalog 4, *Icarus* **198**, 138–155.
- [62] Pravec, P., A. W. Harris, P. Kunirk, A. Gald, & K. Hornoch: 2012, Absolute magnitudes of asteroids and a revision of asteroid albedo estimates from WISE thermal observations, *Icarus* **221**, 365–387.

- [63] Richardson D. C., Michel P., Walsh K. J. & K.W. Flynn: 2009, Numerical simulations of asteroids modelled as gravitational aggregates with cohesion, *Planetary and Space Science* **57**, 183–192.
- [64] Rivkin, A.S., E.S Howell, L.A. Lebofsky, B.E. Clark, & D.T. Britt: 2000, The nature of M.class asteroids from 3- μ m observations, *Icarus* **145**, 351–368.
- [65] Shevchenko, V.G. & E.F. Tedesco: 2006, Asteroid albedos deduced from stellar occultations, *Icarus* **184**, 211–220.
- [66] Schubart, J.: 1991, Additional results on orbits of Hilda-type asteroids, *Astron. Astrophys.* **241**, 297–302.
- [67] E.A. Smirnov & Shevchenko, I.I.: 2013, Massive identification of asteroids in three-body resonances, *Icarus* **222**, 220–228.
- [68] Statler, T.S.: Extreme sensitivity of the YORP effect to small-scale topography: 2009, *Icarus* **202**, 502–513.
- [69] Tanga, P., A. Cellino, P. Michel, V. Zappalà, P. Paolicchi, & A. Dell’Oro: 1999, On the Size Distribution of Asteroid Families: The Role of Geometry, *Icarus* **141**, 65–78.
- [70] Tedesco, E.F., P.V. Noha, M. Noha, & S.D. Price: 2002, The supplemental IRAS minor planet survey (SIMPS), *Astron. J.* **123**, 1056–1085.
- [71] Vokrouhlický, D., A. Milani, & S.R. Chesley: 2000, Yarkovsky Effect on Small Near-Earth Asteroids: Mathematical Formulation and Examples, *Icarus* **148**, 118–138.
- [72] Vokrouhlický, D., M. Brož, P. Farinella & Z. Knežević : 2001, Yarkovsky-Driven Leakage of Koronis Family Members. I. The Case of 2953 Vysheslavia, *Icarus* **150**, 78–93.
- [73] Vokrouhlický, D., M. Brož, W.F. Bottke, D. Nesvorný, & A. Morbidelli: 2006, Yarkovsky/YORP chronology of asteroid families, *Icarus* **182**, 118–142.
- [74] Vokrouhlický, D., Brož, M., Bottke, W.F., Nesvorný, D., & Morbidelli, A. : 2006, The peculiar case of the Agnia asteroid family, *Icarus* **183**, 349–361.

- [75] Vokroulický D., Brož M., Morbidelli A., Bottke W.F., Nesvorný D., Lazzaro D. & A.S. Rivkin: 2006, Yarkovsky footprints in the Eos family, *Icarus* **182**, 92–117.
- [76] Zappalà, V., A. Cellino, P. Farinella, & Z. Knežević: 1990, Asteroid families. I - Identification by hierarchical clustering and reliability assessment, *Astron. J.*, **100**, 2030–2046.
- [77] Zappalà V., A. Cellino, P. Farinella, & A. Milani: 1994, Asteroid families. II: Extension to unnumbered multiopposition asteroids, *Astron. J.*, **107**, 772–801.
- [78] Zappalà V., Ph. Bendjoya, A. Cellino, P. Farinella, & C. Froeschlé: 1995, Asteroid families: Search of a 12,487-asteroid sample using two different clustering techniques, *Icarus*, **116**, 291–314.